Titre: Title:	Broadband design and optimization of balanced subharmonically pumped mixer for Ka-band LMCS subscriber terminal
Auteur: Author:	Huifang Gu
Date:	2001
Type:	Mémoire ou thèse / Dissertation or Thesis
Référence: Citation:	Gu, H. (2001). Broadband design and optimization of balanced subharmonically pumped mixer for Ka-band LMCS subscriber terminal [Thèse de doctorat, École Polytechnique de Montréal]. PolyPublie. https://publications.polymtl.ca/7060/

URL de PolyPublie: PolyPublie URL:	https://publications.polymtl.ca/7060/
Directeurs de recherche: Advisors:	Ke Wu
Programme: Program:	Non spécifié

INFORMATION TO USERS

This manuscript has been reproduced from the microfilm master. UMI films the text directly from the original or copy submitted. Thus, some thesis and dissertation copies are in typewriter face, while others may be from any type of computer printer.

The quality of this reproduction is dependent upon the quality of the copy submitted. Broken or indistinct print, colored or poor quality illustrations and photographs, print bleedthrough, substandard margins, and improper alignment can adversely affect reproduction.

In the unlikely event that the author did not send UMI a complete manuscript and there are missing pages, these will be noted. Also, if unauthorized copyright material had to be removed, a note will indicate the deletion.

Oversize materials (e.g., maps, drawings, charts) are reproduced by sectioning the original, beginning at the upper left-hand corner and continuing from left to right in equal sections with small overlaps.

ProQuest Information and Learning
300 North Zeeb Road, Ann Arbor, MI 48106-1346 USA
800-521-0600

UNIVERSITÉ DE MONTRÉAL

BROADBAND DESIGN AND OPTIMIZATION OF BALANCED SUBHARMONICALLY PUMPED MIXER FOR KA-BAND LMCS SUBSCRIBER TERMINAL

HUIFANG GU
DÉPARTEMENT DE GÉNIE ÉLECTRIQUE
ÉCOLE POLYTECHNIQUE DE MONTRÉAL

THÈSE PRÉSENTÉE EN VUE DE L'OBTENTION
DU DIPLÔME DE PHILOSOPHIÆ DOCTOR (Ph.D.)
(GÉNIE ÉLECTRIQUE)
DECEMBRE 2001

UNIVERSITÉ DE MONTRÉAL

ÉCOLE POLYTECHNIQUE DE MONTRÉAL

Cette thèse intitulée:

BROADBAND DESIGN AND OPTIMIZATION OF BALANCED SUBHARMONICALLY PUMPED MIXER FOR KA-BAND LMCS SUBSCRIBER TERMINAL

présentée par: GU Huifang

en vue de l'obtention du diplôme de: Philosophiæ Doctor

a été dûment acceptée par le jury d'examen constitué de:

BOSISIO Renato G., M.Sc.A, président

WU Ke, Ph.D., membre et directeur de recherche

AKYEL Cevdet, D.Sc.A, membre

ANTAR Yahia, Ph.D., membre

ACKNOWLEDGEMENTS

I would like to warmly thank Professor Ke Wu for his confidence in me from the beginning and throughout this project as well as for the advice he gave and for sharing his technical experience. Under his supervision, I valued his constant concern for innovation. I would also like to thank him for the financial assistance I was accorded throughout this study.

I am also grateful to the laboratory support team. Thank you to Jules Gauthier for his advice, help with measurements and manufacturing, René Archambault for managing the computer networks and Ginette Desparois for taking care of administrative tasks.

My thanks also go to the research members of the Poly-Grames Research Center, particularly Yves Cassivi, Mekki Belaid, Domonic Deslandes and Visan Tiberiu-Marian for their fruitful discussions, co-operation and their friendliness.

I have learned so much from the professors and developed so many friendships in my time at Poly-Grames Research Center. I would like to thank you all for an unforgettable experience.

RÉSUMÉ

Le bloc de transposition de fréquence en bande de base est un élément clé dans les récepteurs LMCS/LMDS utilisés dans les terminaux des abonnés (CPE-Custom Promises Equipment). Il est donc important de concevoir un mélangeur large bande de haute qualité et de dimensions réduites. Le mélangeur équilibré est connu pour avoir des caractéristiques plus intéressantes qu'un mélangeur constitué d'une seule diode, comme une bonne isolation entre les fréquences RF et IF et entre les fréquences RF et LO, une immunité contre le bruit AM issu de l'oscillateur local (LO) et une bonne réjection des produits d'intermodulations non désirés. Les mélangeurs sous-harmoniques SH (SubHarmonically) ont des avantages supplémentaires lorsqu'ils sont utilisés à une fréquence du signal LO deux fois plus petite que la fréquence du signal RF. C'est particulièrement intéressant aux fréquences millimétriques pour lesquelles le coût d'un oscillateur local peut être élevé et quand on sait que le bruit généré par ce dernier augmente rapidement avec la fréquence. Ainsi, nous faisons l'étude et la conception d'un nouveau type de mélangeur SH équilibré qui permettra de combiner les avantages d'un mélangeur équilibré et d'un mélangeur sous-harmonique.

Les mélangeurs SH équilibrés sont très sensibles à la charge d'un composant non-linéaire aux différentes fréquences non désirés. Aux fréquences des signaux LO, RF et IF, le composant a une charge résistive, mais aux fréquences issues des

produits d'intermodulations (dus aux non-linéarités des diodes), on doit avoir une charge réactive pour éviter une perte de puissance. Dans ce travail, nous présentons une approche générique qui peut être utilisée dans le but de déterminer les conditions optimales de charge aux fréquences indésirables, et par la même, obtenir les performances optimales du mélangeur SH équilibré. Ce qui peut constituer une méthode de conception intéressante pour les concepteurs de tels mélangeurs.

Dans le but de valider notre méthode, nous concevons un mélangeur SH équilibré fonctionnant à la fréquence de 14 GHz et en utilisant la technologie des lignes micro-ruban. Le mélangeur est optimisé à la fréquence $2f_{LO} + f_{RF}$. Le circuit est réalisé sur le substrat TMM3 d'épaisseur 10 mil. Les pertes de conversion mesurées sont inférieures à 9dB sur la plage de fréquence 13.5-15.5 GHz et elles sont de 7.2 dB à 14 GHz avec une fréquence IF de 500 MHz. De plus, on a au minimum 30 dB d'isolation entre les ports. Cependant, l'ajout des lignes qui permettent d'obtenir un déphasage de 180 fait qu'il n'est pas possible d'obtenir 180 pour toutes les fréquences, car la variation de la longueur électrique dépend de la fréquence. De plus, les court-circuits qui sont obtenus en plaçant des rivets (pour faire la connexion avec le plan de masse) introduisent des parasites qui perturbent le circuit à haute fréquence. Les lignes de transmission uniplanaires permettent de réaliser facilement les terminaisons court-circuitées. Il est également aisé de placer des composants (passifs ou actifs) montés en surface pour des configurations séries ou parallèles. De plus, il n'est pas nécessaire de percer le substrat pour at-

teindre le plan de masse et il n'est pas difficile de réaliser les transitions entre les différentes lignes de transmission uniplanaires. Par conséquent, certaines architectures uniplanaires sont utilisées pour des conceptions de circuits intégrés hybrides monolithiques (MHMIC) à large bande.

Dans la topologie uniplanaire, il y a généralement deux types de transition pour passer d'une ligne balancée à une ligne non-balancée (cette transition est appelée balun): le balun de Marchand et le balun en double Y. Les baluns de Marchand ont une largeur de bande plus étroite et une géométrie plus grande que ceux en double Y. Ceci est dû à l'asymétrie de la jonction et des stubs de longueur $\lambda/4$. Les baluns double Y permettent, quant à eux, d'obtenir une topologie large bande tout en ayant des dimensions physiques compatibles pour une intégration dans des circuits MMIC.

Dans ce travail, une méthode générale de conception est développée pour des circuits large bande, et ce, dans le but d'améliorer les performances d'un balun uniplanaire en double Y. Selon la technique développée, nous concevons deux nouvelles versions de baluns double Y à large bande. La première version est relative à un plan de masse infini (structure de lignes coplanaires à fentes appelée CPW-slotline) et la seconde relative à un plan de masse fini (structure appelée CPW$_{fpg}$-CPS). Les baluns sont réalisés en technologie MHMIC. Le balun CPW-slotline montre de bonnes performances avec des pertes d'insertions inférieures à 1 dB et une réponse fréquentielle constante sur la plage de fréquence comprise entre 2 et 3 octaves. En

outre, le balun CPW_{fpg}-CPS affiche des pertes d'insertion inférieures à 1.5 dB sur la plage DC-22 GHz.

Un concept de champs électriques modaux en lignes coplanaires anti-symétriques, convergeant "élastiquement" dans une ouverture circulaire, est appliqué à la conception d'une RF-choke et de filtres de découplage DC-RF. Ce qui réduit les pertes par radiation du stub ouvert. En effectuant une étude comparative avec les RF-chokes et les filtres qui existent dans le commerce, il apparaît que les RF-chokes et les filtres DC-RF compensés présentent de meilleurs performances en termes de largeur de bande et de pertes d'insertion.

Finalement, deux nouvelles architectures de mélangeurs uniplanaires SH équilibrés et à large bande sont proposés et fabriqués sur un substrat d'alumine d'épaisseur 10 mil. Le mélangeur avec plan de masse infini permet d'atteindre des pertes de conversion constantes comprises entre 9.5-11.6 dB dans l'intervalle de fréquence 24-38 GHz . La plage de fréquence pour l'oscillateur local est 12.5-17.5 GHz. L'isolation qui a été mesuré entre les ports est supérieure à 45 dB sur la plupart de la plage de fréquence. En outre, on a une excellente annulation des harmoniques LO/RF non désirés et des produits d'intermodulations. L'autre type de mélangeur uniplanaire SH balancé avec plan de masse fini permet d'obtenir des pertes de conversion comprises entre 9 et 11 dB sur la plage 24-30 GHz avec un LO à 11.5-14.5 GHz. L'isolation entre les ports est d'au moins 40 dB sur une grande largeur de bande. On a également une bonne réjection des harmoniques LO/RF et des pro-

duits d'intermodulations. Avec notre mélangeur SH équilibré à large bande, un translateur de fréquence (Ka-band) peut être envisagé pour une application telle que les terminaux des abonnés LMCS à large bande.

ABSTRACT

Downconverter is a key building block in an LMCS/LMDS receiver front-end module for use in the subscriber terminal (CPE-Custom Promises Equipment). It requires the design of a high-quality and small-size broadband mixer, which is critical for the CPE system architecture. Balanced mixer is known to have some advantageous features over its single-diode counterpart, namely, good RF-to-IF and LO-to-RF isolations, and rejection of AM noise from the LO source and some spurious responses. Subharmonically pumped (SH) mixers present additional advantages when operating with an LO at 1/2 RF signal frequency. This is in particular attractive at millimeter-wave frequency where the cost of LO power budget and excessive LO noise increases rapidly with frequency. Combining the advantages of balanced and subharmonically pumped schemes, we study and design new balanced SH mixers.

Balanced SH mixers are very sensitive to the loading of nonlinear devices at various idler frequencies. At LO, RF and IF the device has a resistive load, but at all other mixing frequencies generated in the nonlinear device it should be loaded by reactive load to avoid power loss. In this work, we present a generic approach, which can be used to estimate the optimum loading conditions at various idler frequencies and also to give the best performance of balanced SH mixers for generic circuit model. This provides designer with a practical guideline for designing such

mixers. As an attempt in validating our approach, we design, on the basis of the microstrip technique, a balanced SH mixer at 14 GHz that was optimized at its $2f_{LO} + f_{RF}$ frequency. The circuit was realized on a 10 mil thick TMM3 substrate. The measured conversion loss is less than 9 dB over the RF frequency range of 13.5-15.5 GHz and 7.2 dB at 14 GHz with the IF frequency of 500 MHz. More than 30 dB isolations between ports are achieved. However, the two additional phase difference lines providing 180^o out-of-phase are frequency dependent while the short circuits through via holes introduce troublesome parasitics at higher frequency.

Uniplanar transmission lines have shown the advantages of easy realization of short-circuited ends, simple mounting of lumped (passive or active) components in shunt or series configuration, free from drilling of holes through the substrate needed to reach the ground plane, and great flexibility of inter-transition among different transmission media. Therefore, some uniplanar building blocks are studied for the broadband design of monolithic and hybrid millimeter-wave integrated circuits.

In the uniplanar scheme, there are generally two types of baluns: Marchand baluns and double-Y baluns. The Marchand baluns provide smaller frequency bandwidth and larger geometry than the double-Y baluns due to the asymmetry induced in the junction and almost quarter-wave length of stubs. The double-Y baluns offer a completely different solution for wideband and small-size baluns in comparison to various Marchand baluns modified to fit into the MMIC chip.

In this work, a general method of design is developed for broadband design for performance improvement of a class of uniplanar double-Y baluns. According to the developed technique, we design two kinds of broadband double-Y baluns on two platforms related to the infinite and finite ground planes: CPW-slotline and CPW_{fgp} structures. They are realized in MHMIC format, respectively. The designed CPW-slotline balun exhibits a rather good performance with a low insertion loss of less than 1 dB and a flat response over 2-3 octave frequency range. Also, the designed CPW_{fgp} balun demonstrates a less than 1.5-dB insertion loss over the DC-to-22 GHz frequency range.

Moreover, a concept of anti-symmetrical CPW modal electrical fields that are "elastically" converged into a circular aperture is applied to the design of RF choke and tapered DC-blocking filters, which is able to reduce the radiation loss of the CPW open stub end. Through a comparative study of the different RF chokes and DC-blocking filters, the compensated RF choke and DC-blocking filter experimentally exhibit a better performance with lower loss and wider bandwidth.

Finally, two new architectures of uniplanar broadband balanced SH mixers with the infinite and finite ground planes are proposed and fabricated on 10-mil thick alumina substrate. The proposed uniplanar balanced SH mixer with infinite ground planes achieves a very flat conversion loss of 9.5-11.6 dB over a wide bandwidth of 24-38 GHz RF driven by a subharmonic LO source of 11.5-18.5 GHz. The measured isolations between ports are higher than 45 dB over most of the RF

range. In addition, it demonstrates excellent suppression of some unwanted LO/RF harmonics and mixing frequency responses. The other type of uniplanar balanced SH mixer with finite ground planes experimentally exhibits a low conversion loss of 9-11 dB over a RF bandwidth of 24-30 GHz by a subharmonic LO source of 11.5-14.5 GHz. The isolations between ports are higher than 40 dB over most of the RF range. Similarly, it also has good suppression of some LO/RF harmonics and spurious responses. With our developed broadband balanced SH mixer, a complete Ka-band downconverter can be expected for broadband LMCS subscriber terminal application.

CONDENSÉ EN FRANÇAIS

Les systèmes de communication à multipoints locaux (Local Multipoint Communication Systems) suscitent un vif intérêt à travers le monde, et aussi bien dans les laboratoires de recherche que dans le monde industriel. Opérant autour de 28 GHz, le LMCS, appelé LMDS aux Etats-Unis, est un système de communication sans fils large bande qui permet d'obtenir des débits de données à grande vitesse sur deux canaux de transmission. Une des applications peut être une transmission en temps réel de la voix/vidéo lors d'une conférence. Bien qu'il y ait plusieurs approches de conception pour le transmetteur LMCS à 28 GHz, l'architecture comprend habituellement un transmetteur, un antenne de réception, un circulateur ou un diplexeur, un filtre à 28 GHz, un contrôle automatique de gain (Automatic Gain Control), un amplificateur faible bruit (Low Noise Amplifier), un amplificateur de puissance, un translateur de fréquences en bande de base, un autre translateur de fréquence en haute fréquence et un filtre pour la fréquence intermédiaire (IF). Il est possible de concevoir des modules de transmetteur basés sur la technologie des circuits intégrés micro-ondes (MIC) ou des circuits intégrés monolithiques micro-ondes (MMIC), bien que cela soit délicat dans cette dernière technologie. A 28 GHz, les fortes pertes ohmiques et pertes par radiation (qui donnent naissance à des interférences) peuvent être à l'origine d'une élévation importante du coût du transmetteur. Toutefois, certains composants imprimés à faible coût et présentant

de bonnes performances peuvent être développés.

Le bloc de transposition de fréquence en bande de base est un élément clé dans les récepteurs LMCS qui sont utilisés dans les terminaux des abonnés (CPE). Ce qui nécessite la conception d'un mélangeur large bande de dimensions réduites et de haute qualité. Le mélangeur balancé est connu pour avoir des caractéristiques plus intéressantes qu'un mélangeur constitué d'une seule diode, comme une bonne isolation entre RF et IF et entre LO (Local Oscillator) et RF, une réjection du bruit AM de l'oscillateur local suppression des produits d'intermodulations non désirés. Les mélangeurs sous-harmoniques SH (Subharmonically) ont d'autres avantages lorsque la fréquence du LO est deux fois plus petite que la fréquence du signal RF. C'est particulièrement intéressant dans les fréquences millimétriques car le coût d'un LO peut être élevé et on sait que le bruit dans un LO augmente rapidement avec la fréquence. Ainsi, un mélangeur SH équilibré devrait être en mesure de combiner les avantages d'un mélangeur SH et d'un mélangeur équilibré si la conception est faite selon une certaine procédure.

Sachant que la caractéristique I/V de la jonction de la diode est approximée par des séries, il est possible de mettre en évidence les caractéristiques des mélangeurs SH équilibrés: la suppression des harmoniques d'ordre pairs pour le signal RF et celui issu du LO, des ordres pairs (m et n sont les ordres impairs pour mf_{RF} et nf_{LO} respectivement) et des ordres impairs (m est pair et n est impair) pour les signaux issus du mélangeur de fréquences. De plus, nous déduisons la topologie que nous

devons adopter pour les mélangeurs SH équilibrés: deux paires de diodes en anti - parallèle, un hybride 180° entre ces dernières et le port LO et un hybride 0° entre le port RF et les paires de diodes.

Une Conception Optimale des Mélangeurs Subharmoniques Balancés

Les mélangeurs SH équilibrés sont très sensibles à la charge d'un composant non-linéaire pour différentes fréquences non désirées. Aux fréquences des signaux RF, LO et IF le composant a une charge résistive, mais pour les fréquences issues des produits d'intermodulations (dus à la non-linéarité des diodes), on doit avoir une charge réactive pour limiter les pertes de puissance. Dans ce travail, nous présentons une approche générique qui peut être utilisée pour approximer les conditions de charge optimale aux fréquences indésirables. D'autre part, nous donnerons les performances optimales qui peuvent être obtenues avec des mélangeurs SH équilibrés. Cela peut constituer une méthode de conception pratique pour les concepteurs de tels mélangeurs. Un modèle générique d'un SH équilibré et amélioré est constitué de deux paires de diodes, d'un réseau à quatre ports idéal et d'un réseau de trois ports idéal. L'optimisation est effectuée sur les valeurs de la phase de S11 et de S33 du réseau à quatre ports aux fréquences non désirées, ce qui permet d'obtenir la condition de charge réactive, car le réseau à trois ports est en parallèle avec les paires de diodes. Ainsi, avec l'aide d'un logiciel de simulations tel que MDS, la méthode originale de conception optimisée est la suivante:

1. Saisir le schéma du circuit avec le logiciel MDS qui permet d'effectuer de simulations d'équilibrage harmonique.

2. Créer les deux réseaux idéaux en choisissant des matrices idéales pour les paramètres de dispersion.

3. Simuler les pertes de conversion du circuit en faisant varier, d'une part, les phases des paramètres S_{11} et de S_{33} aux fréquences non désirées dans un intervalle compris entre 0^o et 360^o, et d'autre part, le niveau de puissance du signal du LO.

4. Afficher les résultats obtenus sous forme de courbes.

5. Déterminer le niveau de puissance approprié pour le LO.

6. Déterminer la charge optimale vue par les diodes aux fréquences indésirables.

7. Concevoir un circuit équivalent à partir des éléments obtenus précédemment.

8. Simuler et optimiser tous les sous-circuits linéaires.

9. Utiliser l'analyse par équilibrage harmonique dans la simulation du circuit global, constitué des sous-circuits linéaires et du circuit non-linéaire, pour s'assurer des bonnes performances.

Dans le but de valider notre méthode nous concevons, en utilisant la technologie des lignes micro-ruban, un mélangeur SH équilibré à 14 GHz. Ce dernier est

optimisé à la fréquence $2f_{LO}+f_{RF}$. Le circuit est réalisé sur le substrat TMM3 d'épaisseur 10 mil. Les pertes de conversion mesurées sont inférieures à 9 dB sur la plage de fréquence 13.5-15.5 GHz et elles sont de 7.2 dB à 14 GHz avec une fréquence intermédiaire de 500 MHz. Plus de 35 dB d'isolations sont obtenus entre les ports dans toute la plage de fréquence. Cependant, l'addition des deux différences de phase des lignes qui donne un déphasage de 180° dépend de la fréquence. En effet, la variation de la longueur d'onde électrique dépend de la fréquence, on ne peut donc pas avoir 180° de déphasage pour toutes les fréquences. De plus les courts-circuits qui sont faits en plaçant des rivets pour faire la connexion avec le plan de masse introduisent des parasites qui perturbent le circuit à haute fréquence.

Des Blocs de Conception Large Bande et Uniplanaires

Les lignes de transmission uniplanaires permettent de réaliser facilement des terminaisons court-circuitées. Il est également aisé de placer des composants (passifs ou actifs) monté en surface dans des configurations séries ou parallèles. De plus, il n'est pas nécessaire de percer le substrat pour atteindre le plan de masse, et il n'est pas difficile de réaliser les transition entre les différentes lignes de transmission uniplanaires. Par conséquent, certains systèmes uniplanaires sont étudiés pour des conceptions de circuits intégrés hybrides monolithiques (MHMIC) à large bande.

Dans la topologie uniplanaire, il y a généralement deux types de transition pour

passer d'une ligne balancée à une ligne non-balancée (cette transition est aussi appelée balun) : Le balun de Marchand et le balun en double Y. Les baluns de Marchand ont une largeur de bande plus étroite et une géométrie plus grande que les baluns double-Y, ceci est dû à l'asymétrie de la jonction et des longueurs des lignes quart d'onde des stubs de longueur $\lambda/4$. Les baluns double Y permettent d'obtenir une topologie large bande fréquentielle, et dont les dimensions géométriques sont compatibles avec leur intégration dans les circuits MMIC (Monolithic Millimeter-wave Integreted Circuit). Dans ce travail, une méthode générale de conception est développée pour des circuits large bande, et ce, dans le but d'améliorer les performances d'un type de balun uniplanaire double Y. La règle proposée est la suivante: Toutes les longueurs électriques des stubs doivent être de 30^o lorsqu'on se trouve dans la partie supérieure de la largeur de bande, et elle doit être au moins deux fois plus grande que la valeur du rayon de la jonction double-Y. Si ces considérations sont prises en compte lors de la conception, de bonnes performances peuvent être obtenues en pratique et sur une large bande de fréquence. Selon la technique développée, nous concevons deux nouvelles versions de baluns double-Y à large bande. La première version sera relative à un plan de masse infini (structure de lignes coplanaires à fente, appelée CPW-slotline) et la seconde sera relative à un plan de masse fini (structure CPW$_{fgp}$-CPS). Les dimensions physiques de chaque balun sont synthétisées dans la partie supérieure de notre bande de fréquence d'intérêt avec les logiciels Momentum et IE3D de Hewlett Packard. Les

baluns double Y ont été réalisés en technologie MHMIC. Le balun CPW-slotline montre de bonnes performances avec des pertes d'insertion inférieures à 1 dB et une réponse fréquentielle plate sur la plage de fréquence comprise entre 2 et 3 octaves. De plus, le balun CPW$_{fgp}$-CPS affiche des pertes d'insertion inférieures à 1.5 dB sur la plage de fréquence DC-22 GHz.

De plus, un circuit ouvert en ligne coplanaire (CPW) est indispensable dans les circuits passifs uniplanaires. Cependant, la conversion du mode et les pertes de puissance, conséquences des radiations et des fuites le long des tronçons des stubs ouverts en lignes coplanaires, peuvent être à l'origine d'une dégradation significative des performances du circuit global. De tels problèmes peuvent en particulier réduire la largeur de bande effective. Dans ce travail, un concept de champs électriques modaux en lignes coplanaires anti - symétriques, qui convergent " élasiquement" dans une ouverture circulaire, est appliqué à la conception d'une RF-choke et de filtres de découplage DC-RF. Ce qui permet de réduire les pertes par radiation du stub ouvert. Un type de RF-choke et filtres de découplage (filtre DC) sont choisis dans le but d'effectuer des comparaisons. Leurs dimensions physiques sont synthétisées à la fréquence centrale de 28 GHz, et en utilisant le logiciel de simulation Momemtum. À travers une étude comparative des différentes RF-chokes et filtres DC, il apparaît que les résultats expérimentaux sur les RF-chokes et filtres DC compenss présentent de meilleures performances avec une plus grande largeur de bande et des pertes plus faibles.

Des Mélangeurs Subharmoniques Balancés Uniplanaires Large Bande

A travers les blocs structurels uniplanaires à large bande, une nouvelle architecture de mélangeur SH équilibré à large bande est proposée. Elle est constituée de deux paires de diodes anti - parallèle (ALPHA DMK2308-000), d'un balun en structure CPW-slotline, d'une jonction-T à fente en fuseau, un diviseur en anneau en structure CPW-to-slotline, en structure CPW on a un filtre de découplage (pour bloquer la composante continue), une RF-choke et un filtre passe-bas. Les trois ports qui sont relatifs au signal RF, IF et au signal issu du LO sont interfacés aux lignes coplanaires d'entrée/sortie. Le balun transforme la ligne débalancé en une ligne balancée pour obtenir une même amplitude mais un déphasage de 180°. Un tel balun combiné avec un hybride assure que le signal RF et le signal issu du LO arrivent en phase aux niveaux de la première paire de diodes et avec un déphasage de 180° avec la deuxième paire de diodes. Grâce aux propriétés de la jonction-T en ligne à fente qui est en série et de la jonction-T en CPW-slotline qui est en parallèle, on a une très bonne isolation entre les ports des signaux RF, IF et du signal issu du LO. La combinaison de la RF-choke compensé et des quatre filtres passe-bas permet, d'une part de minimiser le circuit d'adaptation du port correspondant au signal de fréquence IF, et d'autre part d'éliminer les produits d'intermodulations non désirés générés par les non-linéarités des diodes.

Pour une modélisation correcte du mélangeur dans son ensemble, la structure uniplanaire proposée est décomposée en six blocs distincts, à savoir, le balun

double-Y, l'hybride, le filtrage de la composante continue, la RF-choke, le filtre passe-bas et les deux paires de diodes. Chaque bloc structurel du modèle est déterminé par analyse électromagnétique (EM) de circuit planaire en utilisant les logiciels de simulation Momentum ou IE3D. Les paramètres S EM-simulés décrivent des propriétés des modèles du bloc structurel. Les paires de diodes sont simulées en utilisant, pour chacune d'entres-elles, un modèle non linéaire de diode à jonction PN disponible dans la bibliothèque de composants de HP- MDS. En combinant les modèles équivalents en paramètre-S des cinq blocs structurels, on peut établir un modèle équivalent global pour le mélangeur SH équilibré. Avec ce modèle équivalent, le circuit du mélangeur peut être simulé de manière plus efficace. On utilise pour la simulation l'analyse d'équilibrage harmonique qui est implémentée dans MDS. Si nous considérons les pertes additionnelles de chacun des blocs structurels, nous pouvons nous attendre à obtenir une perte de conversion avec le résultat de simulation.

Le circuit du mélangeur proposé est réalisé sur un substrat d'alumine d'épaisseur 10mil. Les pertes de conversion sont comprises entre 9-11 dB, elles sont donc quasi-constante sur toute la largeur de bande 26-36 GHz. La plage de fréquence pour le signal issu du LO est 12.5-17.5 GHz. L'isolation mesurée entre les ports est supérieure à 50 dB sur une grande partie de la plage de fréquence. A partir de la topologie proposée du mélangeur, nous avons apporté des modifications sur un balun, sur le bloc de découplage et sur les filtres passe-bas. Ainsi, nous avons

obtenu une plus grande largeur de bande pour le mélangeur SH équilibré. La variation des pertes de conversion mesurée est très faible et comprise entre 9.5 à 11.7 dBm sur une largeur de bande RF 24-38 GHz. L'isolation entre les ports est supérieure à 45 dB sur presque toute la plage de fréquence RF. Le niveau de puissance aux fréquences $4f_{LO}$-$2f_{RF}$ et $2f_{LO}$ est au-dessous du niveau de bruit de notre HP analyseur de spectre. Néanmoins, on peut facilement affirmer que notre topologie de mélangeur présente des avantages indiscutables quant à l'annulation des harmoniques d'ordre pairs et des produits d'intermodulations non désirés.

Des Mélangeurs Balancés Uniplanaires avec des Plans de Masse Finis

Les mélangeurs proposés ci-dessus ont été ralisés à partir de lignes coplanaires et de lignes à fentes. Ils peuvent être considérés comme un mélangeur SH équilibré uniplanaire avec des plans de masse infinis. Cependant, un autre genre de ligne de transmission coplanaire (CPW), à ruban coplanaire (CPS), est aussi utilisé dans la réalisation des circuits uniplanaires pour réduire l'encombrement et donc rendre les circuits plus compacts. Par extension, la technique de conception du mélangeur SH équilibré à partir de balun double-Y avec une structure CPW_{fpg}-CPS, nous proposons une nouvelle topologie de mélangeur SH équilibré qui est réalisé à partir de lignes en CPW_{fgp}-CPS. Il peut être vu comme un mélangeur SH équilibré uniplanaire avec des plans de masse finis. Le mélangeur est constitué de deux diodes en anti-parallèle (ALPHA DMK2308-000), un balun avec structure CPW_{fpg}-CPS, d'une jonction-T CPS en fuseau, d'un diviseur en anneau en structure CPW_{fpg} vers

CPS en fuseau, et en structure CPW$_{fpg}$, d'un filtre de découplage, d'une RF-choke et d'un filtre passe-bas. Les trois ports relatifs aux signaux de fréquences RF, IF et celui issu du LO sont interfacés avec les lignes d'entrée/sortie CPW$_{fpg}$. Puisque les caractéristiques de la structure CPW$_{fpg}$ sont proches de celles utilisant la structure CPS lorsque $c/b > 3$, l'approche de conception en CPW du filtre de découplage, de la RF-choke et du filtre passe-bas qui constitue le mélangeur SH équilibré avec les plans de masse infinis précédemment proposé, peut être directement appliquée à la structure CPW$_{fgp}$ dans le cas d'un mélangeur SH équilibré avec des plans de masse finis. Le circuit du mélangeur proposé est réalisé sur un substrat d'alumine d'épaisseur 10-mil. Il permet d'obtenir une perte de conversion comprise entre 10 et 12 dB (donc quasi-constante) sur une largeur de bande RF de 24-30 GHz. La plage de fréquence pour le signal issu du LO est 11.5-14.5 GHz. L'isolation mesurée entre les ports est supérieure à 40 dB. De la même façon qu'avec le mélangeur SH équilibré avec des plans de masse finis semblable au mélangeur SH équilibré avec des plans de masse infinis, le mélangeur a également une bonne annulation des harmoniques d'ordre pair et des produits d'intermodulations non désirés. Le mélangeur proposé avec des plans de masse finis a de bonnes performances pour une largeur de bande étroite. Ceci est peut être dû à des discontinuités significatives dans l'anneau en structure CPS et dans la jonction-T en structure CPW$_{fpg}$-CPS.

Évidemment, nous réalisons deux circuits de mélangeurs SH équilibrés qui peuvent présenter de différences de fabrication. La différence réside dans la jonction-T

du diviseur en anneau. Dans la première topologie, la connexion entre les structures CPS et CPW_{fpg} se fait en amenant le conducteur central de la ligne CPW_{fpg} à la ligne CPS. Dans la deuxième topologie, les bandes des deux lignes de transmission sont connectées l'une à l'autre en utilisant du ruban métallique. En comparant les mesures des deux topologies, on peut voir leurs pertes de conversion sont différentes et la dernière topologie a de meilleures performances. Cependant, l'isolation entre les différents ports du dernier mélangeur est moins bonne que dans le cas du premier mélangeur: ce qui tend à prouver que l'inductance du conducteur compense la discontinuité de la jonction-T en structure CPW_{fpg}-CPS dans les hautes fréquences et améliore le couplage entre le mode à fente et le mode CPW.

TABLE OF CONTENTS

LIST OF FIGURES

LIST OF TABLES

LIST OF ANNEXES

LIST OF ABBREVIATION

AC(ac)	Alternating Current
AGC	Automatic Gain Control
AM	Amplitude Modulation
BPF	Bandpass Filter
CPE	Customer Premises Equipment
CPS	Coplanar Strip
CPW	Coplanar Waveguide
CPW_{fgp}	Coplanar Waveguide with Finite Ground Planes
DC(dc)	Direct Current
DSP	Digital Signal Processing
EM	Electromagnetic
FET	Field Effect Transistor
HEMT	High Electron Mobility Transistor
IF	Intermediate Frequency
IC	Integrated Circuit
LANs	Local Area Network
LMCS	Local Multipoint Communication Systems
LMDS	Local Multipoint Distribution Service
LNA	Low Noise Amplifier

LO	Local Oscillator
LPF	Low-pass Filter
MIC	Microwave Integrated Circuit
MHMIC	Miniature Hybrid Microwave Integrated Circuit
MMIC	Monolithic Microwave Integrated Circuit
OES	Open-end-series
RF	Radio Frequency
SES	Short-end-series
SH mixer	Subharmonically Pumped Mixer
VSWR	Voltage Standing-wave ratio
WLLs	Wireless Local Loops

LIST OF NOTATION

a_{RF}	Incident wave of RF signal
a_{LO}	Incident wave of LO signal
b_{RF}	Reflected wave of RF signal
b_{LO}	Reflected wave of LO signal
C_{j0}	Zero-voltage junction capacitance
C(V)	Nonlinear junction capacitance
$\mathcal{F}$	Fourier-transforming
$\mathcal{F}^{-1}$	Inverse Fourier-transforming
f	Frequency
g(V)	Junction conductance
I	Current matrix
i	Small signal current
I_0	Reverse saturation current
K	Boltzmann's constant (1.37×10^{-23} j/K)
P	Power
q	Electron charge (1.6×10^{-19})
Q	Charge variable
R_s	Linear series resistance
S	Scattering parameter

$\tilde{R}$	Normalized resistance
v	Small signal voltage
$\mathbf{V}$	Voltage matrix
X	Reactance variable
$\tilde{X}$	Normalized reactance
R	Resistance variable
$\tilde{R}$	Normalized resistance
$\mathbf{Z}$	Impedance matrix
Z_0	Characteristic impedance
$\tilde{Z}_0$	Normalized characteristic impedance
η	Ideality factor
o_{bi}	Junction's built-in voltage
γ	Exponent in diode junction capacitance equation
λ_g	Waveguide wave-length
ω	Pulsation: $\omega = 2\pi f$

INTRODUCTION

LMCS (Local Multipoint Communication Systems), as a truly advanced wireless application has attracted enormous attention from academic research and industrial development communities around the world. Operating around 28 GHz (the conventional lowest end of millimeter-wave frequency band), LMCS (known also as LMDS in the United Sates) is a wireless broadband technology capable of providing high-speed two-way interactive data transmission, voice/video conferencing and real-time video-on-demand [1,2]. It promises to be the fundamental platform of universal multimedia wireless systems for the next generation of the information highway, offering high-quality diverse wireless service in the local information distribution markets traditionally monopolized by cable or telephone companies. LMCS technology operates through a local transceiver base station that beams signals to and receives signals from subscribers within a few kilometers.

It is generally believed for the next decades that wireless technologies will be more suitable for personal or home-based information transmission than wireline systems and in particular millimeter-wave wireless systems provide a unique ability to cope with these commercial applications usually requiring low installment cost, high transmission capacity, fast deployment time to markets and excellent upgrade flexibility [3]. The LMCS is in particular of interest for use as a complementary platform with respect to existing and planned satellite and broadband long-haul

optical cable systems.

Millimeter-wave transmission [4], unlike the RF and microwave characteristics, presents some interesting features for short-haul high-speed data links, wireless LANs/WLLs (local area networks/wireless local loops), cloud-profiling/weather monitoring and imaging radar as well as collision avoidance sensor applications [5]. These features include easy frequency re-use, line-of-sight signal path, and high-resolution. Millimeter-wave technologies were considered to be intimately associated with military applications for which small-quantity and high-cost system or subsystems are usually designed and made. These technologies are not suitable for low-cost high-volume LMCS applications. The effective deployment of LMCS presents a very challenging issue related to the design of a transceiver for base-station and subscriber terminal or CPE (customer premises equipment). Usually, a primary consideration in the overall LMCS transceiver design (for both base-station and subscriber terminal) should be directed to its 28 GHz front-end module which is essentially responsible for the signal integrity and overall transceiver performance as well as the complete system cost. The DSP (digital signal processing) unit is also considered as an important building block. Nevertheless, this part of LMCS design work is more or less related to the baseband.

Although there are a number of design approaches available for system architecture, the LMCS 28-GHz transceiver front-end module [6] usually consists of transmitter and receiver antenna, circulator or diplexer, 28 GHz filter, AGC (au-

tomatic gain control), LNA (low noise amplifier), power amplifier, downconverter and up-converter and intermediate frequency (IF) filter. It is possible to design a MIC- or MMIC-based transceiver front-end chip, which presents, however, some challenging issues. At 28 GHz, high ohmic and potential radiation losses (converted into interference) may cause serious problem in the power budget planning that in turn contributes to the cost of transceiver and cell design. In order to cope with stringent LMCS requirement, some low-cost and high-performance printed components should be developed.

The downconverter is the key building block in an LMCS receiver front-end for use in the subscriber terminal. It requires the design of a high-quality and small-size broadband mixer, which is used to convert the received signal to the intermediate frequency, and it could be then amplified with good selectivity, high gain, and low noise, and finally demodulated.

CHAPTER 1

REVIEW OF THE FUNDAMENTALS

Before starting our research project, it is important to make clear what kind of mixer circuit is to be developed in order to match the requirements of LMCS application as well as to understand its analysis fundamentals.

1.1 Mixers

A mixer, or frequency converter, has the prime function of converting a signal from one frequency to another with low loss of the signal and low noise performance degradation. It consists of a 'pump' and a network containing a non-linear device with one or more non-linear elements together with a means to extract the required output signal. The output signal is formed by the fundamental or a harmonic component of the pump mixing with the RF or IF signal. The non-linear device can be a non-linear passive element or a non-linear current or voltage generator. The former is a non-linear resistor, capacitor or inductor or a combination of these such as found in a Schottky diode. The latter is the transconductance, g_m, of a FET which varies as a function of gate bias.

Single FETs or diodes can be used as mixers. However, the mixer designs sometimes use combinations of two, four, or even eight devices in a balanced structure.

Balanced mixers have unparalleled performance advantages compared to single-device mixers. One of these advantages is that the LO and RF are inherently isolated. A balanced mixer also rejects the AM noise from the LO source, and suppresses some spurious responses. The amount of the rejection depends on practical aspects of the circuit design, but in most cases it is prone to at least 10 to 20 dB. The rejection takes place because of the phase relationships of the voltage in the circuit, and it does not require any filtering.

Balanced mixers are loosely divided into two classes called single balanced mixers and double balanced mixers. Single balanced mixers usually use two devices, and are usually realized as two single-device mixers connected by a 180- or 90-degree hybrid. Double balanced mixer usually consists of four untuned devices interconnected by multiple hybrids, transformers, or baluns. They are usually too complicated to allow for individual tuning of the devices, so they may have higher conversion loss than a single-device or a single balanced mixer, but the absence of tuning elements, combined with broadband hybrids, often enable such mixers to have very wide bandwidths.

Unlike diodes, FETs cannot be "reversed"; the consequence of this rather obvious characteristic is that balanced FET mixers often require IF hybrids, while diode mixers do not. For such a reason, balanced mixers--especially double balanced mixers--are more difficult to realize with FETs than with diodes. This situation is especially true for hybrid integrated circuits, where the parasitics associated with

interconnections of several FETs limit the mixer's performance. Balanced FET mixers are somewhat more practical in MMICs, but their high-frequency performance is often unspectacular. Of course, FET mixers have a major advantage over diode mixers: providing several decibels of conversion gain. So far, most of balanced mixers for millimeter-wave practical applications are developed with Schottky diodes.

In the past, point-contact diodes, which consist of a pointed-wire contact to a bulk semiconductor, were used extensively in microwave mixers. However, the mechanical contact procedure for this type of diodes is rather difficult and the reproducibility of the characteristics of the contact is poor. The work reported in[7] was stimulated by recent developments in the fabrication of high-quality, low-capacitance planar integrated Schottky-Barrier diodes [8-10]. Schottky-barrier diodes are superior to point-contact diodes because they are fabricated photolithographically on an epitaxial substrate. This type of fabrication results in lower junction capacitance and series resistance, and a better I/V characteristic. The planar Schottky-Barrier diodes show a good reproducibility of their characteristic parameters and they can easily be mounted on a printed circuit.

Figure 1.1 shows the most commonly encountered realizations of three types of mixer. Figure 1.1(a) shows a single-diode mixer with the RF, LO and IF separated by filters. Figure 1.1(b) shows a single balanced mixer, realized with a transformer hybrid, although a different type of 180° hybrids may be used. The ring mixer in

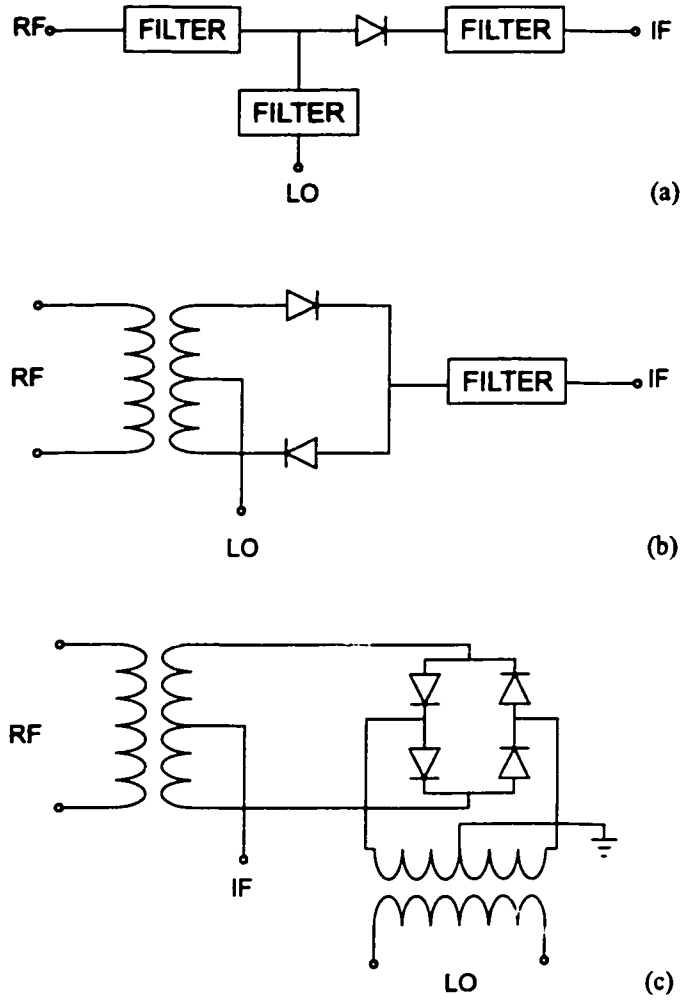

Figure 1.1 The most common forms of three types of mixer: (a) single-diode: (b) single balanced; (c) double balanced.

Figure 1.1(c) is a classical realization of the double balanced mixer.

For many applications, it is expensive, inconvenient, or even impossible to design a fundamental frequency LO that has required frequency stability at millimeter frequency. The conversion loss and noise performance of a millimeter-wave mixer may be limited by the lack of adequate LO power or by excessive LO noise, rather than by the inherent features of the mixer. In these cases, it may be appropriate

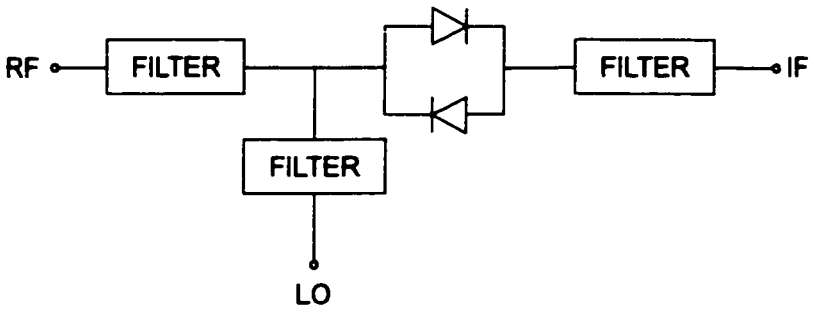

Figure 1.2 A basic form of SH mixer.

to use a mixer that is pumped at half the RF frequency. Such subharmonically pumped mixers (SH mixers) have adequate conversion performance, often only a decibel or two less than a comparable fundamental mixer. Even with a greater conversion loss, the SH mixer often provides the best possible performance when all these factors, especially LO noise and power, are considered.

Figure 1.2 shows a basic realization of the SH mixer. Similar to a single-device mixer (shown in Figure 1.1(a)), the RF, LO and IF are separated by filters. However, since the RF and LO frequencies differ by approximately a factor of two, the filters are rarely difficult to realize.

In millimeter-wave receiver applications, the lowest possible conversion loss may not be required but a minimum LO power leakage at the RF port, less spurious responses and low noise as well as less demand on the LO source are demanded. Combining the advantages of balanced and subharmonically pumped mixer schemes, our objective is to study and design a new class of balanced SH mixer for LMCS practical implementations.

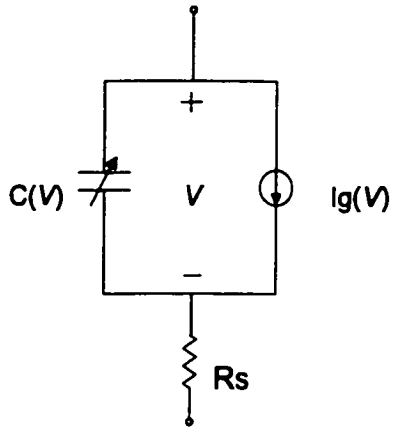

Figure 1.3 Equivalent circuit of the Schottky-barrier diode.

1.2 The Diode Model

The equivalent circuit representation of a Schottky-barrier diode[11], including nonlinear junction capacitance $C(V')$ and fixed linear series resistance R_S is shown in Figure 1.3. The junction I/V characteristics are given by :

$$I_g(V') = I_0(\exp(\frac{qV'}{\eta KT}) - 1) \tag{1.1}$$

and the small-signal junction conductance $g(V')$ is given by:

$$g(V') = \frac{dI_g(V')}{dV'} = \frac{qI_0}{\eta KT} exp(\frac{qV'}{\eta KT}) - 1) \tag{1.2}$$

where I_0 is the reverse saturation current, q is the electron charge (1.6×10^{-19} coul), V' is the junction voltage (not including the voltage drop across the series resistance R_s), η is the ideality factor (usually less than 1.25), K is the Boltzmann's constant

(1.37×10^{-23} J/K), and T is the absolute temperature. The junction capacitance $C(V)$ is known as:

$$C(V) = \frac{C_{j0}}{(1 - \frac{V}{\phi_{bi}})^{\gamma}} \tag{1.3}$$

where C_{j0} is the zero-voltage junction capacitance and ϕ_{bi} is the junction's built-in voltage. The exponent $\gamma = 0.5$ when the diode's expitaxial layer is uniformly doped: if the doping is not uniform, the exponent may deviate somewhat from this value.

Regarding the voltage and current relations for the nonlinear capacitance under large-signal and small-signal excitations, the capacitance is defined as incremental change in depletion-region charge Q in the large-signal analysis. Then, we write:

$$C(V) = \frac{dQ}{dV} \tag{1.4}$$

$$\begin{aligned} I_c(t) &= \frac{dQ_d}{dt} = \left.\frac{dQ_d}{dV}\right|_{V=V(t)} \frac{dV(t)}{dt} \\ &= C(V(t))\frac{dV(t)}{dt} \end{aligned} \tag{1.5}$$

where $V(t)$ is the large-signal junction voltage. In the small-signal analysis, however, the capacitor is not treated as a nonlinear element, but as a linear, time-

varying capacitance. Therefore, $C(t)$ can be written:

$$C(t) = C(V(t)) \tag{1.6}$$

and,

$$\begin{aligned} i_c(t) &= \frac{d}{dt}[C(t)v(t)] \\ &= C(t)\frac{dv(t)}{dt} + v(t)\frac{dC(t)}{dt} \end{aligned} \tag{1.7}$$

where $v(t)$ is the small-signal junction voltage. Equation (1.5) is used in the large-signal analysis, and (1.7) is used in the small-signal analysis.

1.3 Harmonic Balance Analysis

The goal of the large-signal analysis is to determine the control voltage of the junction conductance and capacitance, $V(t)$(or its Fourier components $V_j(n\omega_p)$). Once $V(t)$ is known, it is substituted into Equations (1.2) and (1.7) in order to determine the time-varying conductance and capacitance waveforms. They are subsequently used to determine the conversion loss and input or output impedances [12].

Figure 1.4 shows a general nonlinear circuit, consisting of nonlinear solid-state devices that are connected to a load and source of a large-signal excitation. In

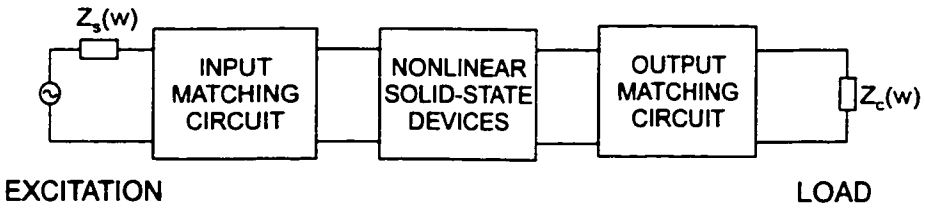

Figure 1.4 Equivalent circuit of a general nonlinear two-port microwave component.

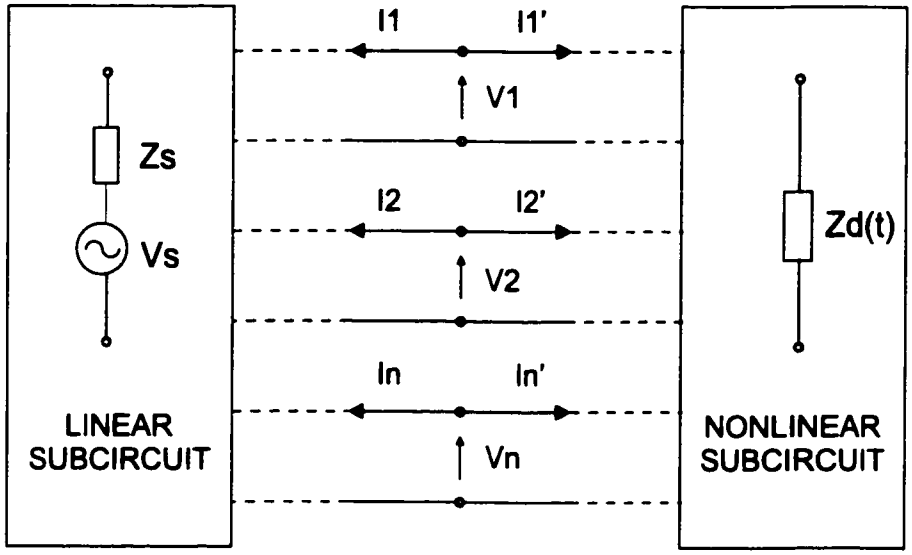

Figure 1.5 A nonlinear microwave circuit, divided into linear and nonlinear subcircuits.

order to use multiport circuit theory, we can simplify at least part of the circuit by lumping all the linear reactances, impedances, transmission lines, and other linear elements into a single matrix of limited size. By describing the linear part of the circuit as one multiport, it needs be evaluated only once for each harmonic, with the results stored as matrices, and no further evaluation is necessary. The circuit elements in Figure 1.4 can be regrouped as shown in Figure 1.5, so that they form a linear subcircuit and a nonlinear subcircuit.

The linear subcircuit can be treated as a multiport and described by its Z-, Y-, S-parameters, or some other multiport matrix. The nonlinear subcircuit is modelled by their nonlinear junction I/V characteristics and must be analyzed in the time domain [11]. The voltages and currents at each port can be expressed in the time or frequency domain. Because of the nonlinearity involved, the port voltages and currents must have frequency components at harmonics related to the fundamental signal. Although in theory an infinite number of harmonics exists at each port, it is adequately considered that the DC component and the first K harmonics (i.e., $k = 0, 1, \ldots, K$) describe all the voltages and currents. Consequently all higher harmonics can be ignored. The linear subcircuit is described in the frequency domain by Z parameters:

$$\mathbf{Z_{m,n}} = \mathbf{diag}[\mathbf{Z_{m,n}(k\omega_p)}], \qquad k = 0, 1, \ldots, K \tag{1.8}$$

that is,

$$\mathbf{Z_{m,n}} = \begin{bmatrix} Z_{m,n}(0) & 0 & \cdots & 0 \\ 0 & Z_{m,n}(\omega_p) & \cdots & 0 \\ \vdots & & & \vdots \\ 0 & 0 & \cdots & Z_{m,n}(K\omega_p) \end{bmatrix} \tag{1.9}$$

The port-voltage **V** and -current **I** between the linear subcircuit and the non-

linear subcircuit must be satisfied by Kirchhoff's law:

$$\mathbf{V} = (\mathbf{Z} + \mathbf{Z}'_{\mathbf{s}})_{\mathbf{N}\times\mathbf{N}} \times \mathbf{I} + \mathbf{V}'_{\mathbf{s}} \tag{1.10}$$

where

$$\mathbf{Z}'_s = \begin{bmatrix} Z'_s & 0 & \cdots & 0 \\ 0 & Z'_s(\omega_p) & \cdots & 0 \\ \vdots & & & \vdots \\ 0 & 0 & \cdots & 0 \end{bmatrix} \tag{1.11}$$

$$\mathbf{V} = \begin{bmatrix} \mathbf{V}_1 & \mathbf{V}_2 & \mathbf{V}_3 & \cdots & \mathbf{V}_N \end{bmatrix} \tag{1.12}$$

$$\mathbf{I} = \begin{bmatrix} \mathbf{I}_1 & \mathbf{I}_2 & \mathbf{I}_3 & \cdots & \mathbf{I}_N \end{bmatrix} \tag{1.13}$$

$$\mathbf{V}'_s = \begin{bmatrix} V'_s & V'_s(\omega_p) & 0 & \cdots & 0 \end{bmatrix} \tag{1.14}$$

where $V'_s(\omega_p)$ and $Z'_s(\omega_p)$ are the equivalent source voltage and impedance respectively. Z'_s and V'_s are the equivalent dc voltage and impedance respectively. If

there are harmonic components of excitation, Equations (1.11) and (1.14) should be given by $V_s'(k\omega_p)$ and $Z_s'(k\omega_p)$, respectively.

The nonlinear element voltages can result from nonlinear capacitors and conductors. Inverse-Fourier-transforming the voltages at each port yields the time-domain voltage waveforms at each port: $\mathcal{F}^{-1}\{\mathbf{V}\} \longrightarrow V(t)$. Therefore, the time-varying characteristics can be determined by $I_g(t) = f_g(V(t))$ and $I_c(t) = \frac{dQ_d(t)}{dt}$ $(Q_d(t) = f_c(V(t)))$.

Fourier-transforming these quantities gives rise to $\mathcal{F}\{I_g(t)\} \longrightarrow \mathbf{I}_g$ and $\mathcal{F}\{I_c(t)\} \longrightarrow \mathbf{I}_c$. From Figure 1.3, $\mathbf{I}'$ is given by:

$$\mathbf{I}' = \left[\begin{array}{cccc} (\mathbf{I}_{g,1} + \mathbf{I}_{c,1}) & (\mathbf{I}_{g,2} + \mathbf{I}_{c,2}) & \cdots & (\mathbf{I}_{g,N} + \mathbf{I}_{c,N}) \end{array} \right] \tag{1.15}$$

and using Kirchhoff's current law, we can obtain in the frequency domain:

$$\mathbf{I} + \mathbf{I}' = 0 \tag{1.16}$$

Substituting Equation (1.15) into (1.10) leads to the expression:

$$\mathbf{V} = -(\mathbf{Z} + \mathbf{Z}_s')(\mathbf{I}_g + \mathbf{I}_c) + \mathbf{V}_s' \tag{1.17}$$

or,

$$F(\mathbf{V}) = \mathbf{V} + (\mathbf{Z} + \mathbf{Z}'_s)(\mathbf{I}_g + \mathbf{I}_c) - \mathbf{V}'_s = \mathbf{0} \tag{1.18}$$

Equation (1.18) is called the harmonic-balance equation. A number of methods to solve this equation have been proposed[12]. There are Optimization, Splitting Algorithm, Reflection Algorithm and Newton's Method. All these methods have the following common procedures: a time-domain voltage is first estimated, and the junction current is then calculated from the diode equations; and a frequency-domain solution is found; testing whether the voltage is estimated correctly, the voltage can be modified and tested again if not. The modification process will cause the voltage to converge to a solution after a number of iterations.

The whole harmonic balance analysis is available in some commercial software packages, such as HP's MDS. As a result, in our work the harmonic balance simulator in MDS is used when dealing with nonlinear analysis.

CHAPTER 2

OPTIMUM DESIGN OF BALANCED SUBHARMONICALLY PUMPED MIXERS

2.1 Introduction

Subharmonically pumped (SH) mixer is very useful at millimeter wave frequencies with its advantages of subharmonic pumping and inherent local oscillator (LO) AM noise suppression [13,14], both alleviating the demand for the LO source. Several authors have demonstrated the attractiveness of SH mixer performance [15-17]. Balanced mixer is also widely used due to its better power-handling capability and rejection of certain spurious signals as well as enhancement of inherent LO-to-RF isolation [11]. Balanced SH mixer essentially shares the common advantages with SH mixers and balanced mixers. For this kind of mixers, little work has been reported to date [18].

In a balanced SH mixer, the mixing action is performed between the radio frequency (RF) or the intermediate frequency (IF) signals and one of the harmonics of the LO. Thus, the nonlinear device performs both mixing and multiplication. Usually, the conversion loss of such mixers is higher than the fundamental harmonic counterpart. However, a careful design can yield comparable performance. Balanced SH mixers are very sensitive to the loading condition of the nonlinear

device at various idler frequencies. At the LO, RF and IF frequencies, the device has resistive loads, but at all other mixing frequencies generated in the nonlinear device it would be better to use reactive loads to avoid any power loss that in turn contributes to the conversion loss of such mixers.

In this chapter, we will at first theoretically prove the inherent features of balanced SH mixers under the condition of the adequate excitation of the LO and RF signals. Then, we present a generic approach to optimizing the design of balanced SH mixers in determining reactive loads of nonlinear devices at various idlers. Through this method, a design guideline is generated with some ideal networks with a generic mixer circuit representation. Finally we validate our proposed approach with a design example of 13.5-15.5 GHz balanced SH mixer. Our proposed method for the optimum design of balanced SH mixers has already been presented in [19].

2.2 The Features of Balanced SH Mixers

A balanced SH mixer must share the common advantages with balanced mixers and SH mixers. In order to extract the inherent features of balanced SH mixers, we approximate the diode junction's I/V characteristic by power series[11] and derive useful results.

In Figure 2.1(a), the relation between the current and voltage is defined by:

$$i_1 = a_1 v_1 + a_2 v_1^2 + a_3 v_1^3 + a_4 v_1^4 + \cdots. \tag{2.1}$$

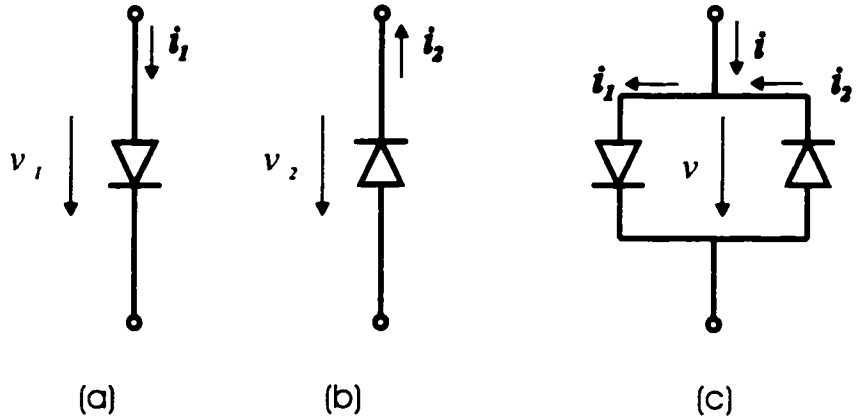

Figure 2.1 Currents and voltages in diodes.

where v_1 is the total ac voltage across the diode (the RF plus the LO voltage), i_1 is the current, and a_i (i=1,2,$\cdots$) is constant. If the diode is reversed, as shown in Figure 2.1(b), only the applied voltage is reversed so the signs of the odd-power terms become negative:

$$i_2 = -a_1 v_2 + a_2 v_2^2 - a_3 v_2^3 + a_4 v_2^4 - \cdots. \tag{2.2}$$

From Figure 2.1(c), the i current of an anti-parallel diode pair is given by:

$$i = i_1 - i_2 = 2a_1 v + 2a_3 v^3 + 2a_5 v^5 + \cdots, \tag{2.3}$$

where v is the total ac voltage across the diode pair.

Currents and voltages in the diode pairs of a balanced SH mixer are shown in Figure 2.2, where v_1 and v_2 are ac voltages applied to the two diode pairs

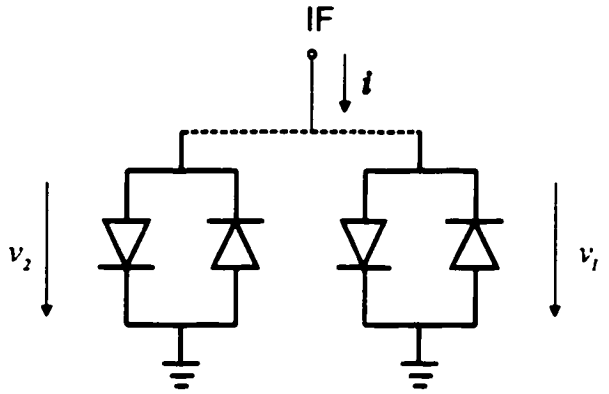

Figure 2.2 Currents and voltages in the two diode pairs of an 180-deg balanced mixer.

respectively. The i current is

$$i = a_1(v_1 + v_2) + a_3(v_1^3 + v_2^3) + a_5(v_1^5 + v_2^5) + \cdots, \tag{2.4}$$

Considering the LO and RF applied by 180° out-of-phase and in-phase, respectively,

$$v_1 = -V_{LO}\cos(\omega_{LO}t) + V_{RF}\cos(\omega_{RF}t), \tag{2.5}$$

and,

$$v_2 = V_{LO}\cos(\omega_{LO}t) + V_{RF}\cos(\omega_{RF}t), \tag{2.6}$$

where V_{LO} and V_{RF} are the magnitudes of LO and RF signals, ω_{LO} and ω_{RF} are the frequencies of LO and RF signals, respectively.

Substituting Equations (2.5) and (2.6) into (2.4),

$$
\begin{aligned}
i &= a_1\{[-V_{LO}\cos(\omega_{LO}t) + V_{RF}\cos(\omega_{RF}t)] + [V_{LO}\cos(\omega_{LO}t) \\
&\quad + V_{RF}\cos(\omega_{RF}t)]\} + a_3\{[-V_{LO}\cos(\omega_{LO}t) + V_{RF}\cos(\omega_{RF}t)]^3 \\
&\quad + [V_{LO}\cos(\omega_{LO}t) + V_{RF}\cos(\omega_{RF}t)]^3\} + a_5\{[-V_{LO}\cos(\omega_{LO}t) \\
&\quad + V_{RF}\cos(\omega_{RF}t)]^5 + [V_{LO}\cos(\omega_{LO}t) + V_{RF}\cos(\omega_{RF}t)]^5\} \\
&\quad + \cdots. \\
&= \underbrace{[a_1 2V_{RF} + a_3(3/2V_{RF}^3 + 3V_{RF}V_{LO}^2)]\cos(\omega_{RF}t)}_{Signal} \\
&\quad + \underbrace{a_3 1/2V_{RF}^3\cos(3\omega_{RF}t)}_{Signal-third-harmonic} \\
&\quad + \underbrace{a_3 3/2V_{RF}V_{LO}^2\cos[(\omega_{RF} - 2\omega_{LO})t]}_{Difference-or-intermediate-frequency} \\
&\quad + \underbrace{a_3 3/2V_{RF}V_{LO}^2\cos[(\omega_{RF} + 2\omega_{LO})t]}_{Sum-frequency} + \cdots. \qquad (2.7)
\end{aligned}
$$

From the above equations, if the mixing frequency is expressed by $mf_{RF}+nf_{LO}$, we can conclude the features of the balanced SH mixers in which the two diode pairs are excited by the out-of-phase LO and in-phase RF signals:

- kth-order responses arise only from the terms of the kth power in (2.3).
- All even-order spurious responses are eliminated.
- All (m,n) spurious responses are eliminated if m is even and n is odd, but not if m is odd and n is even.

Interchanging the LO and RF ports, namely, the LO and RF applied with in-phase and 180° out-of-phase, respectively,

$$v_1 = V_{LO}\cos(\omega_{LO}t) + V_{RF}\cos(\omega_{RF}t), \tag{2.8}$$

and,

$$v_2 = V_{LO}\cos(\omega_{LO}t) - V_{RF}\cos(\omega_{RF}t), \tag{2.9}$$

another equation quite different from Equation (2.7) is

$$\begin{aligned} i &= a_1\{[-V_{RF}\cos(\omega_{RF}t) + V_{LO}\cos(\omega_{LO}t)] + [V_{RF}\cos(\omega_{RF}t) \\ &\quad + V_{LO}\cos(\omega_{LO}t)]\} + a_3\{[-V_{RF}\cos(\omega_{RF}t) + V_{LO}\cos(\omega_{LO}t)]^3 \\ &\quad + [V_{RF}\cos(\omega_{RF}t) + V_{LO}\cos(\omega_{LO}t)]^3\} + a_5\{[-V_{RF}\cos(\omega_{RF}t) \\ &\quad + V_{LO}\cos(\omega_{LO}t)]^5 + [V_{RF}\cos(\omega_{RF}t) + V_{LO}\cos(\omega_{LO}t)]^5\} \\ &\quad + \cdots. \\ &= [a_1 2V_{LO} + a_3(3/2V_{LO}^3 + 3V_{LO}V_{RF}^2)]\cos(\omega_{LO}t) \\ &\quad + a_3 1/2V_{LO}^3\cos(3\omega_{LO}t) \\ &\quad + a_3 3/2V_{LO}V_{RF}^2\cos[(\omega_{LO} - 2\omega_{RF})t] \\ &\quad + a_3 3/2V_{LO}V_{RF}^2\cos[(\omega_{LO} + 2\omega_{RF})t] + \cdots. \end{aligned} \tag{2.10}$$

From Equation (2.10), it can be seen that it is impossible to realize a balanced SH mixer in which the two anti-parallel diode pairs are excited by the in-phase LO and out-of-phase RF signals.

The features of balanced SH mixers are derived with some ideal conditions where the balanced SH mixer circuit has the same magnitude and phase of the RF signal, and same magnitude and opposite phase of the LO signal, and when two pairs of diodes are identical. Also, it is important to note that if the two diodes forming one diode pair are not identical, this unbalancing causes circulating currents in the diode pair in question, and in that case all of mixing frequencies should exist. However, by using a monolithic diode pair, the effect becomes minimal.

2.3 A Novel Generic Approach

A generic circuit model of a balanced SH mixer is shown in Figure 2.3. The mixer incorporates two diode pairs, one ideal four-port network (0-DEG HYBRID) and one ideal three-port network (180-DEG HYBRID). Each diode pair consists of two Schottky anti-parallel diodes. The four-port circuit supplies equal magnitude and phase of RF signal, whereas the three-port circuit supplies equal magnitude and opposite phase of LO signal. All ideal networks are presented by S parameter matrices as follows:

1. Three-port network

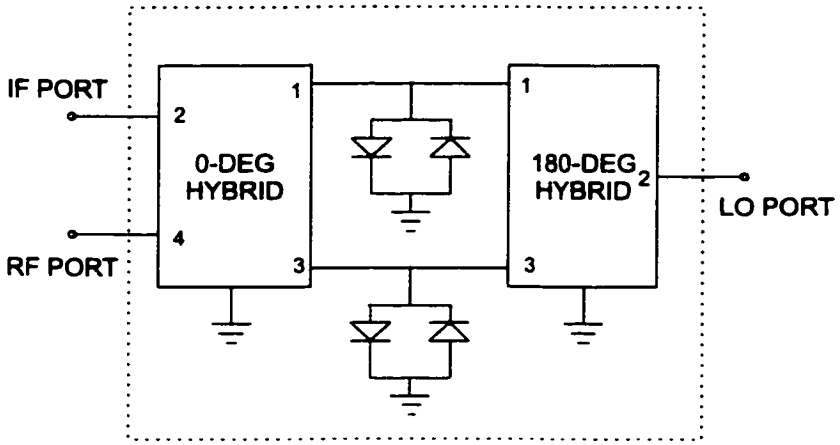

Figure 2.3 A generic circuit of a 180-deg balanced SH mixer.

at the LO frequency,

$$\mathbf{S} = \begin{bmatrix} 0 & 0.707 & 0 \\ 0.707 & 0 & -0.707 \\ 0 & -0.707 & 0 \end{bmatrix} \tag{2.11}$$

at other frequencies.

$$\mathbf{S} = \begin{bmatrix} 1 & 0 & 0 \\ 0 & 1 & 0 \\ 0 & 0 & 1 \end{bmatrix} \tag{2.12}$$

2. Four-port network

at the RF frequency.

$$\mathbf{S} = \begin{bmatrix} 0 & 0 & 0 & 0.707 \\ 0 & 0 & 0 & 0 \\ 0 & 0 & 0 & 0.707 \\ 0.707 & 0 & 0.707 & 0 \end{bmatrix} \tag{2.13}$$

at the IF frequency.

$$\mathbf{S} = \begin{bmatrix} 0 & 0.707 & 0 & 0 \\ 0.707 & 0 & 0.707 & 0 \\ 0 & 0.707 & 0 & 0 \\ 0 & 0 & 0 & 0 \end{bmatrix} \tag{2.14}$$

at other frequencies.

$$\mathbf{S} = \begin{bmatrix} e^{j\theta} & 0 & 0 & 0 \\ 0 & 1 & 0 & 0 \\ 0 & 0 & e^{j\theta} & 0 \\ 0 & 0 & 0 & 1 \end{bmatrix} \tag{2.15}$$

At the idler frequencies it is enough to vary the angle θ of S_{11} and S_{33} of the four-port network alone while keeping the angle of S_{11} and S_{33} of the three-port

network at zero (namely, open circuit), since the three-port network is in parallel to the diode pairs.

These ideal networks are subject to the ideal conditions for operation of the balanced SH mixer. The optimization is performed on the phase of S_{11} and S_{33} of the four-port network at the idler frequencies, which sets the reactive loading condition. In the case that uses ideal anti-parallel diode pairs (odd nonlinear terms) the mixing frequency signals which are considered in the analysis are of the form: $f = nf_{LO} \pm mf_{RF}$, where n is an even number and m is an odd number. Thus, the phase of S_{11} and S_{33} of the four-port network at the above frequencies should be optimized. In addition, the AC characteristics of diodes are related with the LO power level that determines the input or output impedance of diodes at all the mixing frequencies. Therefore, the optimization is performed under the condition of an appropriate LO power level drive. The novel generic approach for the optimum design of balanced SH mixers can be implemented by using a commercial harmonic simulator, such as MDS. The optimal design process is as follows:

- Build the circuit as shown in Figure 2.3 in a harmonic balance simulator.
- Create the two ideal networks by ideal S parameter matrices as outlined above.
- Simulate the conversion loss of the circuit by varying the phase of S_{11} and S_{33} at the idler frequencies between 0° to 360° and the LO power level.

- Plot curves of the performance.
- Determine an appropriate LO power level.
- Determine the optimum load in view of the diodes at the various idlers.
- Design an equivalent circuit, which approximates the above requirements.
- Simulate and optimize all individual linear sub-circuits.
- Use the harmonic balance analysis simulator to calculate the performance of the whole circuit consisting of all the linear sub-circuits and the nonlinear device, in order to verify the actual performance.

In a practical circuit, it is difficult or even impossible to realize the optimum conditions simultaneously at all the idler frequencies, but the optimal conditions can serve as a design guideline for the actual design of balanced SH mixers. The performance essentially depends on the reactive load at the idler frequencies. However, it is not a sharp optimum, and variations around the optimum point do not have significant effect on the wanted performance. This allows to some extent a derivation from optimum point in the circuit.

2.4 Design Example

As an attempt in validating our approach, the generic approach is applied to the design of a balanced SH mixer at 14 GHz, namely, an RF frequency of 14

GHz and an LO frequency of 6.75 GHz as well as an IF frequency of 500 MHz ($f_{RF} - 2f_{LO}$). Under small signal conditions, the harmonic balance analysis takes into account up to four LO harmonics, and thus there are three important idler signals: the sideband around the second LO harmonic 27.5 GHz ($f_{RF} + 2f_{LO}$) and the two sidebands around the fourth LO harmonic 13 GHz ($4f_{LO} - f_{RF}$) and 41 GHz ($4f_{LO} + f_{RF}$). In this application, commercial anti-parallel diode pairs (MA/COM-MA40422) are selected.

2.4.1 Optimum Loading Condition

Following the procedure outlined above, the generic model for the balanced SH mixer is established in HP MDS. It is simulated using a nonlinear harmonic balance simulator implemented in the MDS. Figure 2.4 depicts the simulated conversion loss versus the phase of S_{11} and S_{33} of the four-port network (for each plot the phase angle at the other idlers is zero) and the LO power level. Figure 2.4(a) shows the conversion loss as a function of the LO level and the phase of S_{11} and S_{33} at 27.5 GHz ($2f_{LO} + f_{RF}$); Figure 2.4(b) shows the conversion loss as a function of the LO level and the phase at 13 GHz ($4f_{LO} - f_{RF}$); Figure 2.4(c) shows the conversion loss as a function of the LO level and the phase at 41 GHz ($4f_{LO} + f_{RF}$). From these curves, it is obvious that the conversion loss sensitively depends on the load conditions at idler frequencies and it is tightly associated with the LO power drive. Thus, the optimum loads at the idlers should be determined under the condition

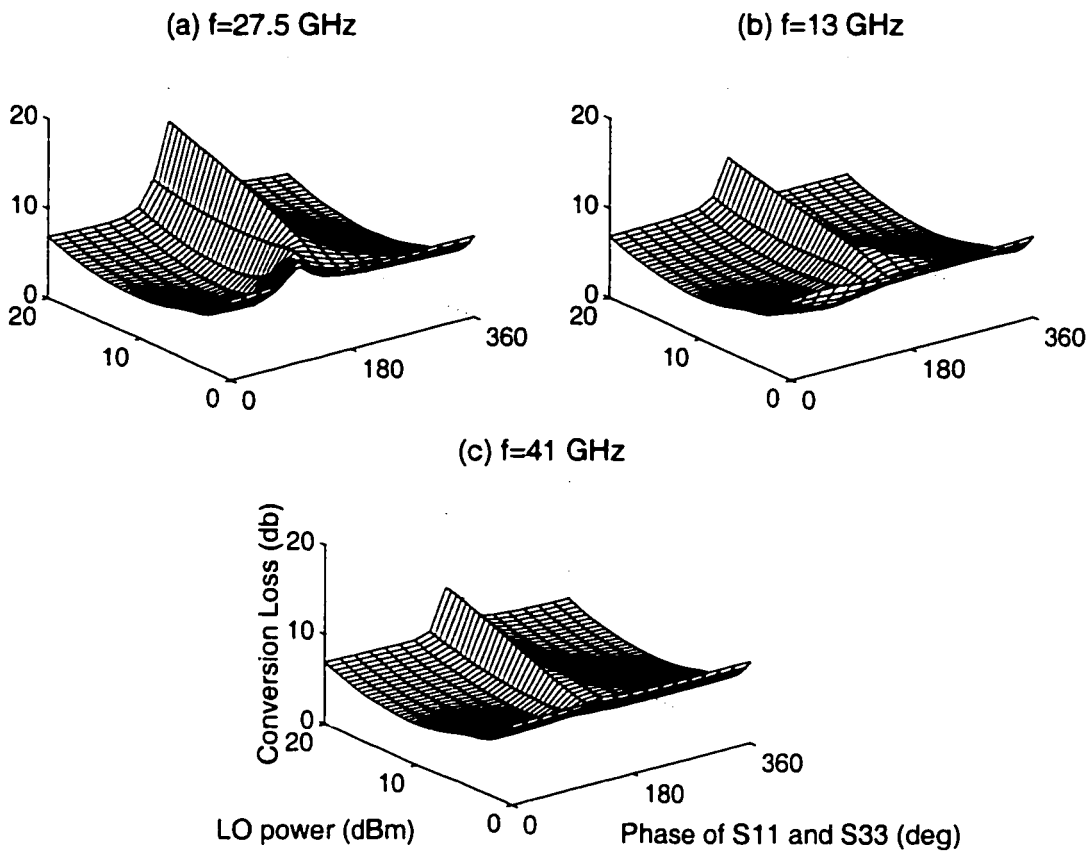

Figure 2.4 Conversion loss versus phase angle of S_{11} and S_{33} and LO power level.

of an appropriate LO power level.

When the LO power level of 7 dBm is appropriately selected, the conversion loss only versus the phase of S_{11} and S_{33} of the four-port network is highlighted in Figure 2.5. From these curves it can be seen that the maximum conversion loss occurs at angles around 180°. With this phase, the circuit acts as an effective short circuit, which maximizes the idler currents via the diode pair (power loss). The largest sensitivity is at the idler $2f_{LO} + f_{RF}$: the conversion loss varies from an optimum of 3.9 dB at angle of 90° to a maximum of 12.8 dB at angle of 180°. At

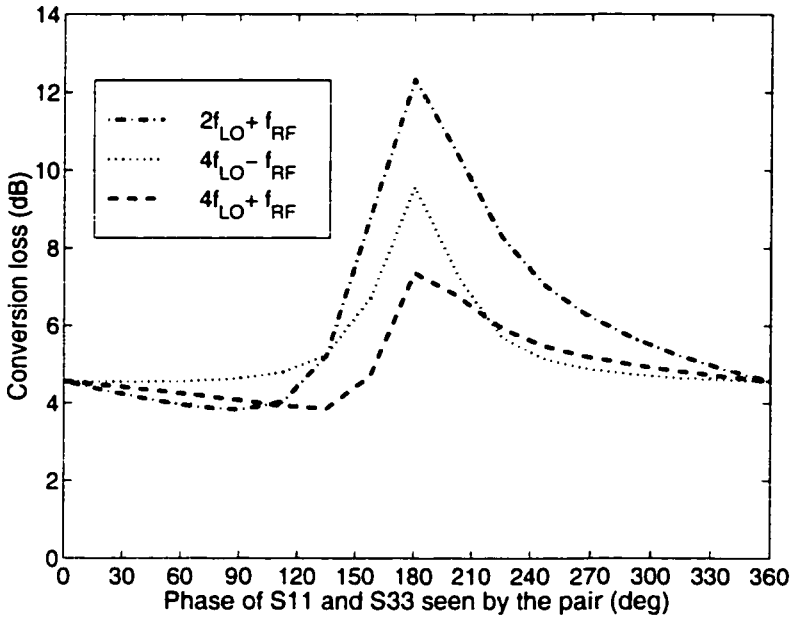

Figure 2.5 Conversion loss versus phase angle of S_{11} and S_{33} ($P_{LO} = 7dBm$)

the other idlers, the sensitivity is smaller. The optimum performance is achieved for 90° at the idler $f_{RF} + 2f_{LO}$, 0° at the idler $4f_{LO} - f_{RF}$ and 135° at the idler $4f_{LO} + f_{RF}$.

With these values the conversion loss is 3.9 dB. This is an extremely good result. Despite this satisfactory result, we note that it is obtained for the ideal case. It is very difficult in practice to realize ideal networks with the S parameters as outlined above. However, the simulated results can serve as the limiting case. Here, our goal is that the analysis based on the ideal model serves as design guideline, namely, practical circuits are as close as possible to the optimum ones derived from the ideal generic circuit.

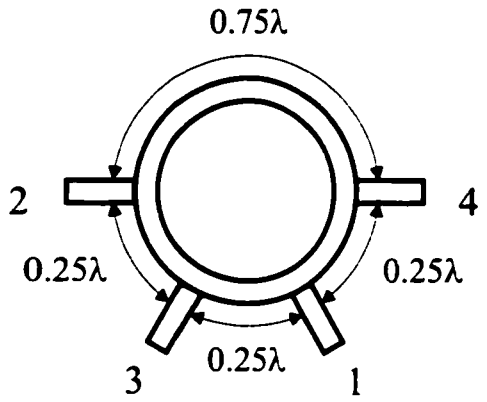

Figure 2.6 A 180-deg ring hybrid.

2.4.2 Balanced SH Mixer at 14 GHz

2.4.2.1 Structure and Design

In the microstrip realization of an 180-deg balanced mixer, a simple and conventional type of 180-deg hybrid is the ring hybrid as shown in Figure 2.6. It consists of a ring of transmission line with 1.5 wavelenghs in circumference. Because the path from port 4 to port 2 is one-half wavelengh longer than the path from port 3 to port 2, the waves arriving at port 2 are 180- deg out of phase at the fundamental frequency of LO. In a balanced SH mixer, however, the LO frequency is approximately half of the RF frequency, it is obvious that the phase difference of 180° in the balanced SH mixer cannot possibly be realized with such a ring hybrid.

The proposed balanced SH mixer circuit is sketched in Figure 2.7. It consists of two anti-parallel diode pairs (MA/COM MA40422 used in our design), a bandpass filter, a low-pass filter, a RF choke, two shorted stubs and a ring.

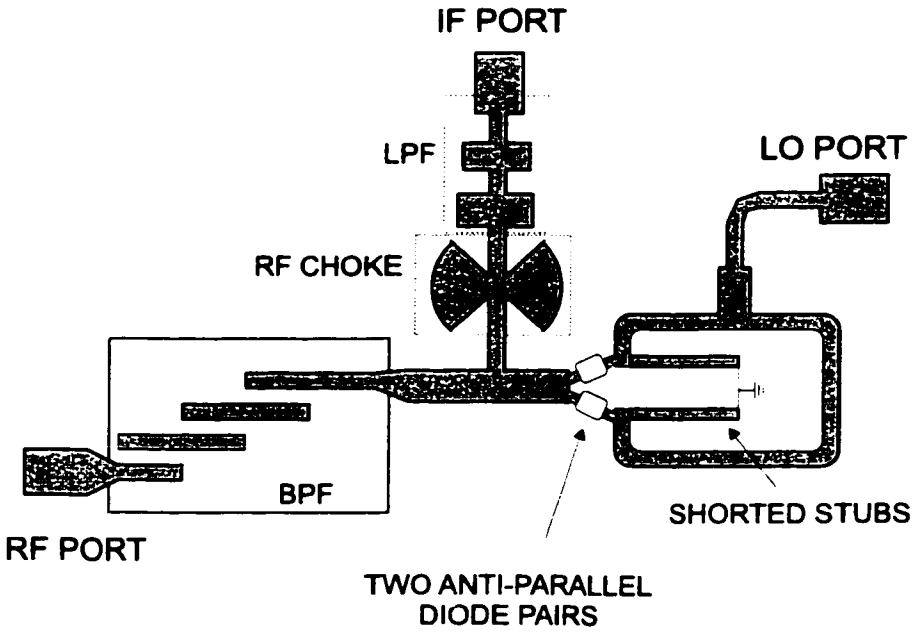

Figure 2.7 A circuit schematic for the balanced SH mixer.

Table 2.1 MA40422 Diode Parameters

C_{j0}(pF)	I_s(A)	$R_s(\Omega)$	η	ϕ_{bi}(V)
0.04	7.14×10^{14}	4	1.21	0.7

The two $\lambda_{g,RF}/2$ ($\lambda_{g,LO}/4$) shorted stubs are located on the LO side of the diode pairs such that the diodes are terminated with a short circuit at the RF frequency, but the LO signal is less affected because the LO frequency is set to be half the RF frequency. The use of the two shorted stubs also provide dc/IF return paths to ground. Through the ring with two additional $\lambda_{g,LO}/2$ length series lines towards the two diode pairs, the LO signal is split equally and applied by the phase difference of 180°. Therefore, the point of interconnection between the two diode

pairs is a virtual ground at the LO frequency for the LO excitation.

The low-pass filter is connected to the IF port for IF extraction. It employs multiple sections of low/high characteristic-impedance microstrips. The RF choke is an open-circuited radial stubs located $\lambda_{g,RF}/4$ away from the main line in the IF output circuit to prevent the IF port (RF choke) from the RF leakage. The length of the radial stubs is approximately a quarter-wavelength at 14 GHz. The combination of the low-pass filter and the RF choke effectively provides an approximate open circuit at both the RF and LO frequencies, and also may suppress some spurious responses caused by the nonlinear device.

The bandpass filter is a four-stage Lange-coupler filter. It is designed to pass the RF signal from 13 to 16 GHz, while approximately providing an open circuit to the IF signal and rejecting the spurious signal of $2f_{LO} + f_{RF}$ in order to realize the optimal reactive condition at the idler frequency $2f_{LO} + f_{RF}$ for good performance. The fabricated filter is measured with a 13-16 GHz 1-dB passband response and a 0.6-dB port-to-port insertion loss at the centre frequency of 14 GHz. Using the previous generic approach, the distance from the filter to the interconnection point between the two diode pairs is easily determined in the vicinity of the 90° phase at $2f_{LO}+f_{RF}$ frequency for achieving performance as good as possible.

The DC characteristic parameters of our used diodes are given in Table 2.1. The whole circuit is simulated using the harmonic-balance analysis routine implemented in the MDS. Figure 2.8 shows a conversion loss of 7 dB ±2 dB over the LO level

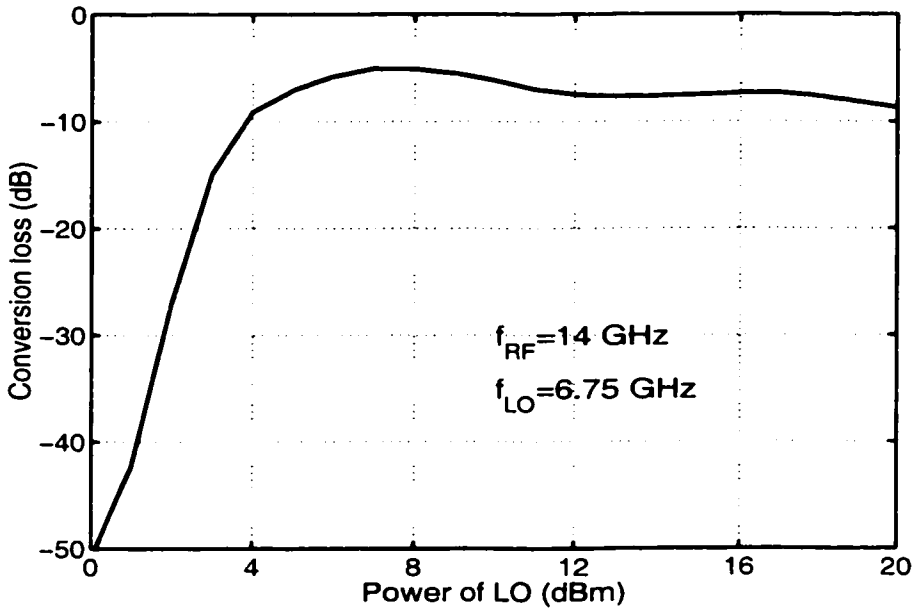

Figure 2.8 Simulated conversion loss versus the power of LO (P_{RF}=-20 dBm).

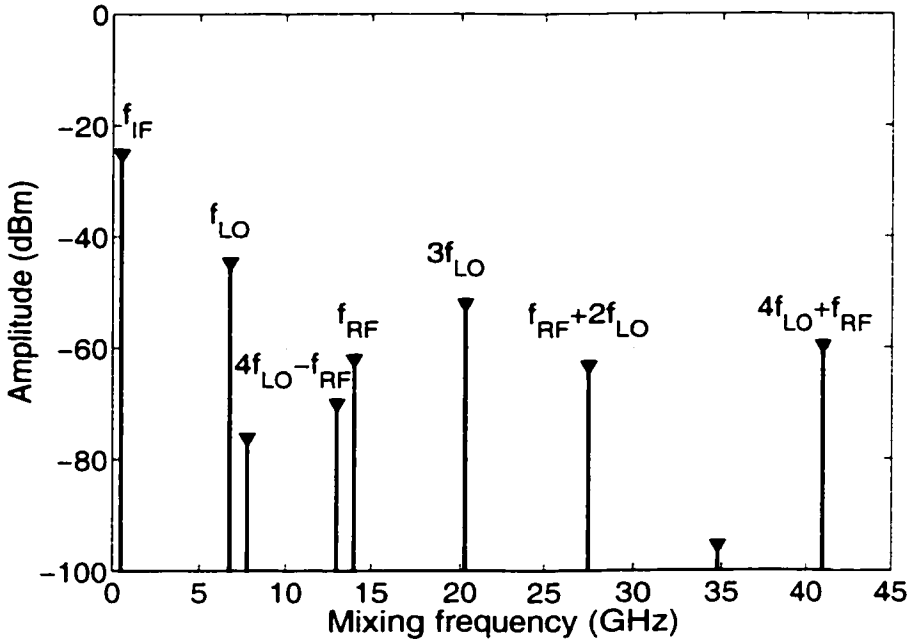

Figure 2.9 Simulated IF output power spectrum (P_{RF}=-20 dBm, P_{LO}=7 dBm).

of 4-20 dBm, and the minimum conversion loss of 5 dB at the LO level of 7 dBm.

Figure 2.9 gives the output power spectrum at the IF port. From this figure, we observe the absence of the fundamental mixing products ($f_{RF}-f_{LO}$) and ($f_{RF}+f_{LO}$) as well as all of the terms $mf_{RF} \pm nf_{LO}$ with even $m+n$. The main power flow takes place in the two sidebands around the second harmonic LO: $f_{RF}+2f_{LO}$ and $f_{RF}-2f_{LO}$, and the two sidebands around the fourth harmonic LO: $4f_{LO}+f_{RF}$ and $4f_{LO}-f_{RF}$. It is important to point out that the level of the frequency $f_{RF}+2f_{LO}$ is well enhanced for a good mixer design. In addition, the outputs at the even-order harmonics of LO and RF are absent, and all of the terms $mf_{RF} \pm nf_{LO}$ in which m is even and n is odd are well rejected. It is obvious that the mixer has the advantageous features, namely, the rejection of some spurious responses and even-order harmonics of RF and LO.

2.4.2.2 Performance

The designed balanced SH mixer is fabricated on a 15-mil TMM3 substrate with a dielectric constant of 3.2. The overall size is 40×30 mm^2. Two beam diode pairs were bonded on the line. To measure the mixer, the measurement set-up is built as shown in Figure 2.10. LO power is 8 dBm, RF input power is -20 dBm, and IF is constantly at 500 MHz.

Figure 2.11 shows the measured conversion loss when the RF is swept from 13 to 16 GHz and the LO is from 6.25 to 7.75 GHz with the 8-dBm power level. The

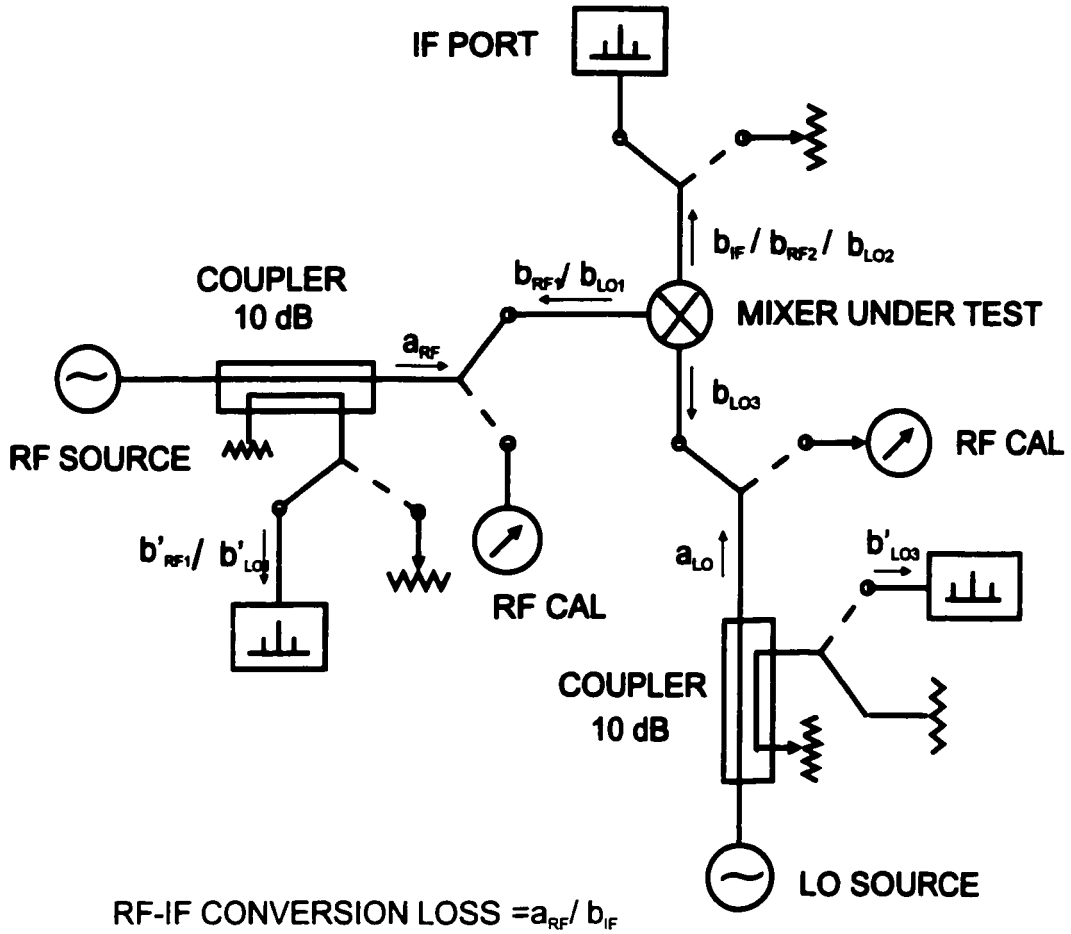

RF-IF CONVERSION LOSS $= a_{RF} / b_{IF}$
LO-RF ISOLATION $= a_{LO} / b'_{LO1}\, b'_{LO1} / b_{LO1}$
LO-IF ISOLATION $= a_{LO} / b_{LO2}$
RF-IF ISOLATION $= a_{RF} / b_{RF2}$
RF RETURN LOSS $= a_{RF} / b'_{RF1}\, b'_{RF1} / b_{RF1}$
LO RETURN LOSS $= a_{LO} / b'_{LO3}\, b'_{LO3} / b_{LO3}$

Figure 2.10 The measurement set-up for the mixer.

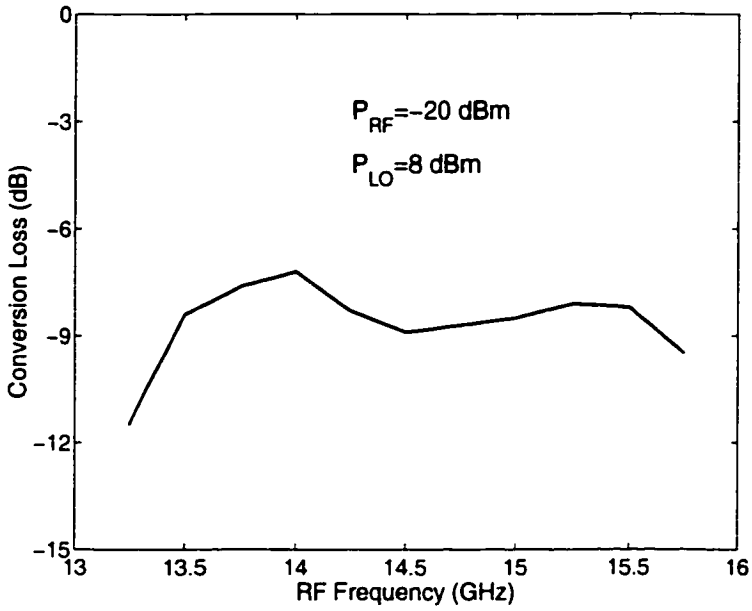

Figure 2.11 Measured conversion loss of the balanced SH mixer. The LO and RF are swept from 6.25 to 7.75 GHz and 13 to 16 GHz, respectively.

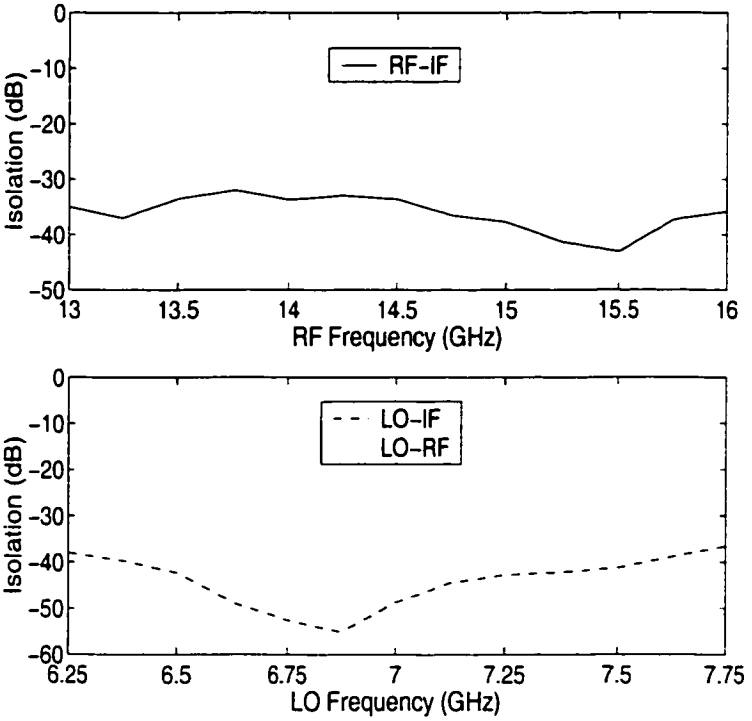

Figure 2.12 Measured RF-to-IF, LO-to-IF and LO-to-RF isolations of the balanced SH mixer.

conversion loss is less than 9 dB over the RF frequency range of 13.5-15.5 GHz. The best port-to-port conversion loss is measured at 14 GHz and is equal to 7.2 dB. Considering roughly 2 dB losses from RF and IF paths in the physical circuit, the measured conversion loss is almost identical to the simulated result.

Figure 2.12 depicts the measured LO-to-RF and LO-to-IF isolations as well as RF-to-IF isolation. The LO-to-RF and LO-to-IF isolations are higher than 45 dB and 35 dB over the LO frequency range of 6.25-7.75 GHz. The RF-to-IF isolation is higher than 30 dB over the RF frequency range of 13-16 GHz.

2.5 Conclusion

We examine the inherent properties of balanced SH mixers theoretically. Through our modeling derivation, the basic conditions for the realization of such mixers are obtained, namely, the LO signal with 180^o out-of-phase and the RF signal with in-phase at two anti-parallel diodes.

A novel generic approach of optimum design of balanced SH mixers is presented. The approach makes the optimum design of such mixers much more simple. With the aid of our proposed method, we can estimate the best achievable performance of the mixers and the loading conditions, which are necessary to achieve that performance. This can serve as both performance limit and design guideline.

As a design example, a balanced SH mixer at 14 GHz on the basis of the microstrip technique is realized and it demonstrates a good performance.

CHAPTER 3

BROADBAND UNIPLANAR DOUBLE-Y BALUNS FOR MONOLITHIC AND HYBRID MILLIMETER-WAVE INTEGRATED CIRCUITS

3.1 Introduction

Balun is the structure that transforms an unbalanced transmission line to a balanced transmission line. It is a key building block in the microwave and millimeter-wave components such as balanced mixers, push-pull amplifiers, frequency multipliers and phase shifters. A properly designed balun is essential for these types of circuits. It is often the performance of the balun which predominately determines the performance of the entire circuits.

The development of the printed microwave baluns dates back to 1969, when S. B. Cohn[20] suggested the first microstrip-slot transition. Various microstrip-slot transitions have subsequently been reported [21-24], following the development of double-sided MIC technology, based on the combination of microstrip and slot lines. In the last decade, the development of MMIC and miniaturized IC technology has generated much interest in the uniplanar structure and various uniplanar baluns made of CPW (coplanar waveguide), slotline and CPS (coplanar strip) have been proposed [25-27,30-32] for innovative uniplanar designs.

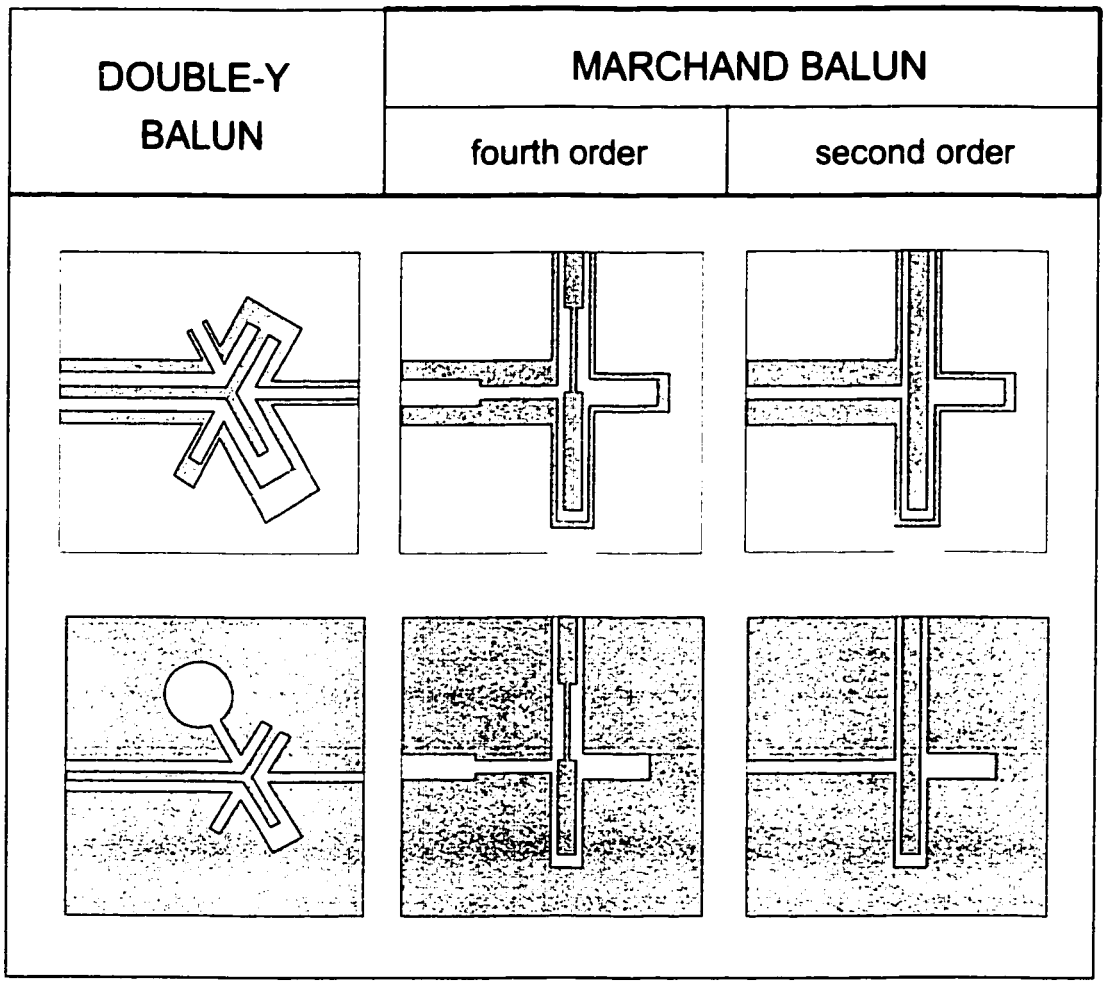

Figure 3.1 Review of uniplanar microwave baluns.

A review of uniplanar baluns is presented in Figure 3.1. Generally speaking, the uniplanar baluns are divided into two groups: Marchand baluns (the last two column) and Double-Y balun (the first column). Marchand baluns of the second order, the most popular Marchand baluns in practice, are shown in a separate column, although they represent only a special case of fourth order Marchand baluns. The Marchand balun is one of the most popular forms of broadband microwave balun used today. It is well known that its configuration is actually a bandpass network [28]. It is theoretically possible [29] to widen the bandwidth of this structure even over one-octave. The baluns realized so far mostly have bandwidths significantly below one-and-half-octave. Its bandwidth depends on balun order and relation between circuit impedances.

However, the uniplanar Marchand baluns provide smaller frequency bandwidth and larger geometry than the Double-Y baluns. The main reason is due to the asymmetry introduced in the junction and almost quarter-wave length of stubs. The double-Y baluns offer completely different solutions for wideband and small-size baluns in comparison to various Marchand baluns modified to fit into the MMIC chip. The uniplanar double-Y baluns are theoretically all-pass networks. Conditions for this network to be all-pass are defined by a very simple theoretical model presented in [30]. Modifications of such a balun leads to a balun with bandwidth over multi-octave.

A simple method for the design of double-Y baluns was already proposed in [30].

On the basis of this analysis scheme, broadband double-Y baluns were presented [31,32]. However, several disadvantages were found in connection with those design methods.

In this chapter, we present a new analysis approach that was published in [33] to effectively design low-loss broadband double-Y baluns. According to the developed technique, we design two new versions of low-loss and broadband double-Y baluns on two platforms relative to the infinite and finite ground planes: CPW-slotline and CPW$_{fgp}$-CPS structures, in which the subscript "fgp" refers to the finite-ground plane. The fabricated samples effectively validate our proposed method with achieved low-loss and wideband performance with experimental results.

3.2 A New Analysis Approach

Double-Y baluns are designed as six port double-Y junction topology that usually consists of three balanced and three unbalanced transmission lines placed alternately around the center of the junction. In this structure, each pair of two opposite ports is uncoupled while the other four ports are matched provided that the junction effects can be neglected. The incident RF signal at the unbalanced port will be equally divided among the other four ports. Similarly, an input signal at the balanced port will be equally divided among the four output ports, but one pair of the opposite ports will be operated in opposite phase.

In order to design a structure that works as a balun with perfect transmis-

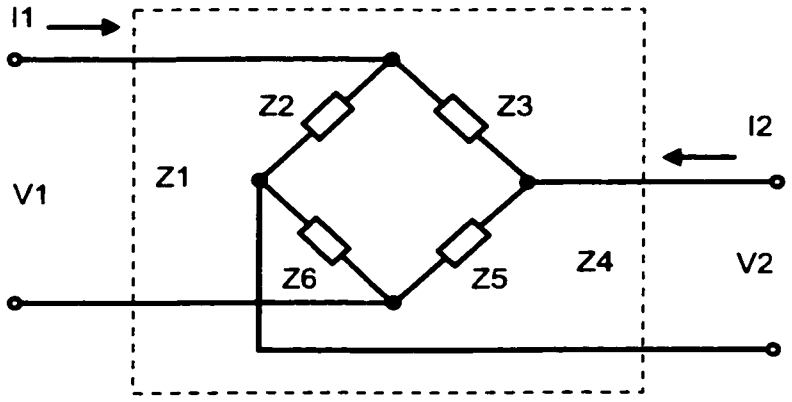

Figure 3.2 Equivalent circuit of double junction.

sion between an opposite balanced and unbalanced ports, the other opposite ports should be terminated by opposite-characteristic reactive loads (short and open).

Similar to the proposed analysis technique in [30], the equivalent circuit of a double-Y balun can be expressed in the form of an impedance bridge as shown in Figure 3.2. The impedances in the bridge are transformed along the corresponding lines onto the junction point. The influence of the junction itself is neglected in the equivalent circuit.

A simple analysis of the impedance bridge gives the following equation for the input impedance at port 1:

$$Z_{in} = Z_A - \frac{Z_B^2}{Z_A + Z_A} \tag{3.1}$$

where $Z_A = (Z_a + Z_b)/2$ and $Z_B = (Z_b - Z_a)/2$, and it is assumed that $Z_2 = Z_5 = Z_a$, $Z_3 = Z_6 = Z_b$.

For $Z_a = jX_a$, $Z_b = -jX_b$, Equation (3.1) can, after a basic transformation, be expressed by

$$R_{in} = Z_4 \frac{[\frac{1}{2}(X_a + X_b)]^2}{[\frac{1}{2}(X_a + X_b)]^2 + (Z_4^2 - X_a X_b)} \tag{3.2}$$

$$X_{in} = \frac{1}{2Z_4}(X_a - X_b)(Z_4 - R_{in}) \tag{3.3}$$

If all the stubs are of the same electrical length βl and have equal characteristic impedance Z_0, then we write:

$$R_{in} = Z_4 \frac{[\frac{1}{2}Z_0(\tan(\beta l) + \cot(\beta l))]^2}{[\frac{1}{2}(Z_0(\tan(\beta l) + \cot(\beta l))]^2 + (Z_4^2 - Z_0^2)} \tag{3.4}$$

$$X_{in} = \frac{Z_0}{2Z_4}(\tan(\beta l) - \cot(\beta l))(Z_4 - R_{in}) \tag{3.5}$$

Further normalizing the impedances in Equations (3.4) and (3.5) with respect to the characteristic impedance Z_4 leads to:

$$\tilde{R}_{in} = \frac{[\frac{1}{2}\tilde{Z}_0(\tan(\beta l) + \cot(\beta l))]^2}{[\frac{1}{2}(\tilde{Z}_0(\tan(\beta l) + \cot(\beta l))]^2 + (1 - \tilde{Z}_0^2)}. \tag{3.6}$$

$$\tilde{X}_{in} = \frac{1}{2}\tilde{Z}_0(\tan(\beta l) - \cot(\beta l))(1 - \tilde{R}_{in}), \tag{3.7}$$

in which $\tilde{R}_{in}$, $\tilde{X}_{in}$ and $\tilde{Z}_0$ are the input normalized resistance, reactance and characteristic impedance, respectively. Equations (3.6) and (3.7) are fulfilled on the assumption that there are short and open circuits alternately set in the bridge, at the same electric distance from the double junction point.

To highlight the generic characteristics of double-Y baluns, our derived results (Equations (3.6) and (3.7)) are plotted in the multilevel 3D form of curves for the normalized input resistance $\tilde{R}_{in}$ and reactance $\tilde{X}_{in}$ versus electrical length βl of the stub and normalized characteristic impedance $\tilde{Z}_0$ as illustrated in Figure 3.3.

Considering the case of $Z_0 = Z_4$, the balun characteristics are actually represented by two straight lines: $\tilde{R}_{in} = 1$ and $\tilde{X}_{in} = 0$. That means that the input impedance is real and equal to the impedance at port 4 when all the stubs have the same characteristic impedance as the impedance at port 4. It implies that, in theory, if all stubs are the same electric lengths, all stubs and transmission lines have the same characteristic impedance, then a perfect match is maintained regardless of frequency. As such, double-Y baluns are all-pass networks according to the simple theory presented. However, in practice, the baluns are band-pass networks. The main reason for the frequency bandwidth limitation is due to imperfect stub terminations, unequal dispersions between different transmission lines, junction parasitics, and mode conversions. These factors are frequency dependent.

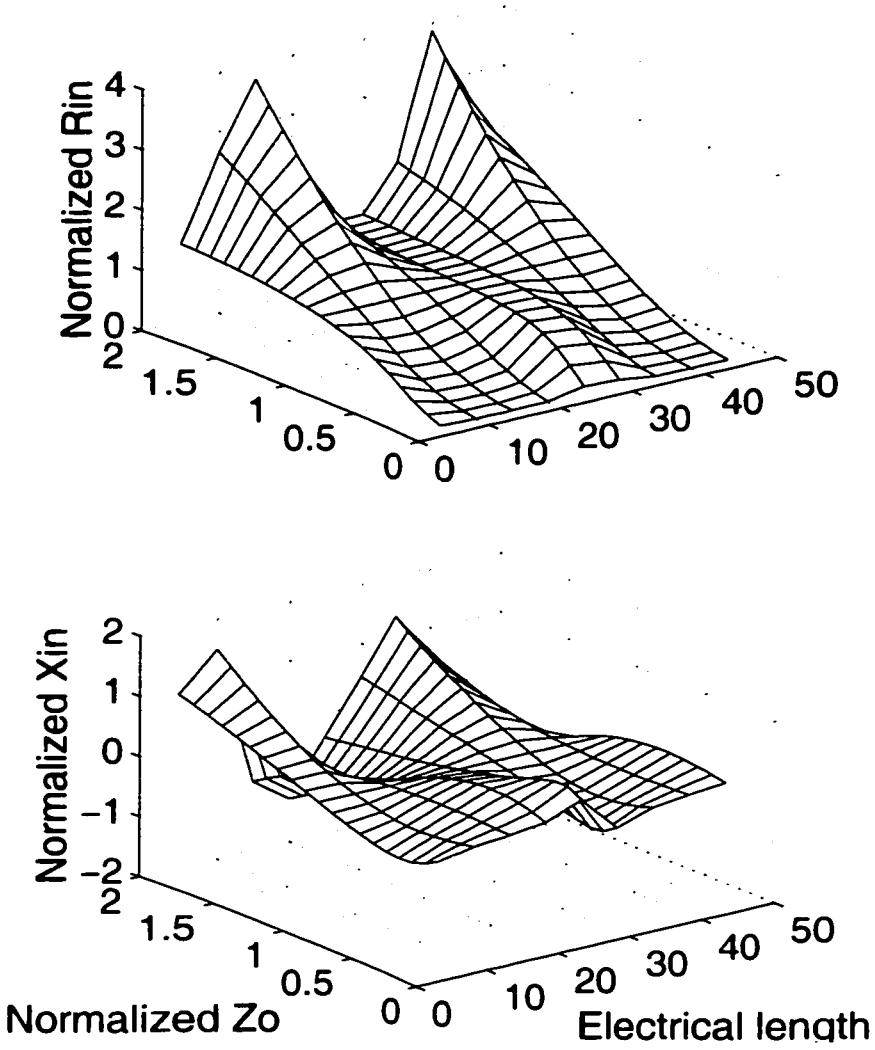

Figure 3.3 Input normalized impedance vs. βl and $\tilde{Z}_0$.

Therefore, in order to minimize potential attenuation of line and effects of dispersion and junction parasitics, we can derive the same design considerations of double-Y baluns as presented in work [27,30–32] : keeping the stub length short, selecting the stub electric length of 45° at the upper edge of the operating bandwidth for possible maximum bandwidth, and ensuring the stub length a few times larger than the radius of the double-Y junction.

However, it is not easy to design the exactly same electrical length of all stubs as well as to keep the characteristic impedance of all stubs and transmission lines to be the same due to non-negligible fabrication tolerance and other electrical and mechanical errors. Taking a look at the case of $Z_0 \neq Z_4$ in which there is a deviation of Z_0 from Z_4 as shown in Figure 3.3, we can find that the normalized input impedance is much sensitive around the electric length of 45° and less sensitive over the $25° \sim 30°$ range, even though there is somewhat a deviation of the stub characteristic impedance from the output impedance. Therefore, we suggest the following rules. For a good match within the maximum bandwidth, all the stub electric length should be selected to be 30° at the upper edge of bandwidth, and the stub length is ensured at least twice larger than the radius of the double-Y junction. It is to say that a careful design with such considerations may yield a possible broadband performance in practice.

3.3 Design and Experimental Results

According to the developed technique, we design two types of broadband double-Y baluns on the two platforms relative to the infinite and finite ground planes: CPW-slotline and CPW$_{fgp}$-CPS structures. The physical dimensions for each balun are synthesized at the upper edge of our desired frequency range with the aid of a commercial full-wave simulator such as Hewlett-Packard's Momentum and IE3D, which are a two-and-one-half dimensional (2.5-D) field solver using the planar surface meshing but including vertical currents between layers.

The electrical length of each stub is selected to be 30^o at the upper edge. The CPW lines, slot lines and CPS lines are synthesized with the smallest slot width of 1 mil that we are able to build in our laboratories. Under these conditions, the electrical field remains well confined in the vicinity of the slots, and it allows an equivalent characteristic impedance approach for both CPW and slotline or CPW$_{fgp}$ and CPS. This design also provides a substantial size miniaturization, which should considerably reduce parasitic influences of the discontinuities involved in the balun circuits.

For the purpose of measurements, the back-to-back balun structures are arranged as shown in Figure 3.4. Each of them consists of two back-to-back connected baluns with certain transmission line, and also two CPW or CPW$_{fgp}$ tapers matching relative to the 50 Ohm measurement system. Their measured scattering

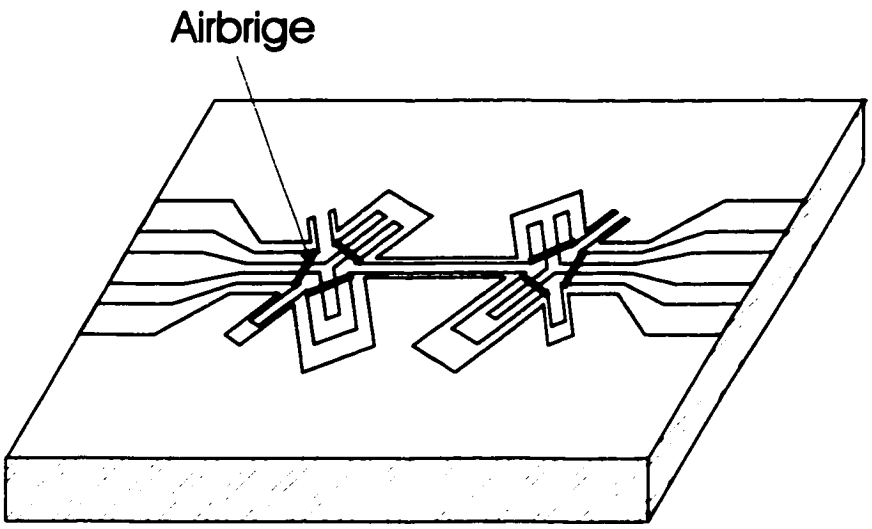

(a)

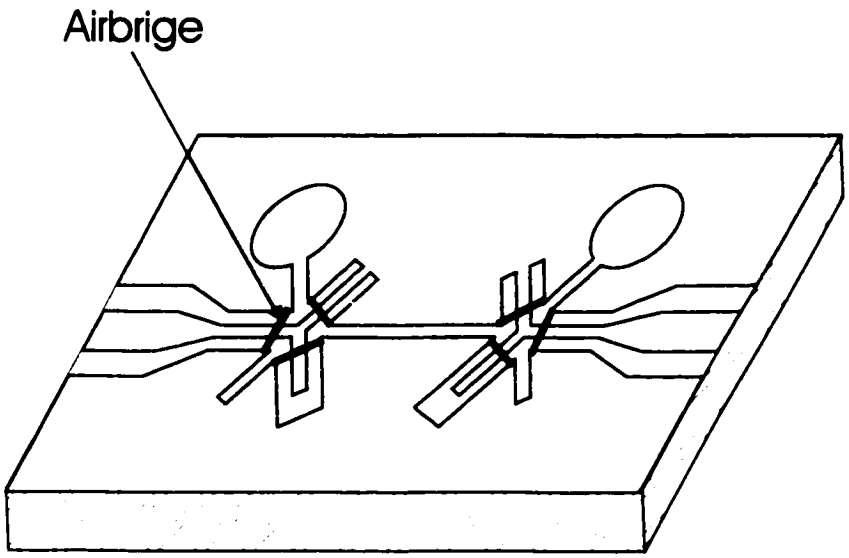

(b)

Figure 3.4 A back-to-back CPW$_{fgp}$-CPS balun structure and a back-to-back CPW-slotline balun structure.

parameters are expressed by

$$S'_{11} = s_{11} + s_{22}\frac{s_{21}^2}{1 - s_{22}^2} \tag{3.8}$$

$$S'_{21} = \frac{s_{21}^2}{1 - s_{22}^2} \tag{3.9}$$

where S'_{ij} are the measured scattering parameters for the back-to-back balun structure, s_{ij} are the scattering parameters for a single balun. Therefore, the insertion loss for a single balun can approximately be calculated as a half of the measured value in dB when s_{22} is much smaller than 1 (very low reflection along the interconnecting line). However, the return loss for a single balun is impossible to be determined from the measured value since there is another unknown variable in Equation (3.8). As such, the measured return loss for the back-to-back balun structure is used to demonstrate our designed baluns.

The samples are fabricated on Epsilon 9.9 alumina substrate with a thickness h=10 mil. Some wire bonds are attached over balun junctions and quarter-wavelength intervals on the CPW or CPW$_{fgp}$ line to suppress potential odd mode effects of the CPW or CPW$_{fgp}$ line. The circuits are measured using a vector network analyzer HP 8510C and a probe measurement system, with 68 μm-pitch 40 GHz coplanar waveguide probes. The system is calibrated at the probe tips over

the desired frequency range, using TRL (through-reflect-line) to obtain a fixed reference plane of zero phase shift, zero magnitude and known impedance over a broad band.

3.3.1 CPW$_{fgp}$-CPS Balun

A CPW$_{fgp}$-CPS balun consists of a six port CPW$_{fgp}$-CPS junction with two short circuited stubs and two open circuited stubs. The short and open stubs are realized with almost ideal short and open circuits. Furthermore, CPW$_{fgp}$ and CPS lines, due to their low dispersion, enable the balun to operate over wider frequency bandwidth. The lower edge of the frequency bandwidth is practically DC, while the upper edge of the bandwidth depends on transverse dimensions of the lines forming the double-Y junction.

Based on our proposed design rules, the physical dimensions of the double-Y baluns are synthesized at the upper edge of 16 GHz. The electrical lengths at the CPW$_{fgp}$ and CPS lines from the short and open circuits to the center of the junction are designed to be equal and to be 30^o at the upper edge of 16 GHz. Since the open and short circuits behave as being capacitive and inductive, respectively, the end capacitance and inductance associated with the short-end and open-end stubs are introduced in the equivalent circuit. The real lengths from the open and short circuits to the center of the junction should include the length extension associated with the fringing fields of these discontinuities at the open and short

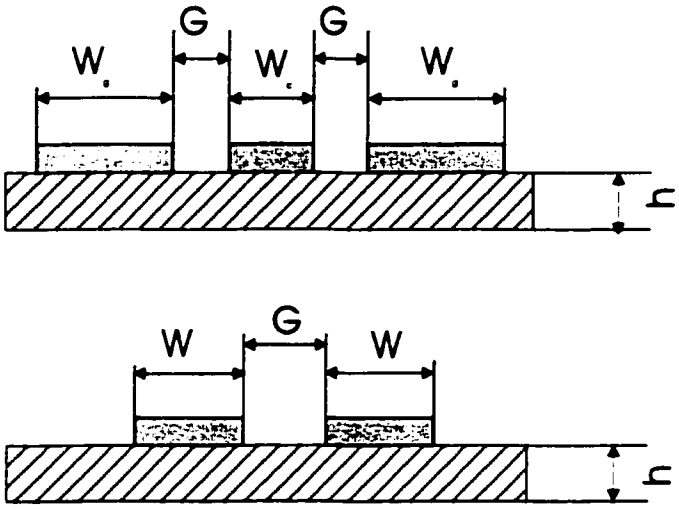

SUBSTRATE		CPW$_{fgp}$ [[mil]					CPS [mil]			
ε_r	h[mil]	W_g	W_c	G	L_s	L_o	W	G	L_s	L_o
9.9	10	4	1.1	1.2	28	27	1.6	1	27	26

L_s: short stub length

L_o: open stub length

Figure 3.5 Dimensions of CPW$_{fgp}$-CPS balun structure.

ends. The length extensions are evaluated by electromagnetic (EM) modeling of planar circuit using commercial EM simulators such as HP Momentum. The finally designed dimensions of the balun are shown in Figure 3.5.

The initial three back-to-back CPW$_{fgp}$-CPS balun structures with three different spacing lengths are fabricated and measured. Figure 3.6 illustrates measured results for the single balun performance along with the three spacing lengths be-

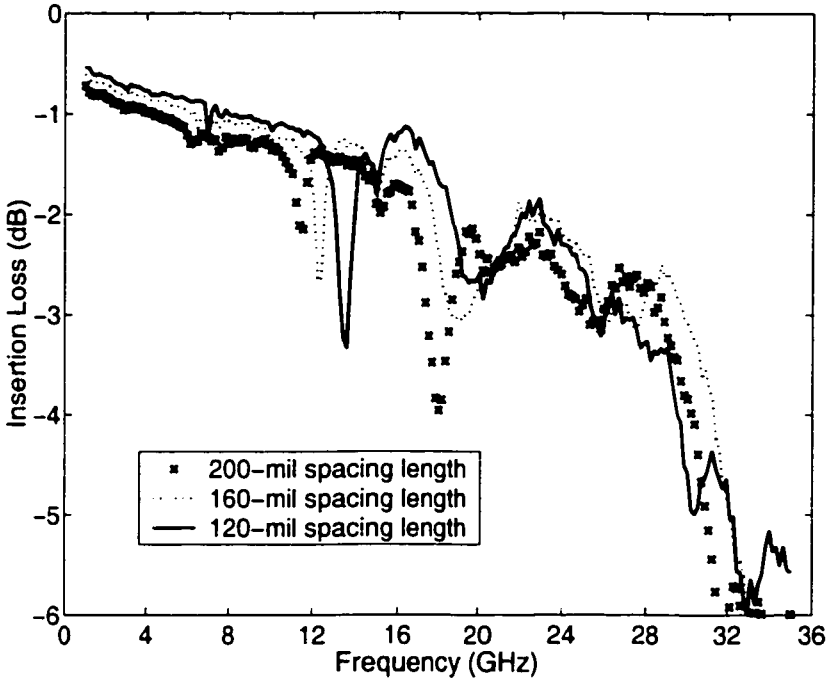

Figure 3.6 Measured complete single balun characteristics with initial tapers.

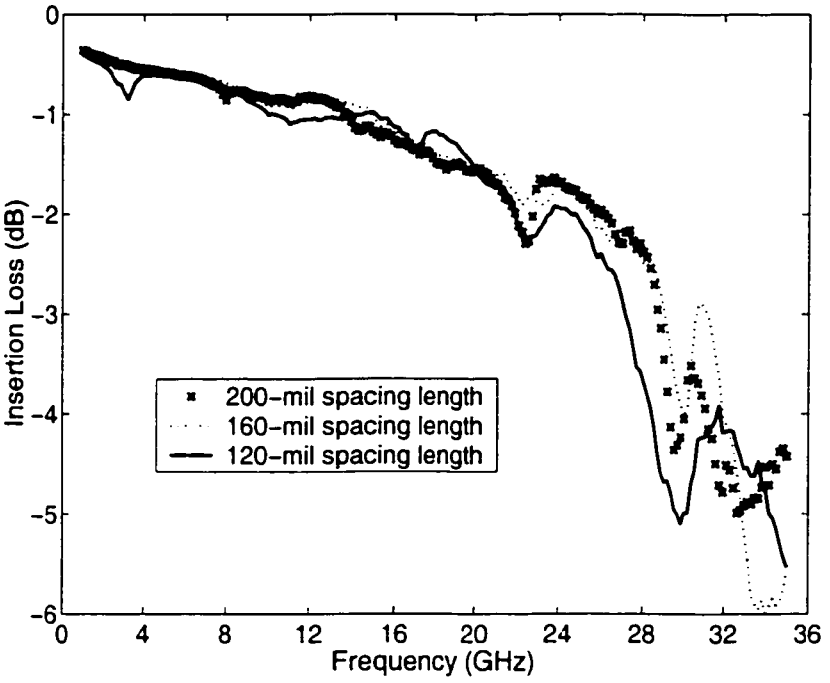

Figure 3.7 Measured complete single balun characteristics with modified (optimized) tapers.

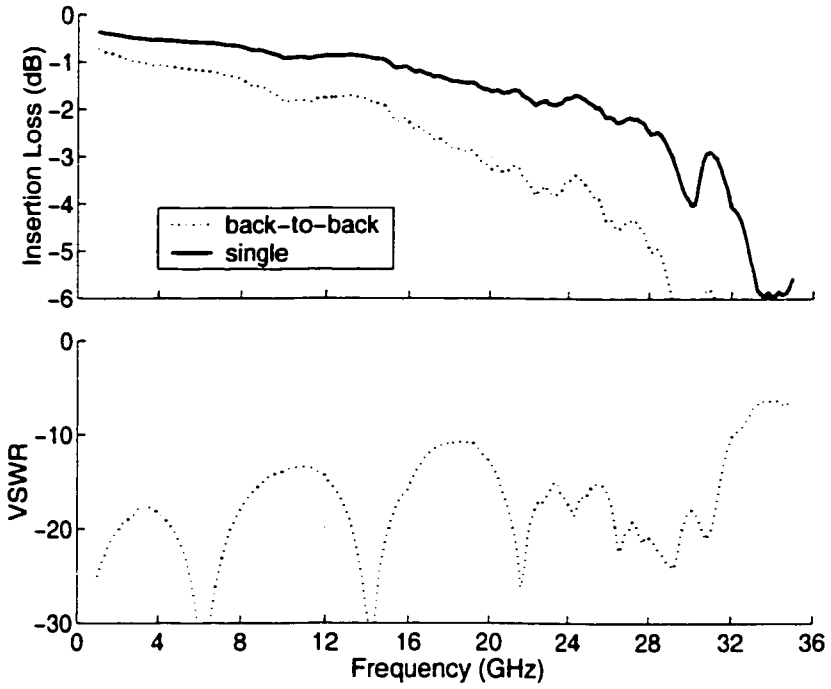

Figure 3.8 Measured results of the CPW$_{fgp}$-CPS balun.

tween the two back-to-back junctions. It can be seen from the curves that there are some dips in the frequency sweeping response except for a slight shift. This suggests that the dips are not caused by the space between two junctions, and no resonance takes place between the back-to-back experimental samples.

By replacing the two CPW tapers by a set of optimized tapers, measured results are shown in Figure 3.7 for the same structures. It is found that the dips are significantly reduced, and the insertion loss response becomes much smooth and flat. Hence, we can conclude that the proposed CPW$_{fgp}$-CPS double-Y balun is able to offer a flat frequency response and also a broadband performance.

To highlight the experimental results, one of them is plotted in Figure 3.8. The

lower edge of the frequency bandwidth is nearly in the DC range although the balun characteristics are measured starting from 1 GHz because of our TRL calibration limitation. The upper edge of the bandwidth goes up to 22 GHz if a small higher radiation loss is neglected in the CPS line, as it can be seen from the solid line curves. The measured insertion loss is less than 1.5 dB, and slightly higher in the remainder of the bandwidth, the return loss is less than 10 dB for the back-to-back balun structure including the CPW taper below 32 GHz. Such results indicate that our proposed design considerations ensures the designed balun to have a good reliable performance around 16 GHz at the upper edge of the desired frequency bandwidth.

3.3.2 CPW-slotline Balun

A CPW-slotline balun consists of a six-port CPW-slotline junction with two short circuited stubs and two open circuited stubs. The slotline open circuit is realized as a circular slot line.

We design two different CPW-slotline double-Y baluns which are synthesized at the upper edges of 16 GHz and 26 GHz, respectively. As a result, the electrical lengths at the CPW and slot lines from the short and open circuits to the center of the junction are designed to be equal and they are 30^o at the upper edge of 16 GHz and 26 GHz, respectively. Similarly, the stub lengths should include the length extension associated with the fringing fields of these discontinuities at the open

and short ends. The real dimensions of the two different baluns obtained using HP Momentum are shown in Figure 3.9.

With the previously optimized CPW taper, the two designed CPW-slotline balun circuits are fabricated and measured in the symmetric (back-to-back) configuration. Figure 3.10 shows the measured back-to-back characteristics and the calculated results from its measured data for the first single balun design having a 110-mil diameter of the circular slot line. The insertion loss is about 1 dB over a 3-20 GHz frequency range, and slightly higher in the remainder of the bandwidth. The return loss is less than 10 dB from 5 GHz up to the measured highest frequency of 35 GHz.

According to the simple theory described above, the operating bandwidth is supposed to be wider. However, the first CPW-slotline double-Y balun sample demonstrates a low insertion loss and a flat response over a 2-3-octave frequency range. The limitation of bandwidth is caused by the circular slot line. The main reason is that a circular slot line has a good open circuit only in a 2-3 octave frequency range. Otherwise, a further wider bandwidth can be expected.

Figure 3.11 shows the measured back-to-back characteristics of the other balun sample having a 66-mil diameter of the circular slot line. The insertion loss is about 1 dB over the frequency range of 5-30 GHz, and slightly higher in the remainder of the bandwidth. The return loss is less than 10 for the back-to-back balun structure from 6 GHz up to the measured highest frequency of 40 GHz. It can also be seen

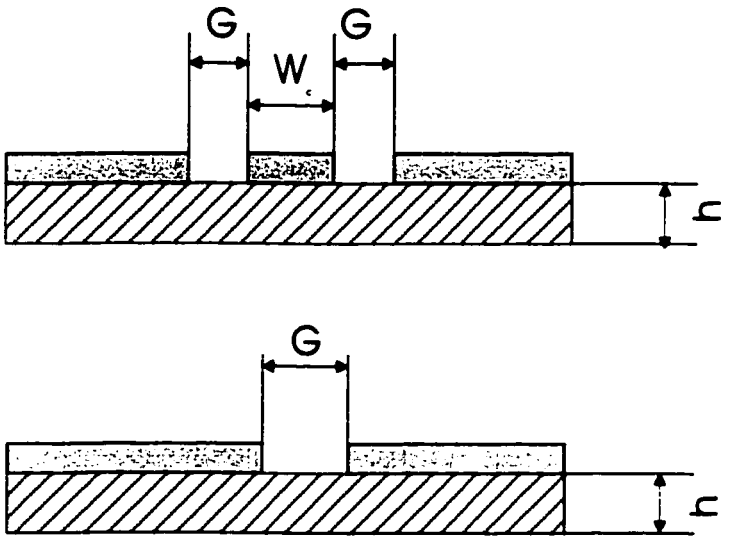

SUBSTRATE		CPW [[mil]				SLOTLINE [mil]			
ε_r	h[mil]	W_c	G	L_s	L_o	G	L_s	L_o	D
9.9	10	1.6	1	22.5	22	1	21	24.5	110
9.9	10	1.6	1	13	12.5	1	10	15	66

L_s: short stub length
L_o: open stub length

Figure 3.9 Dimensions of two CPW-slotline double-Y balun structures.

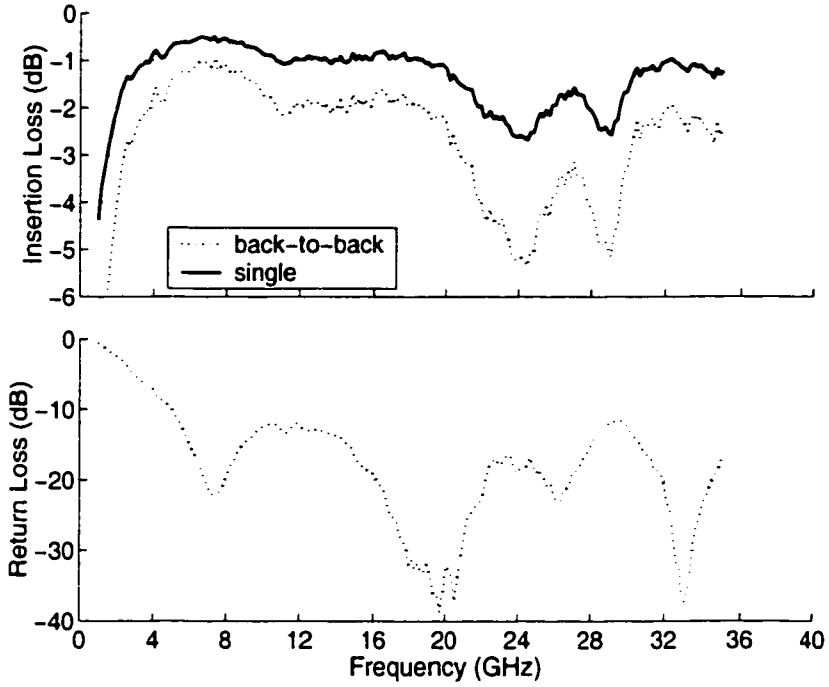

Figure 3.10 A CPW-slotline double-Y balun with 100-mil diameter, arranged results.

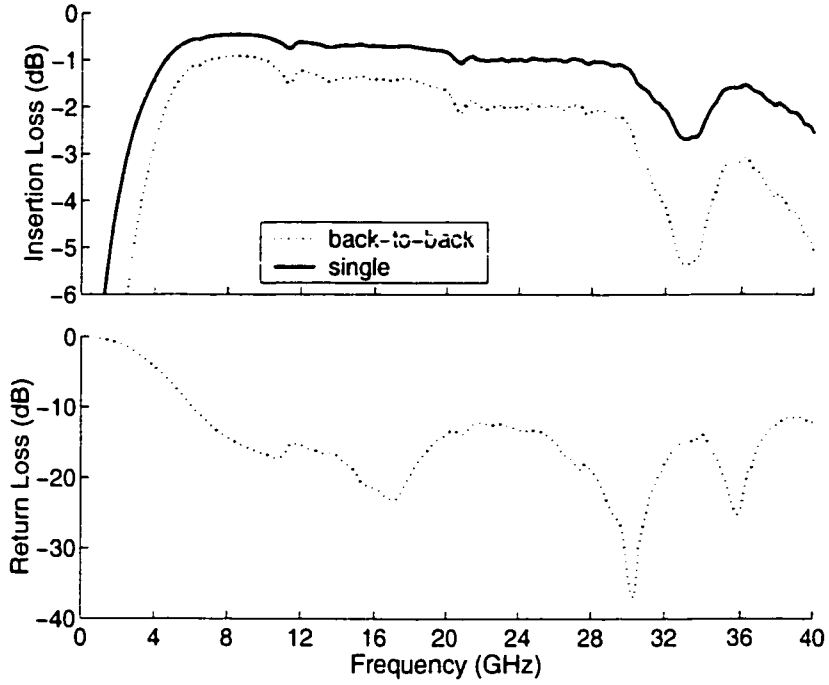

Figure 3.11 A CPW-slotline double-Y balun with 66-mil diameter, measured result.

that the second sample has a low insertion loss and a flat response over 2-3-octave frequency range.

Through the measured results, it is further seen that our proposed design consideration ensures the balun to have a good reliable performance around the desired upper edge of the frequency bandwidth.

With the comparison of the experimental performance of the two different CPW-slotline double-Y balun samples, it is found that the bandwidth of 3-20 GHz for the first balun is shifted up to the bandwidth of 5-30 GHz for the second one. Therefore, we conclude that reducing the diameter of the circular slot line causes an increase of the upper edge of the bandwidth somewhat but also the increase of the lower edge.

3.4 Conclusion

In this chapter, we present a simple but effective network model for the design of low-loss and broadband double-Y balun structures involving various dissimilar planar transmission lines. Basic design equations are derived for the network analysis.

According to the derived design equations, we obtain the simple rules for the design of such low-loss and broadband baluns. In our work, two types of baluns, namely, CPW-slotline and CPW$_{fgp}$-CPS structures, are studied for uniplanar and multilayer broadband circuit design. They demonstrate a pretty good performance

with a low-loss of around 1 dB and a multi-octave bandwidth.

Baesd on our theoretical predictions and measured results, we can find that specific considerations in connection with critical design parameters can lead to a multi-octave broadband performance with a very flat frequency response.

CHAPTER 4

A CLASS OF NOVEL UNIPLANAR BUILDING BLOCKS FOR MONOLITHIC AND HYBRID MILLIMETER-WAVE INTEGRATED CIRCUITS

4.1 Introduction

Uniplanar transmission lines such as Coplanar Waveguide (CPW) and Slotline have already found many applications in today's rapidly-developed microwave, millimeter-wave hybrid and monolithic integrated circuits. They have the advantages of easy realization of short-circuited ends, simple mounting of lumped (active or passive) components in shunt or in series configuration, free from drilling of holes through the substrate needed to reach the ground plane, and great flexibility of inter-transition among different transmission media. As all conductors are in the same side of substrate, it permits a high-level integration and it is well-suited to high-frequency design since the grounding connection through via-hole is eliminated and potential parasitic effects related to active device implementation may be minimized.

Low-loss small-size broadband design of passive integrated building blocks is of critical importance in the design of a large variety of monolithic and hybrid active integrated circuits and devices at microwave and millimeter-wave frequencies. As

MMIC and miniaturized IC technology are in rapid progress, the need for broadband uniplanar structures becomes evident, and various schemes of circuits made of CPW, slotline and CPS have been proposed for innovative uniplanar designs.

The CPW open circuit is indispensable in uniplanar passive circuits. However, potential mode conversion[36] and main radiation [37] along open CPW stubs may significantly deteriorate overall circuit performance. Such problems may in particular reduce the effective frequency bandwidth. In this work, a concept of the anti-symmetrical CPW modal electric fields that are "elastically" converged into a circular aperture[35] is applied to the design of RF choke and tapered DC-blocking filters[38] that is able to reduce the radiation loss of the CPW open stub end. Through a comparative study of different RF chokes and different DC-blocking filters, the compensated RF choke and DC-blocking filter experimentally exhibit a better performance with lower loss and wider bandwidth. This work was published in [39].

4.2 CPW Open Stubs

A class of CPW open stubs is shown in Figure 4.1. Figure 4.1a is a broadband radial open stub similar to a conventional wideband open microstrip circuit. Figure 4.1b is a rectangular open stub, which is used as reference for the purpose of comparison. Figure 4.1c and d present circular CPW open stubs without and with the central conductor compensations, respectively.

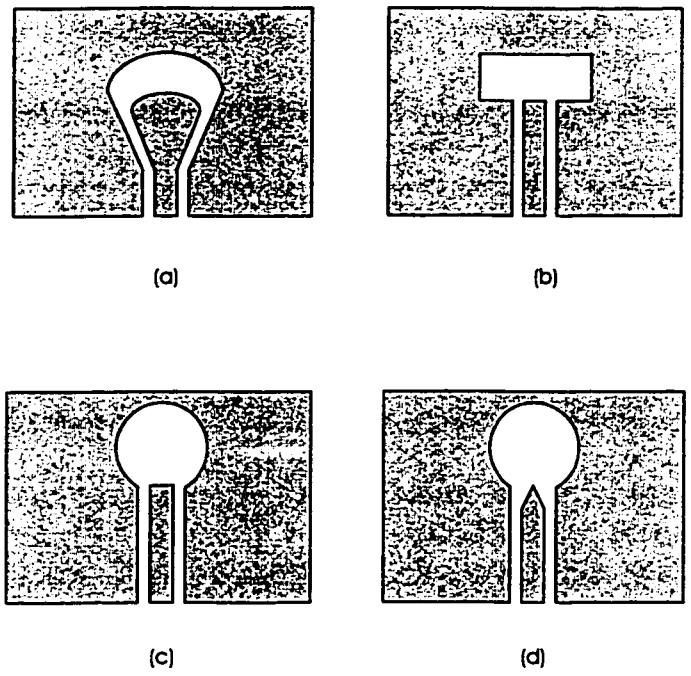

Figure 4.1 A class of CPW open stubs: (a) radial open; (b) rectangular open; (c) uncompensated circular open; (d) compensated circular open.

Judging from the impedance point of view, these CPW opens have similar terminal conditions with a gradually higher impedance towards the end, thereby achieving the open circuit. However, there is a fundamental difference regarding the radiation loss properties. With reference to the last structures in Figure 4.1, it can be seen that due to the anti-symmetrical property, the electric fields of the CPW fundamental modes are cancelled out against each other as the coupled slots converge into the open aperture. In this way, the electrical fields spread out more over the open aperture with lower frequency and the contrary situation takes place with higher frequency. Considering the situation of the uncompensated circular stub (Figure 4.1c), the electric fields converge "elastically" and "smoothly" with

different frequencies into a circular aperture. Therefore, a virtual open effect is expected over a broadband of frequency at the intersection between the circular stub and the CPW branch line. Nevertheless, there is still a current discontinuity due to the central conductor, which may cause a small radiation loss. To solve this problem, a technique of compensation was proposed[35] by taping the conductor shape, as shown in Figure 4.1d.

4.3 RF Chokes

Based on the open structures outlined above, a class of RF chokes is arranged for the purpose of comparison, as shown in Figure 4.2. Their physical dimensions are synthesized at the center frequency of 28 GHz, using the commercial full-wave simulator of HP Momentum. During the synthesis, more EM simulations may be done. If the computed EM characteristics of the circuits do not satisfy the circuit performance requirement, the geometry of the circuits needs to be modified. In such situations, numerous EM simulations are conducted to optimize the circuits' dimensions.

The class of RF chokes with four different CPW open ends are fabricated on a 10-mil alumna substrate with a thickness h=10 mil. Some bonds are attached in the vicinity of the CPW cross-junction to suppress the potential odd mode of CPW line. The circuits are measured using a vector network analyzer HP 8510C and a probe measurement system, with 68 μm-pitch 40 GHz coplanar waveguide

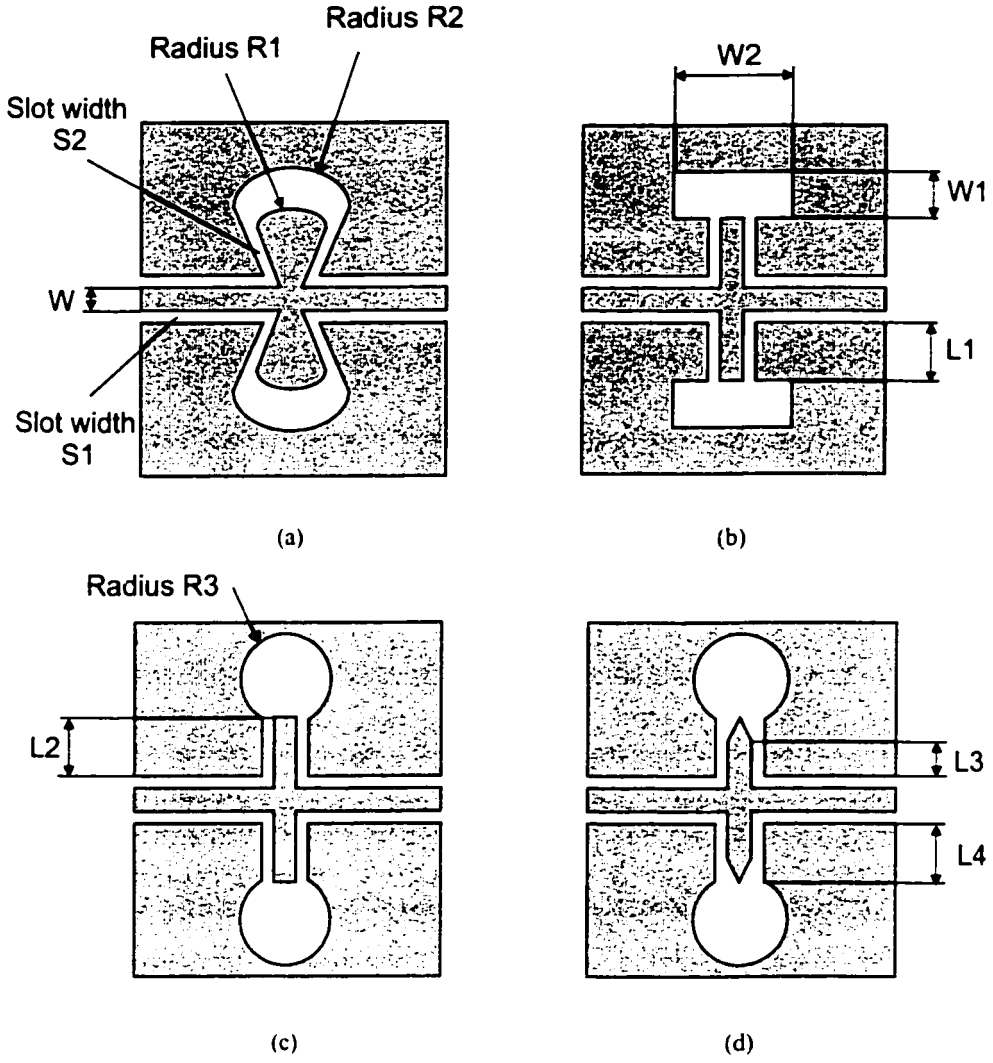

Figure 4.2 RF choke circuits of CPW: (a) radial open; (b) rectangular open; (c) uncompensated circular open; (d) compensated circular open.

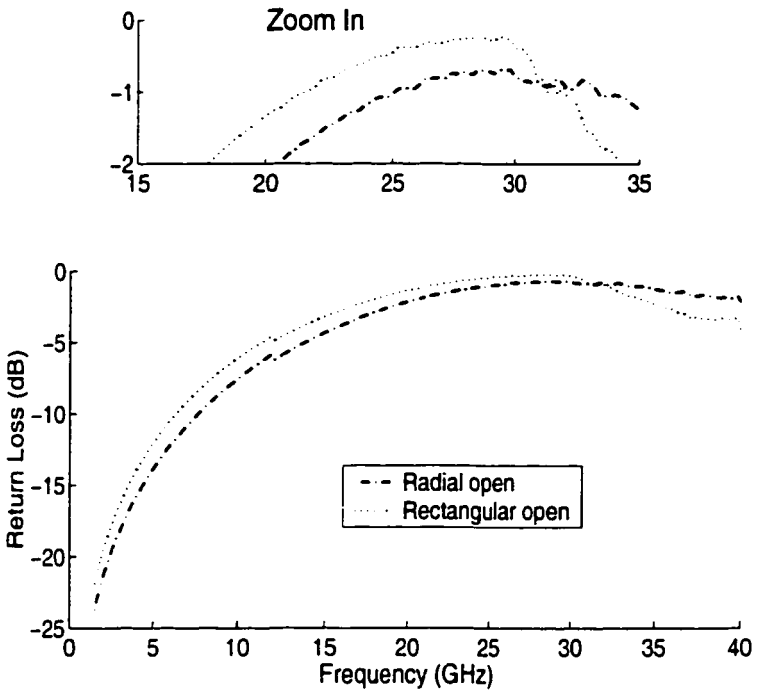

Figure 4.3 Measured results of two RF chokes with the radial and rectangular open stubs. Geometrical dimensions are S_1 = 1.3 mil, S_2 = 2 mil, W=3 mil, R_1 = 31.5 mil, R_2 = 65 mil, L_1 = 45.7 mil, W_1 = 12 mil, W_2 = 17 mil and thickness of alumina is equal to 10 mil.

probes. The system is calibrated at the probe tips over the range of 1.5-40 GHz, using TRL (through-reflect-line) to obtain a fixed reference plane of zero phase shift, zero magnitude and known impedance over a broad band.

Figure 4.3 shows experimental results for the RF chokes with the radial and rectangular open stubs. The overall loss of the radial-open RF choke is higher than its counterpart. This may be due to the radiation loss because the slot fields are gradually separated over the radial line and hence cannot be cancelled out with each other. In this case, the wideband characteristics are obtained by the elasticity and smoothness of electric fields along the radial line.

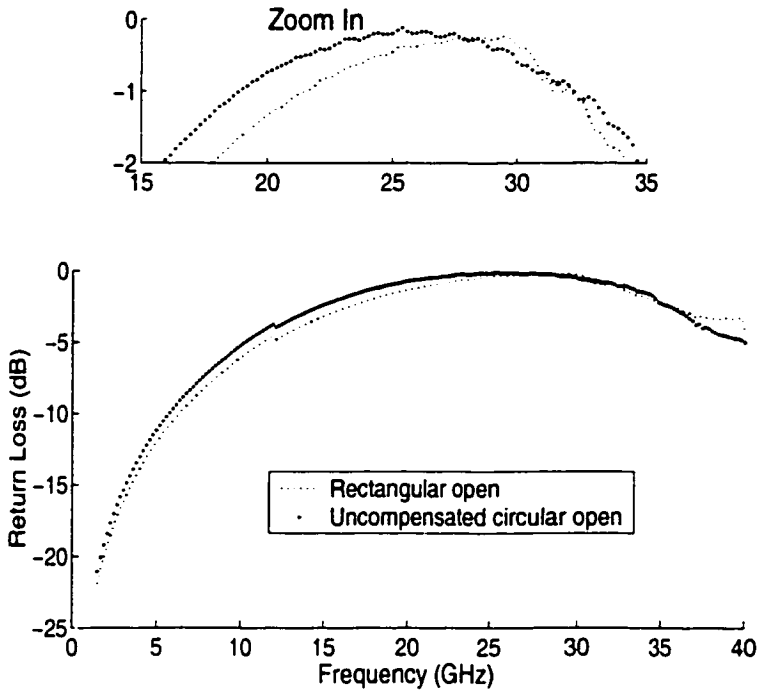

Figure 4.4 Measured results of both the rectangular-open RF choke and the circular-open RF choke without taping the central conductor shape. Geometrical dimensions are S_1 = 1.3 mil, W=3 mil, L_1 = 45.7 mil, W_1 = 12 mil, W_2 = 17 mil, L_2 = 50.7 mil, R_3 = 6 mil and thickness of alumina is equal to 10 mil.

Figure 4.4 displays a comparison of electrical performance for the rectangular-open RF choke and the circular-open RF choke without taping the central conductor shape. Obviously, the circular-open RF choke presents a better performance than its rectangular-open counterpart. This is well explained by the concept of the anti-symmetrical CPW modal electric fields that are "elastically" converged into a circular aperture. Although low loss characteristic is observed over the wide-band range for the circular-open RF choke, the bandwidth of this choke is still incomparable with the compensated RF choke.

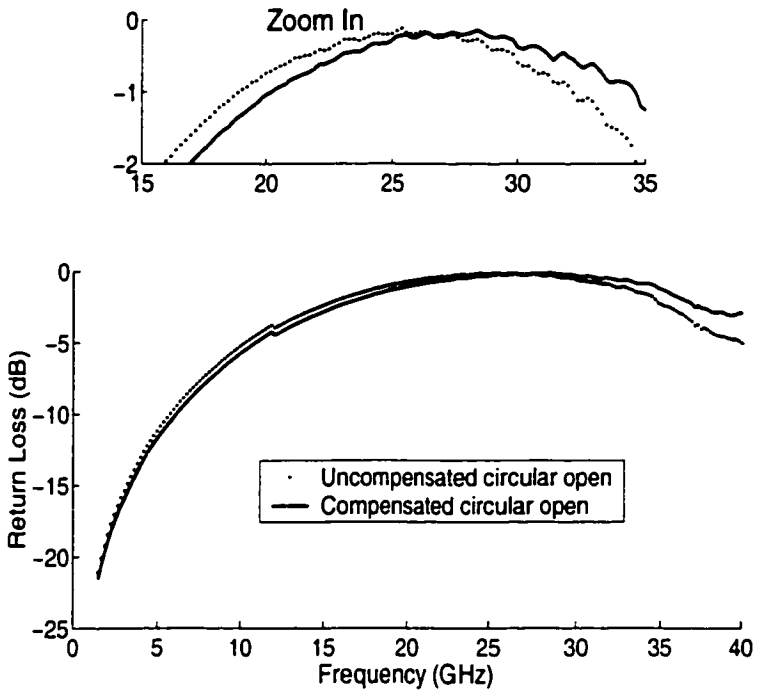

Figure 4.5 Measured results of two circular-open RF chokes without and with the central conductor compensation. Geometrical dimensions are S_1 = 1.3 mil, W=3 mil, L_2 = 50.7 mil, L_3 = 44.7 mil, L_4 = 50.7 mil, R_3 = 6 mil and thickness of alumina is equal to 10 mil.

Figure 4.5 shows the comparison for the circular-open RF chokes without and with the central conductor compensation. The RF choke with the compensated CPW circular open stubs exhibits the better performance with radiationless and wider bandwidth.

To highlight the comparison of the experimental results, the results for four different RF choke circuits are plotted together as shown in Figure 4.6. Obviously, the RF choke with the compensated CPW circular open stubs demonstrates the best performance: radiationless and extremely wide frequency bandwidth.

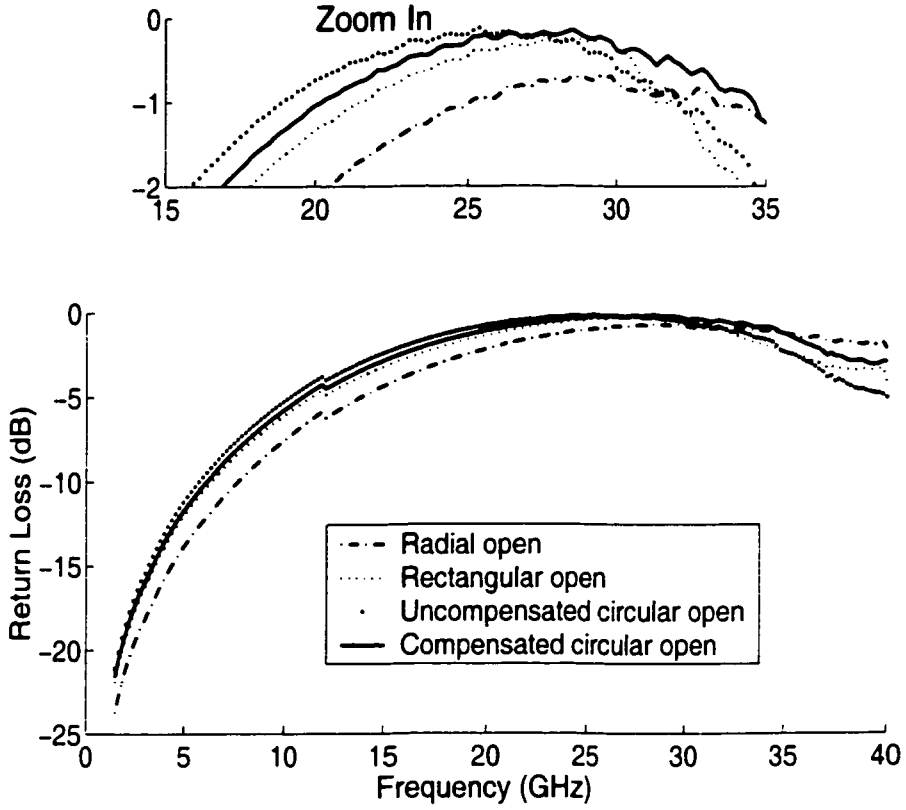

Figure 4.6 Measured results of a class of CPW RF-chokes.

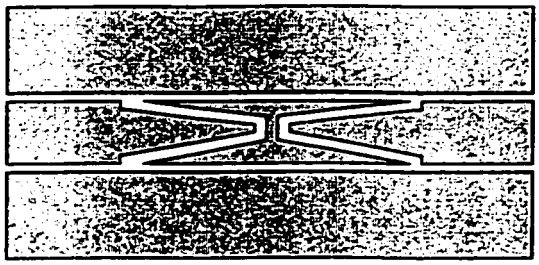

(a)

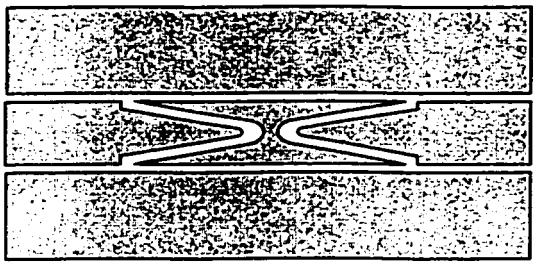

(b)

Figure 4.7 CPW DC-blocking filter structures, (a) with uncompensated open ends, (b) with compensated open ends.

4.4 DC-blocking Filters

Basically a DC-blocking filter is made out of a single cell of bandpass filter, consisting of an open-end series (OES) stub. With the conventional OES CPW stub, the value of the center spacing influences the bandwidth of the OES. At finite inner slot width, a small spacing yields a high characteristic impedance for the inner CPW formed by the inner slots, hence causes a rapid variation of the series stub phase around resonance. Taking a moderate to large value for the spacing enlarges the bandwidth, but also increases the coupling between inner and outer slots: the impedances at access ports are different and the reflection levels

increase. Huynen [38] proposed a novel CPW topology DC-blocking filters (see Figure 4.7a) to obtain a large bandwidth and a low return loss, in which the center spacing linearly varies between the inner slots of the OES CPW stub. Linearly varying the spacing confines the coupling effects into a small fraction of the OES length only, while minimizing the characteristic impedance of inner CPW stub at access ports. Therefore, the tapered CPW DC-blocking filter has the improvement of the input and output reflection levels over a wide band.

However, the performance of the tapered CPW DC-block can be improved a bit if doing a further modification, because there are some discontinuities in the inner CPW open stub, which may cause unwanted radiation loss. With the scheme outlined previously, we propose a novel CPW DC-blocking filter (see Figure 4.7b). For comparison, the two topologies shown in Figure 4.7 are designed. Their analysis and synthesis are performed using HP's Momentum.

The two DC-blocking filter circuits are fabricated on a 10-mil alumna substrate. Accurate measurements are performed over the 1.5-40 GHz frequency band. Figure 4.8 compares experimental results for the two configurations. The dashed curve depicts the frequency response of the tapered CPW DC-block filter, while the solid curve is for the compensated tapered CPW DC-blocking filter. It indicates a visible improvement of bandwidth and return loss for the compensated tapered DC-block filter over its uncompensated counterpart. The return loss of less than 16 dB is obtained over a 25-40 GHz bandwidth.

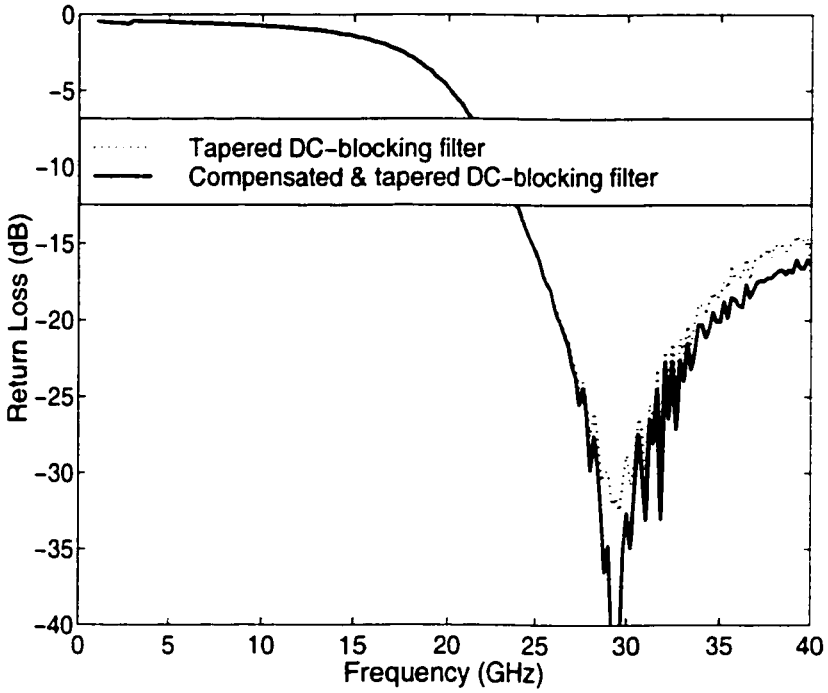

Figure 4.8 Measured results of two types of CPW DC-blocking filter.

4.5 Conclusion

Based on the concept of the anti-symmetrical CPW modal electric fields that are "elastically" converged into a circular aperture, we proposed our novel structures for RF choke and DC-blocking filter circuits. Compared to conventional CPW circuits, the proposed RF chokes and DC-blocking filters exhibit radiationless and broadband properties. The developed circuit capability in achieving broadband and good performance is well confirmed by measurements.

CHAPTER 5

A NOVEL UNIPLANAR BROADBAND BALANCED SUBHARMONICALLY PUMPED MIXER

5.1 Introduction

Rapid growth in radio-frequency (RF) commercial sectors at microwave and millimeter-wave frequencies has triggered the search for new solutions in the design of cost-effective MHMICs and MMICs. Such a demand has a significant impact on a number of design parameters both at component and system levels, such as size reduction, broadband operation and low-power consumption and low-noise requirement.

As we presented in Chapter 2, subharmonically pumped (SH) mixer is very useful at millimeter wave frequencies since it has the advantages of subharmonic pumping and inherent suppression of local oscillator (LO) noise, both alleviating the demand for the LO source. On the other hand, the balanced mixer is also widely used due to its rejection of certain spurious responses, its reduction of LO noise and spurious signals as well as its enhancement of inherent LO-to-RF isolation. Therefore, a balanced SH mixer should be able to combine the advantages of both SH and balanced mixers if the mixer design is made in an adequate manner. In such mixers, anti-parallel diode pairs are used to replace single diodes, the LO is applied

at 1/2 the frequency necessary to provide the desired frequency conversion, and the RF and IF are separated from each other only by filters. These design features make it possible to effectively reduce the demand on the LO source while broadband properties are achievable.

In our previous work, we designed a balanced SH mixer at 14 GHz, which was realized in microstrip. Although it demonstrated a good performance, its operating frequency bandwidth was very narrow. The main reason is due to the two additional $\lambda_{g,LO}/2$ length series microstrip lines and the two $\lambda_{g,RF}/2$ length short-circuited stubs. The two additional phase difference lines provide the two anti-parallel diode pairs with 180^o out-of-phase. The short-circuited stubs on the LO side of the diodes are used to prevent the RF signal from propagating in the direction of the LO port and also serve as the IF/DC return. Both are frequency dependent and limit the RF and LO operating frequency ranges. In addition, the short circuits were realized by connecting the conductor to the backside ground plane through via holes. Obviously, the via-holes introduce troublesome parasitics into the short-circuited stubs at higher frequency.

With the scheme of coplanar lines and new double-Y balun building block, we propose a new architecture of broadband balanced SH mixer operating at millimeter-wave frequencies, which is implemented in a uniplanar configuration. This uniplanar architecture allows for shunt and series connections of circuit element, simple grounding without the need for backside metallization or associated

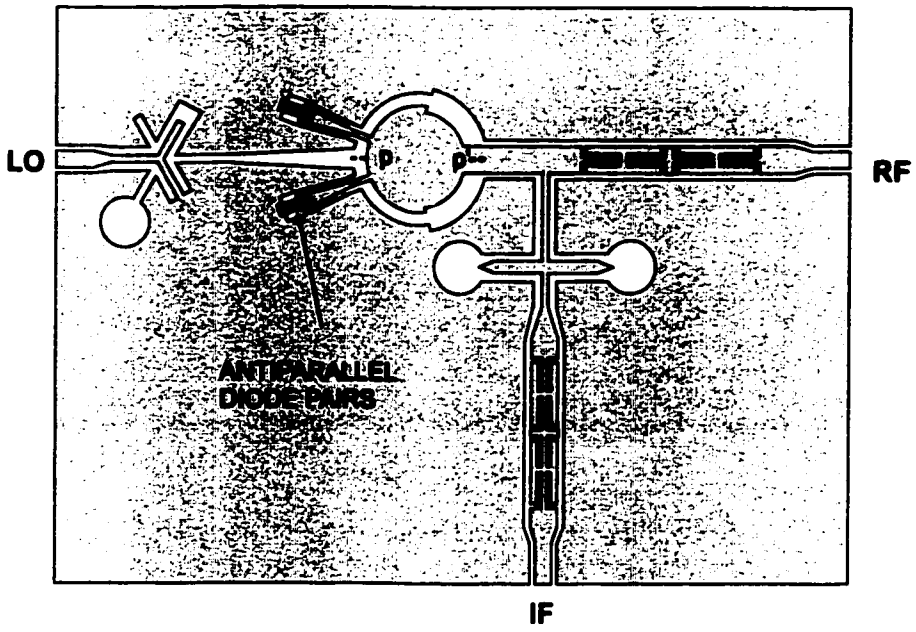

Figure 5.1 The proposed uniplanar architecture of broadband balanced subharmonically pumped mixer.

via-holes, and also flexible inter-transitions among different uniplanar transmission lines to realize a broadband transition between unbalanced and balanced lines. As such, the proposed mixer also has advantages of easy fabrication, good performance, and small size. Part of this work was published in [41].

5.2 Balanced SH Mixer

5.2.1 Mixer Structure

The proposed balanced SH mixer is shown in Figure 5.1. It consists of two anti-parallel diode pairs, a CPW-slot line balun, a tapered slot line T-junction, a tapered CPW-to-slot line ring divider, a CPW DC-blocking filter, a CPW RF-

choke and a CPW low-pass filter. All the three ports related to RF, LO and IF signals are interfaced to CPW input/output lines.

The balun makes use of a double-Y junction design strategy that transforms unbalanced line to balanced line with equal magnitude and 180° out-of-phase outputs. This is the key building block in realizing our broadband balanced SH mixer. In the uniplanar scheme, there are generally two types of baluns: Marchand baluns and double-Y baluns. The selection of the double-Y balun is because it features broadband and small-size properties. Such a balun combined with a hybrid circuit, namely, a tapered slotline T-junction and a tapered CPW-to-slotline ring divider, ensures that the LO and RF signals arrive at the diode pairs with 180° out-of-phase and in-phase, respectively, regardless of frequency. This is an important consideration of design for broadband operation.

In the topological arrangement of our mixer, the hybrid consists of the tapered slotline T-junction and the tapered CPW divider in connection with a $\lambda_{LO}/2$ slotline ring and two balanced CPW-format outputs. It is realized in a CPW-slotline configuration that makes use of the properties of a series slotline T-junction and a parallel CPW-slotline T-junction. The slotline T-junction has such a property that its outputs have a phase difference of 180° between them while the CPW-slotline T-junction offers in-phase outputs. Therefore, the reference point denoted by P' at which it yields a short circuit is a virtual ground (electrical wall) for the LO excitation (the right-hand side). The reference point P, on the other hand,

presents a virtual open circuit (magnetic wall) for the RF excitation (the left-hand side). As a consequence, the unbalanced signal from the CPW feed port cannot propagate cross the slotline T-junction into the slotline port, and also the balanced signal from the slotline feed port cannot propagate into the CPW port through the CPW-slotline junction where it faces a short circuit (grounding air-bridge). This is a very important design strategy that guarantees an inherent high isolation between the LO and RF/IF ports.

The low-pass filter is connected to the IF port for IF extraction. It is a four-section low-pass filter designed with CPW short-end-series (SES) stubs. The RF choke in the IF output circuit prevents the RF signal from propagating in the direction of the IF output. To reduce the radiation loss at the CPW open stub end of the RF chock circuit, the center conductor is tapered and the slot line open stub is circular. As such, anti-symmetrical CPW modal electric fields are cancelled out against each other as the coupled slots converge into the open aperture while the current smoothly varies from CPW branch line to circular stub. In the IF output branch, the combination of the RF choke and low-pass filter minimizes the matching requirement at the IF port, and it may suppress undesired spurious responses caused by the nonlinear devices. A DC-blocking filter is included in the RF port to serve IF and dc blocking. This DC-blocking filter is made with CPW open-end-series (OES) stubs having four sections.

Table 5.1 MDK2308-000 Diode Parameters

C_{j0}(pF)	I_s(A)	$R_s(\Omega)$	η	ϕ_{bi}(V)
0.05	0.5×10^{12}	4	1.02	0.82

5.2.2 Mixer Design

The proposed new type of balanced SH mixer is designed to operate at Ka-band for wideband applications. ALPHA DMK2308-000 GaAs antiparallel Schottky diodes are used in our design. The diode chip is 300μm $\times$ 660μm. The diode spice parameters (per junction) are shown in Table 5.1 as given by the manufacturer. The Schottky diode offers the high performance of low junction capacitance as well as low series resistance. Due to its leadless, it eliminates the problems associated with mounting of beam lead diodes.

The whole circuit design procedures are based on our developed generic algorithm in conjunction with linear and nonlinear simulations, presented in Chapter 2. This algorithm allows designing and optimizing the whole mixer structure with 5 decomposed blocks: the CPW-slotline double-Y balun, the hybrid, the DC-blocking filter, the low-pass filter and the RF-choke.

5.2.2.1 Optimum Loading Conditions

Balanced SH mixers are very sensitive to the loading of the nonlinear device at various idler frequencies. At LO, RF and IF, the device has a resistive load, but at

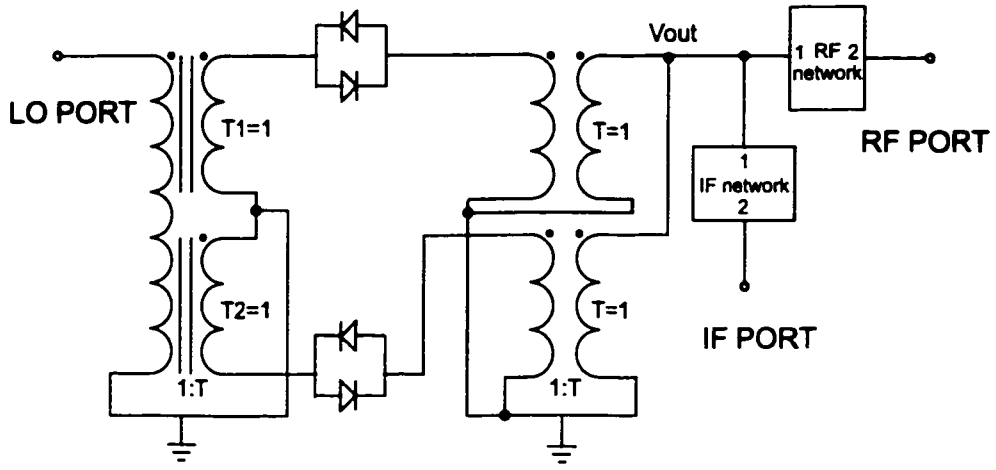

Figure 5.2 A modified generic circuit of a 180-deg balanced SH mixer.

all the other frequencies generated in the nonlinear device it should be loaded by reactive load to avoid power loss, which increases the conversion loss of the mixer. However, the mixer performance strongly depends on the nature of the reactive load (short, open, capacitive or inductive). According with our developed generic algorithm, it is possible to estimate optimum loads at idler frequencies derived from the ideal generic circuit model.

Considering the inherent properties of our new balanced SH mixers, namely, the reference point P is a virtual open circuit for the (even) CPW mode whereas the reference point P' presents as a short circuit for the (odd) slotline mode, we propose a modified model for the analysis of optimum loading conditions at idler frequencies. The model is shown in Figure 5.2. It incorporates two antiparallel diode pairs, two ideal transformers and two two-port ideal networks. The only two-port networks are presented by S parameter matrices as follows:

1. RF network:

   at the RF frequency,

$$\mathbf{S} = \begin{bmatrix} 0 & 1 \\ 1 & 0 \end{bmatrix} \tag{5.1}$$

   at all the other frequencies,

$$\mathbf{S} = \begin{bmatrix} e^{j\theta} & 0 \\ 0 & 1 \end{bmatrix} \tag{5.2}$$

2. IF network:

   at the IF frequency,

$$\mathbf{S} = \begin{bmatrix} 0 & 1 \\ 1 & 0 \end{bmatrix} \tag{5.3}$$

   at all the other frequencies,

$$\mathbf{S} = \begin{bmatrix} 1 & 0 \\ 0 & 1 \end{bmatrix} \tag{5.4}$$

At the idler frequencies it is enough to vary the angle θ of S_{11} of the RF network alone while keeping the angle of S_{11} of the other network at zero (namely, open

circuit), because the two networks are in parallel to the common point V_{out}.

The two networks provide the conditions necessary for the bandpass and low-pass filters. Using the harmonic balance simulator in MDS, the nonlinear analysis is performed to calculate the conversion loss versus the phase angle to be presented to diodes at various idler frequencies. The generic approach is implemented for the single frequency, namely, an RF frequency of 28 GHz and an LO frequency of 13.5 GHz as well as an IF frequency of 1 GHz ($f_{RF} - 2f_{LO}$). The harmonic balance analysis accounts for up to four harmonics, and thus there are three important idler signals: the $2f_{LO} + f_{RF}$ frequency of 55 GHz, the $4f_{LO} - f_{RF}$ of 26 GHz and the $4f_{LO} + f_{RF}$ of 82 GHz.

We follow the procedure outlined before. The results are depicted in Figure 5.3 and 5.4. In Figure 5.3 the conversion loss is plotted versus the S_{11} angle θ of the RF two-port network and the LO power level, varying the angle θ from 0^o to 360^o at the three idler frequencies and the power level from 0 dBm to 20 dBm. It indicates that the conversion loss is sensitively dependant on the load conditions at idler frequencies and tightly associated with the LO power drive. In Figure 5.4 the conversion loss under 10 dBm power level is highlighted versus the S_{11} angle θ of the RF two-port network. From these curves, it is seen that the worst performance occurs for an angle around 180^o, and the largest sensitivity is at the $2f_{LO} + f_{RF}$ frequency of 55 GHz as well as the optimum performance is achieved for 120^o at the $2f_{LO} + f_{RF}$ frequency of 55 GHz, 120^o at the $4f_{LO} - f_{RF}$ of 26 GHz and 150^o at

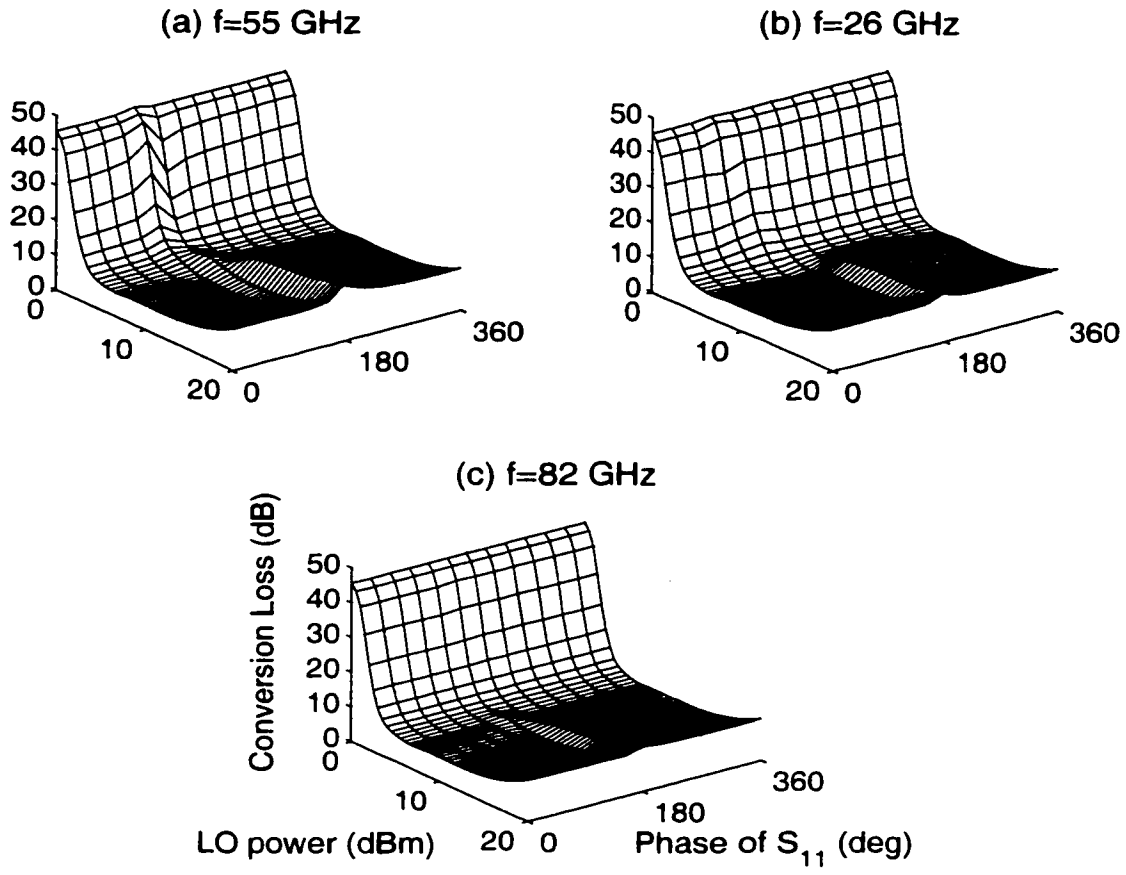

Figure 5.3 Conversion loss versus phase angle of S_{11} and LO power level.

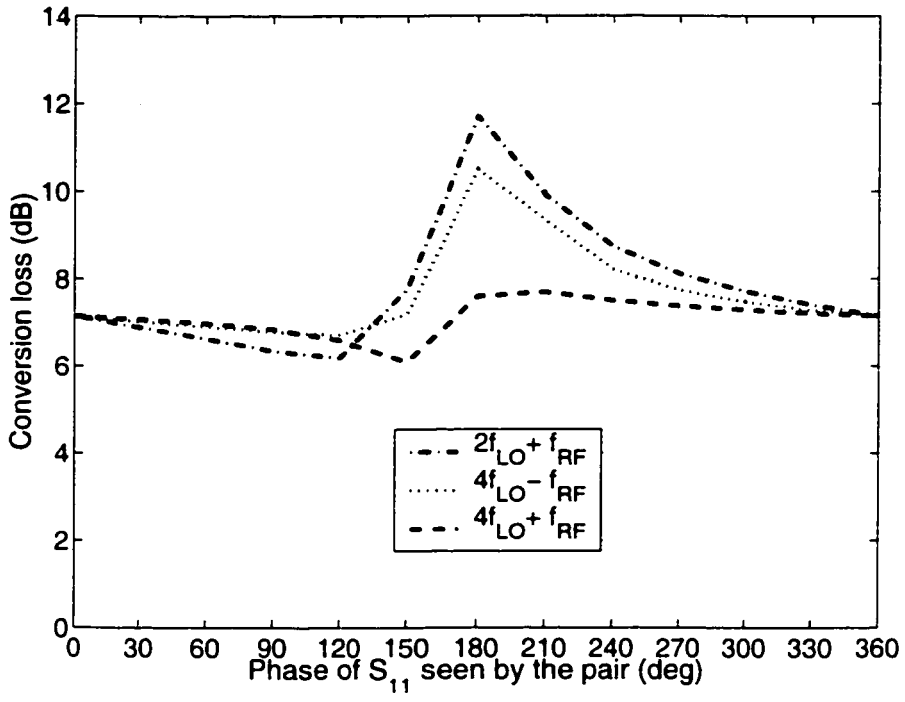

Figure 5.4 Conversion loss versus phase angle of S_{11}.

the $4f_{LO} + f_{RF}$ of 82 GHz. For these values, the best conversion loss is 6.2 dB. This is extremely good result for this type of mixer, and we do not expect to achieve it in practice. Nevertheless, this result can serve as the limiting performance. In our particular mixer, the RF and LO bandwidths are very large, and we do not expect to be able to design and build an optimal circuit over the entire bandwidth. Our objective is to design a practical circuit, which presents to the diode pair impedances as close as possible to the optimum derived from the ideal model.

Considering that the largest sensitivity takes place at the $2f_{LO} + f_{RF}$ frequency of 55 GHz, the optimum loading is determined only at the idler of $2f_{LO} + f_{RF}$ frequency. It also yields the flexibility in the design of band-pass and low-pass

filters because the $2f_{LO} + f_{RF}$ frequency is away from the RF bandwidth and the 3-dB frequency upper edge of the low-pass filter. The optimum termination of the diodes at such an idler frequency of $2f_{LO} + f_{RF}$ can be adjusted by varying the distance from the filters to the hybrid.

5.2.2.2 Design

Each building block is designed and optimized by use of the commercial electromagnetic (EM) simulators. The EM-based optimization may require more EM simulations. If the computed EM characteristics of the element circuits do not satisfy the overall circuit performance requirement, the geometry of the element circuits needs to be modified. In such a situation, numerous EM simulations are conducted to optimize the element circuits.

For the balun, a broadband CPW-slotline balun was well characterized and designed before. Our measured results show a very good performance with a low loss of about 1 dB over 3-20 GHz frequency range for the CPW-slotline balun. Since the balun is used for the subharmonic LO signal path, the low-loss frequency range is well suited to our Ka-band mixer design.

In Chapter 4, we compare a class of RF chokes with four different CPW open ends. As we know, the RF choke with the compensated CPW circular open stubs experimentally exhibits the best performance: radiationless and extremely wide bandwidth. It is good for use in the IF path to prevent the RF signal from propa-

gating in the direction of the IF port.

The hybrid is made of the tapered slotline T-junction and the tapered CPW divider in connection with a $\lambda_{LO}/2$ slotline ring and two balanced CPW-format outputs. Concerning the out-of-phase slotline feed port, the $\lambda/4$ sections used in the circuit are, in effect, quarter-wave shorted stubs and hence the input slotline with a characteristic impedance $2Z_0$ is matched to each Z_0 at the two balanced CPW ports. For the in-phase CPW feed port, the terminal impedances in the open-circuit plane P are infinite, so they have no electrical effect on the two balanced ports. Since the LO frequency approximately equals to 1/2 the RF frequency in our balanced SH mixers, we also use the $\lambda/4$ length section of the ring to design two-section impedance transformers to obtain a good match over a broadband of frequency that effectively transform the input CPW line to each Z_0 at the two balanced ports by the two intermediate sections: $Z_1 = 1.53Z_0$ and $Z_2 = 1.16Z_0$. At the two balanced CPW ports, there are two tapered CPW lines needed for matching Z_0 to the RF impedance of the anti-parallel diode pair. The whole hybrid is designed and optimized through the electromagnetic simulations with the aid of HP Momentum.

The DC-block filter is a four-section filter. Its physical dimensions are synthesized with the aid of HP Momentum. An experimental circuit is fabricated on alumina substrate ($\epsilon = 9.9$, h=10 mil). Its experimental and simulated results are shown in Figure 5.5, which are in good agreement. It should be explained that we measure the circuit over 1-40 GHz frequency range since the probe pitches

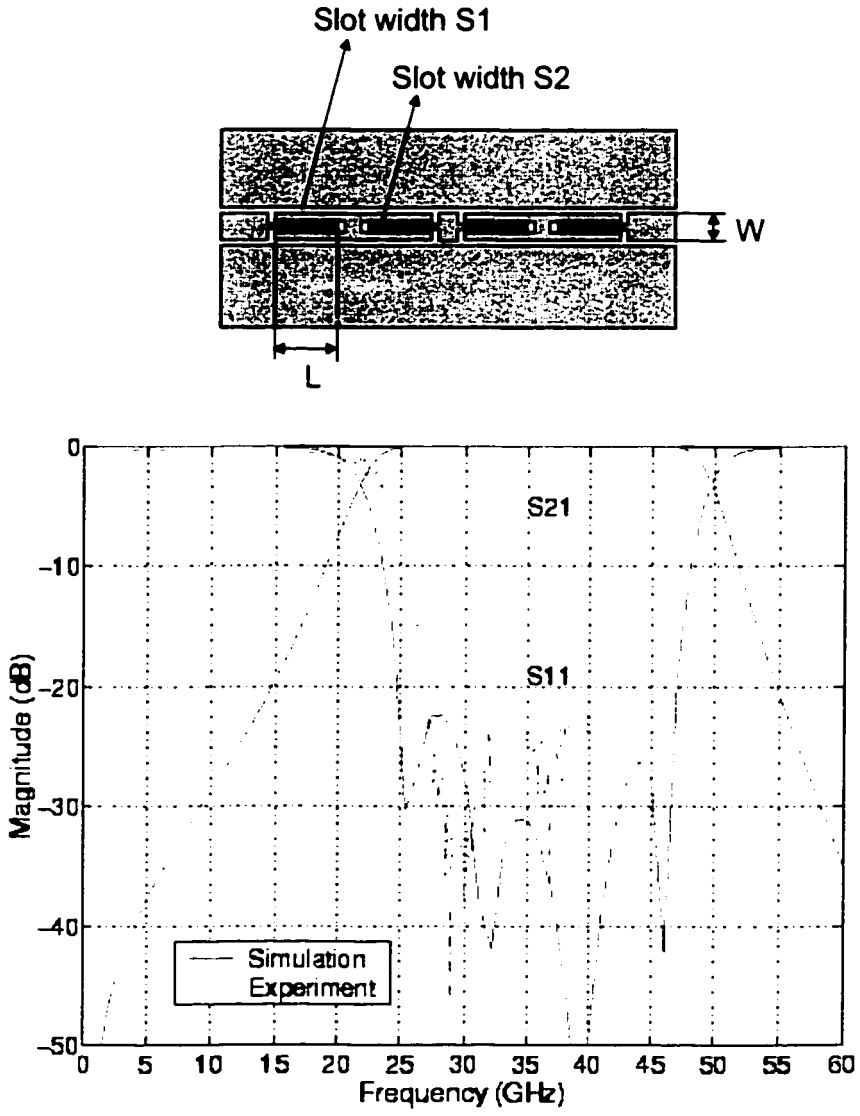

Figure 5.5 Frequency response of the DC-blocking filter. Geometrical dimensions are $S_1 = 3.2$ mil, $S_2 = 1$ mil, W=8 mil, L=32 mil and thickness of alumina is equal to 10 mil

work well up to 40 GHz. However, from the simulated result it would be expected that the designed filter may have a good rejection of the idler at the frequency of $2f_{LO} + f_{RF}$ from the devices.

The low-pass filter is also a four-section filter. Its physical dimensions are synthesized using HP Momentum. An experimental circuit is fabricated on alumina substrate. Its experimental and simulated results are shown in Figure 5.6, which are also in good agreement. Similarly, the measured upper edge is 40 GHz due to our probe pitches. From the simulated results, it can be seen that the designed filter may have a good rejection of the idler at the $2f_{LO} + f_{RF}$ frequency.

For an effective theoretical modeling of the whole mixer, the proposed uniplanar structure is decomposed into six parts (see Figure 5.1), namely, the double-Y balun, the hybrid, the DC-blocking filter, the RF choke, the low-pass filter and the two diode pairs. Each building block model is determined by electromagnetic (EM) studies of planar circuit using HP Momentum. EM-simulated S parameters describe properties of the building block models. The diode pairs are simulated by a nonlinear PN junction diode model available in the HP-MDS component library. By combining the S-parameter equivalent models for the five building blocks, one may establish a complete equivalent model for the balanced SH mixer as shown in Figure 5.7. With this equivalent model, we can more effectively simulate the mixer circuit using a nonlinear harmonic balance simulator implemented in MDS.

Figure 5.8 shows the simulated performance of the proposed balanced SH mixer

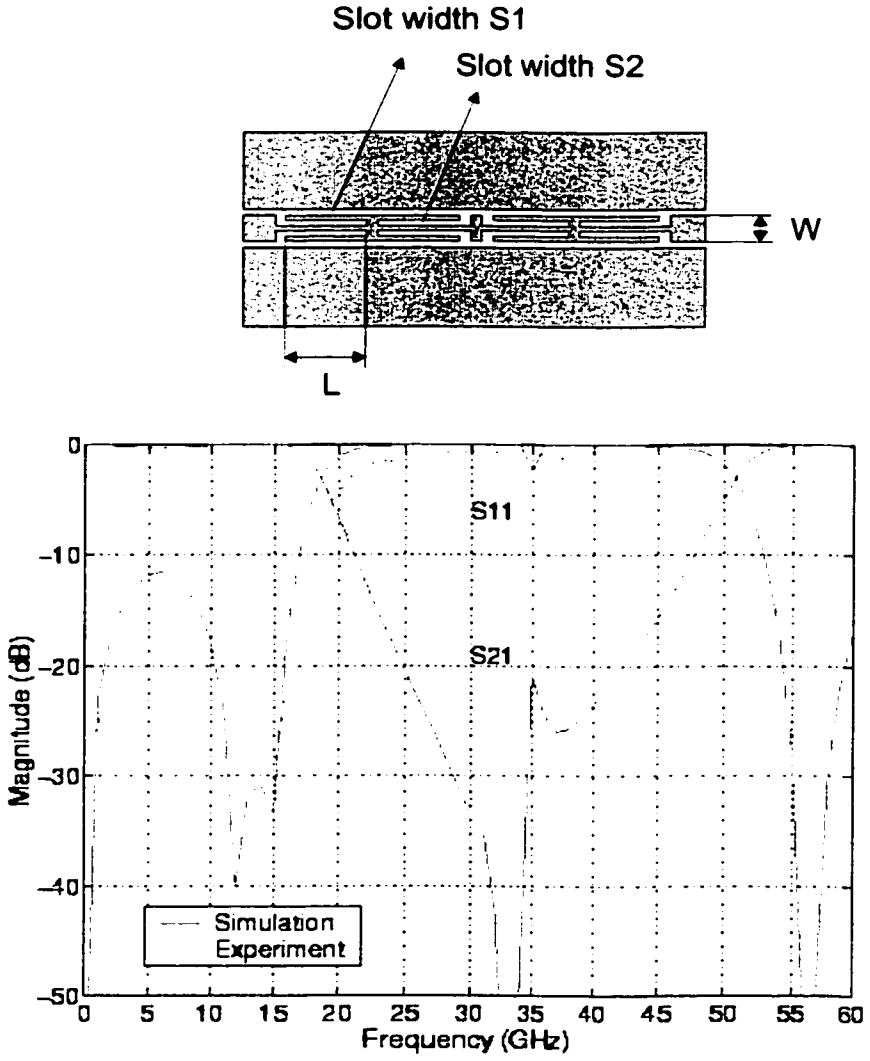

Figure 5.6 Frequency response of the low-pass filter. Geometrical dimensions are $S_1 = 3.2$ mil, $S_2 = 1$ mil, W=8 mil, L=35 mil and thickness of alumina is equal to 10 mil.

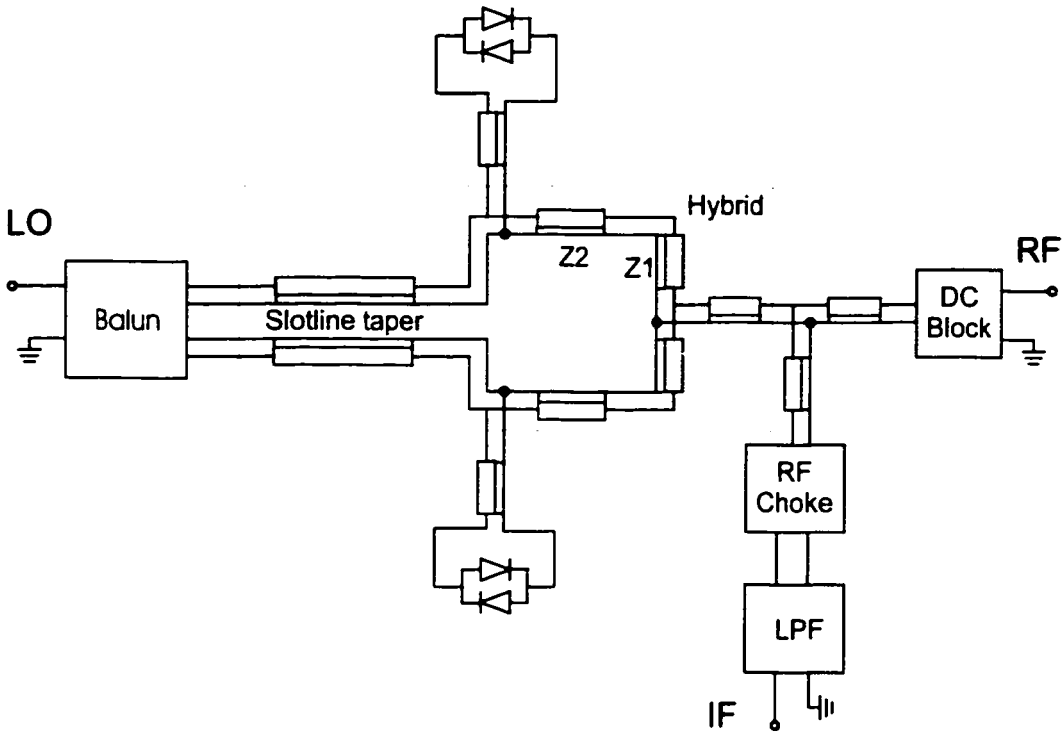

Figure 5.7 Equivalent network model for the proposed broadband uniplanar balanced SH mixers.

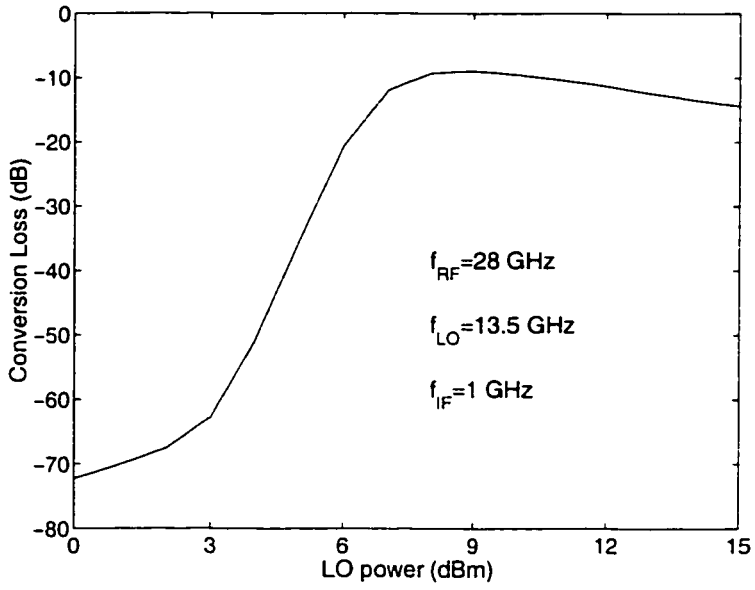

Figure 5.8 Model-simulated conversion loss versus the LO pumped power level.

as shown in Figure 5.1. A minimum conversion loss of 8.9 dB is predicted for 28-GHz RF, 1-GHz IF and 9 dBm LO power. Since the simulations are based on the idealized transmission line components, additional losses due to ohmic effects and radiations are not accounted for in the models. The additional loss in the DC-blocking filter over the simulated loss is determined from the measured S-parameter value that is about 1.2 dB from 26 to 36 GHz (see Figure 5.5). The measured insertion loss of the fabricated low-pass filter is approximately 1 dB below 8 GHz (see Figure 5.6). As such, the combined RF and IF losses in the passive networks will result in a realistic conversion loss that should be roughly 2 dB higher than predicted by the simulation. Therefore, we expect to obtain a conversion loss around 11 dB with this design scheme.

5.2.3 Mixer Performance

The balanced SH mixer sample is fabricated with our miniaturized hybrid MIC process on a 10 mil thick ceramic substrate with a dielectric constant of 9.9. The overall chip size is 590×430 mil^2. Two diode pair chips are flip-chip mounted on the line with silver epoxy. Air-bridges are included at various points in the circuit, particularly junctions, to suppress the excitation of some undesired slotline (even) modes in the CPW lines. The mixer is tested with 68 um-pitch 40 GHz coplanar waveguide probes. The RF source is an HP 8510C Network Analyzer. The LO source is a 68147A Synthesized Sweep Generator. The IF signal is extracted by a

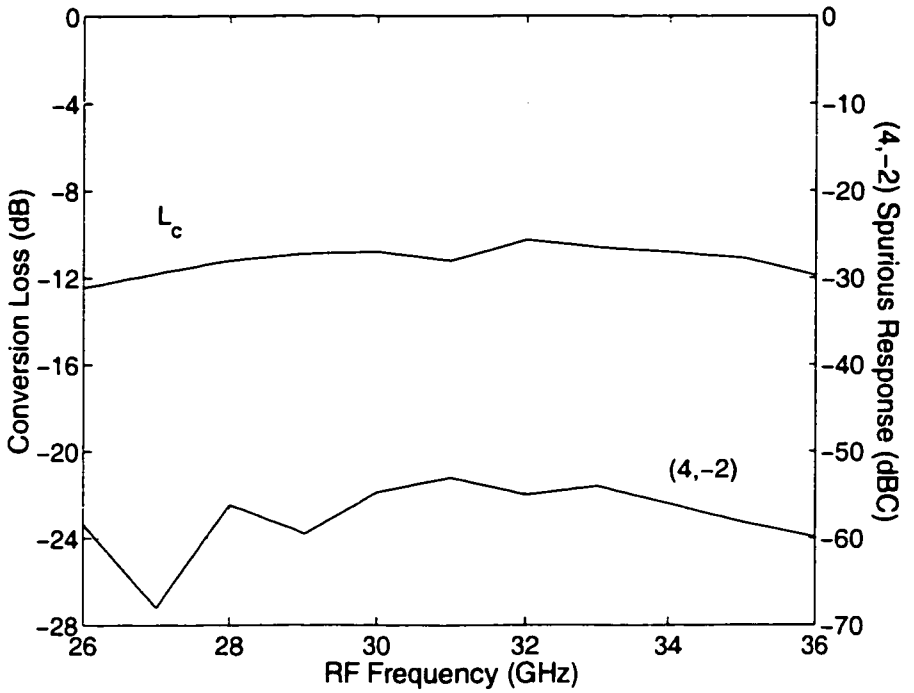

Figure 5.9 Measured frequency response of the conversion loss and (4, -2) spurious-response output level; $P_{RF} = -15$ dBm, $P_{LO} = 11$ dBm. The LO and RF signals are swept from 12.5 to 17.5 GHz and 26 to 36 GHz, respectively.

third probe and the IF power level is measured using a spectrum analyzer. The cable, probe and connector transition losses at the RF, LO and IF frequencies are determined using a calibration approach and are de-embedded from the measured data.

Figure 5.9 shows the measured conversion loss and (4, -2) spurious-response level at a fixed IF frequency of 1 GHz; the RF signal is swept from 26 to 36 GHz and the LO is from 12.5 to 17.5 GHz with the 11-dBm power injected at the LO port. The conversion loss is found to smoothly vary from 10 to 12 dB. Considering that the above-assessed 2-dB loss is added to the simulated conversion loss, a very good

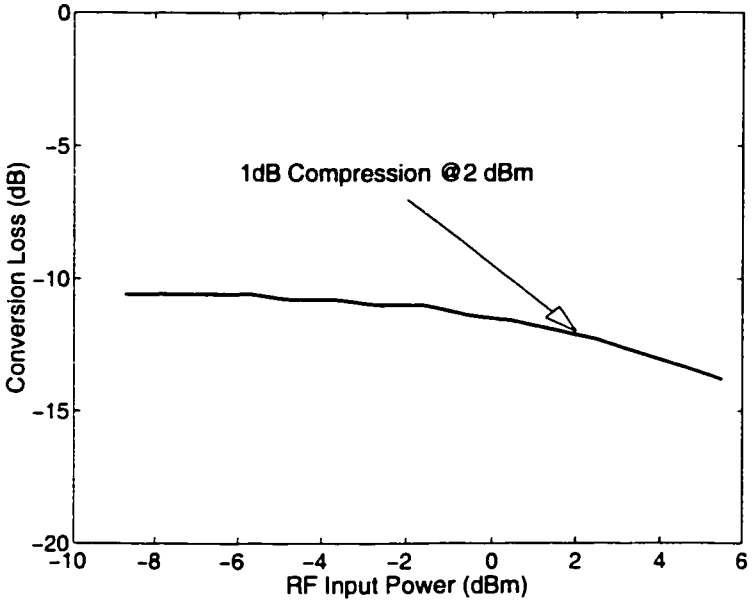

Figure 5.10 Measurement of input 1 dB compression power: f_{RF} = 28 GHz, f_{LO} = 13.5 GHz and P_{LO} = 11 dBm.

agreement can be observed between measurement and simulation. The measured (4, -2) spurious response is well below -50 dBC over the entire band of interest. Such a good suppression of (4, -2) spurious response significantly reduces the distortion on the IF signal. In addition, the (4, -1) spurious response and the second-order LO harmonic level are not easy to read over most of the 28-36 GHz RF frequency range due to the noise floor of our HP spectrum analyzer. Nevertheless, it can readily be estimated that the proposed mixer architecture has the distinct advantages of high suppression of even-order harmonics and some spurious responses.

Figure 5.10 shows the measured conversion loss versus the RF power used to determine a 1-dB compression level of the mixer. When the RF is fixed at 28 GHz and the LO is at 13.5 GHz with the 11-dBm LO power, a swept power measurement

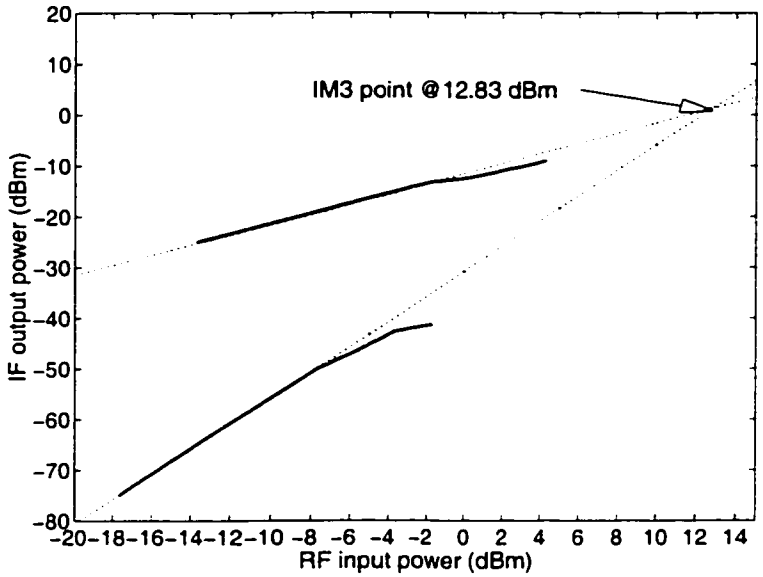

Figure 5.11 Measured first- and third-order IF power outputs as a function of the RF input power for third-order intermodulation product measurements of the proposed balanced SH mixer: f_{RF1} = 28 GHz, f_{RF2} = 28.006 GHz. The LO is fixed at 13.5 GHz with 11 dBm.

yields an input P_{1dB} of about 2 dBm.

Figure 5.11 plots the IF output power and its third-order intermodulation product (IM3) versus the RF input power. The mixer is excited by two RF input signal tones having equal magnitude and two closely spaced frequencies of 6 MHz. The two RF signal tones are delivered via a 3-dB combiner applied at two input ports by two RF sources: one is 8510C Network analyzer while the other is 6740B Sweep Frequency Synthesizer. The third-order input intercept point (IP3) is determined to be 12.83 dBm under the 11-dBm LO driving at a fixed IF frequency of 1 GHz.

Figure 5.12 depicts the measured LO-to-RF and LO-to-IF isolations as well as RF-to-IF isolation characteristics. Generally, the measured LO-to-RF and LO-to-

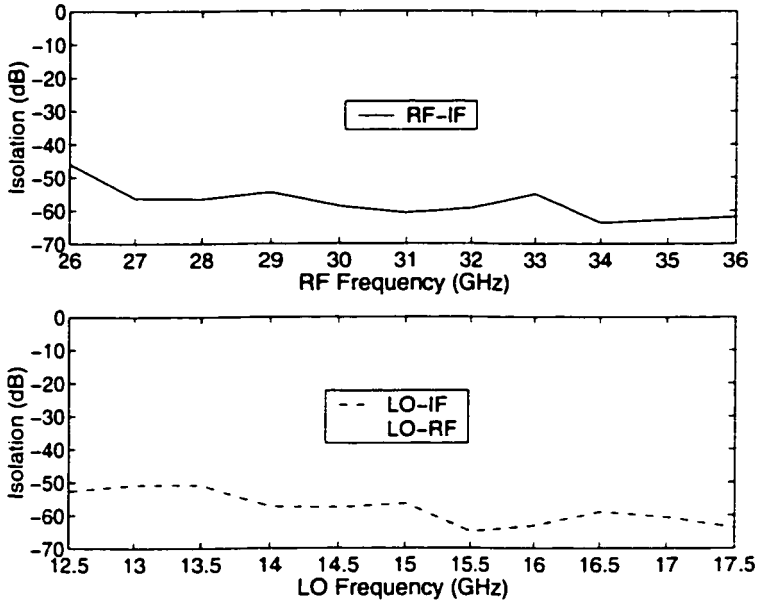

Figure 5.12 Broadband characteristics of the LO-to-RF, LO-to-IF and RF-to-IF isolations of the balanced SH mixer.

IF isolations are higher than 50 dB over the LO frequency range spanning 12.5-17.5 GHz. The RF-to-IF isolation is also higher than 50 dB over the RF frequency range of 27-36 GHz. To our knowledge, this is the first time to report such a high isolation performance for a uniplanar mixer operating at millimeter-wave frequencies.

5.3 Improved Broadband Balanced SH Mixer

The previous mixer sample experimentally demonstrated a good performance over a RF bandwidth of 26-36 GHz driven by a subharmonic LO source of 12.5-17.5 GHz. However, the operation of such a type of uniplanar balanced SH mixer can be improved, over a wider bandwidth, if a few modifications are made on the basis of the previously designed mixer.

In the chapter 3, two versions of CPW-slotline double-Y baluns have been presented. The second one synthesized at the upper edge of 26 GHz shows an extremely good performance with a smaller size and a low insertion loss of less than 1 dB over a 5-30 GHz. This circuit is used as the balun block instead of the old one in the previous mixer circuit. Regarding the slot line ring, the two-section impedance transformers are redesigned to obtain a good match over a wider broadband of RF frequency. The two intermediate sections of the impedance transformers are designed as $Z_1=1.51Z_o$ for first section and $Z_2=1.15Z_o$ for second section.

The low-pass filter and DC-block filter characteristics are redesigned by changing the lengths of open-end series stubs and short-end series stubs, in order to achieve a wider bandwidth operating performance. An adequate combination of low-pass filter and DC block filter as well as RF choke in front of the slot line ring is made to be a trade-off between low conversion loss and high isolations.

The modified balanced SH mixer is fabricated on a 10 mil think ceramic substrate with a dielectric constant of 9.9. The overall size chip is 620×460 mil^2. Similarly, two diode pair chips (ALPHA DMK2308-000) are flip-chip mounted on the line with silver epoxy. Air-bridges are included at various points in the circuit, particularly junctions, to suppress the excitation of some undesired slotline (even) modes in the CPW lines. The mixer is tested with 68 μm-pitch 40 GHz coplanar waveguide probes.

Figure 5.13 shows the measured conversion loss at a fixed IF frequency of 1

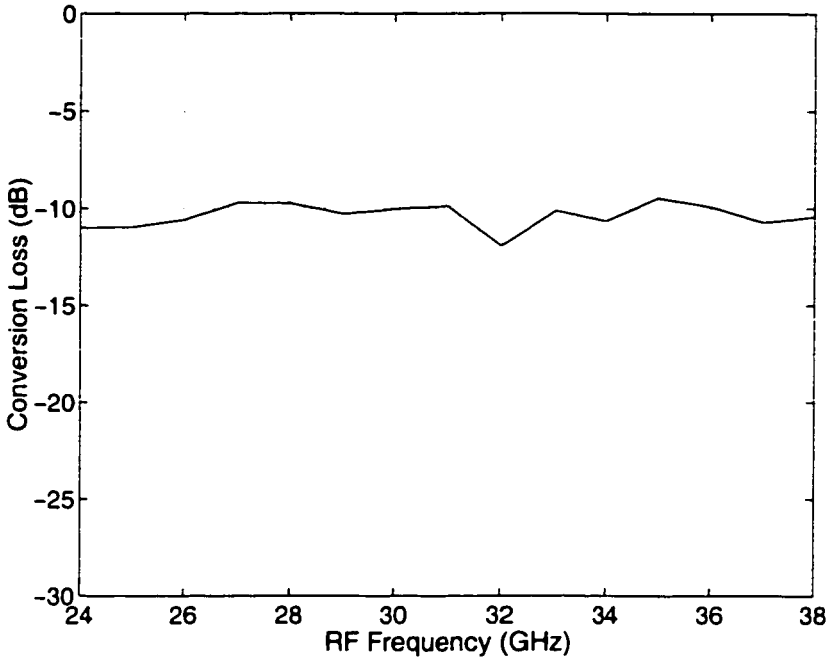

Figure 5.13 Measured conversion loss of the modified mixer. The LO and RF are swept from 11.5 to 18.5 GHz and 24 to 38 GHz.

GHz: the RF signal is swept from 24 to 38 GHz and the LO is from 11.5 to 18.5 GHz with the 10-dBm power injected at the LO port. The conversion loss is found to smoothly vary from 9.5 to 12 dB over the entire range of RF frequency. The (4, -1) and (4, -2) spurious response at the IF port are not easy to read over most of RF frequency range due to the noise floor of our HP spectrum analyzer. Nervetheless, it can readily be estimated that the new version of mixer architecture has the distinct advantages of high suppression of some spurious responses.

Figure 5.14 depicts the measured LO-to-IF and RF-to-IF isolations. The LO-to-IF isolation is higher than 50 dB over the 11.5-18.5 GHz LO frequency range. The RF-to-IF isolation is higher than 45 dB over the 25-38 GHz RF frequency

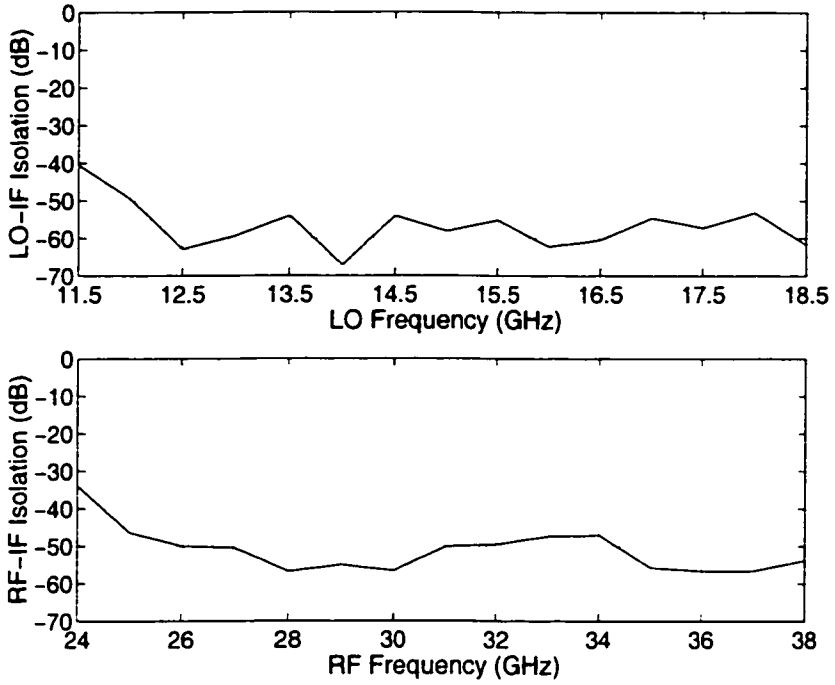

Figure 5.14 Measured LO-to-IF and RF-to-IF isolations.

range. In addition, the 2LO-to-IF isolation can be estimated to be higher than 55 dB since the output power level at the IF port is below the noise floor of the spectrum analyzer over most of the 2LO frequency range.

Figure 5.15 plots the measured LO-to-RF and 2LO-to-RF isolations. The LO-to-RF isolation is higher than 45 dB over the LO frequency range of 11.5-18.5 GHz. The 2LO-to-RF isolation is higher than 55 dB over the entire LO frequency range.

The modified mixer indicates a visible improvement of bandwidth and conversion loss over the first version of mixer, even though the isolations between ports are not so high as for its counterpart. Also we expect that the modified mixer may work well up to 40 GHz because the measured upper edge of 38 GHz is limited by

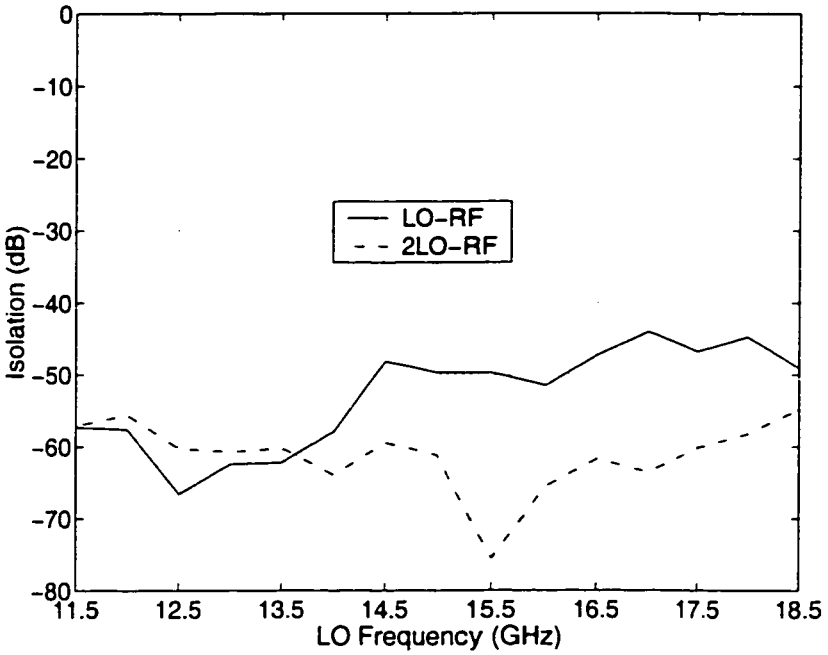

Figure 5.15 Measured LO-to-RF and 2LO-to-RF isolations.

the LO power level of our 68147A Synthesized Sweep Generator.

5.4 Conclusion

A new uniplanar architecture of broadband balanced subharmonically pumped mixer has been proposed and demonstrated with a small-size hybrid chip. This mixer scheme studied both theoretically and experimentally consists of a broadband miniaturized double-Y balun and other innovative uniplanar building blocks that enable achieving some unparalleled advantages.

This architecture has shown an impressive broadband performance that features very good conversion loss, record-high isolation between ports and excellent suppression capability of even-order harmonics and some spurious signals. The

proposed architecture allows reducing the demand on LO source so that it is very useful for low-cost millimeter-wave transceiver design.

CHAPTER 6

A NOVEL UNIPLANAR BALANCED SUBHARMONICALLY PUMPED MIXER WITH FINITE GROUND PLANES

6.1 Introduction

As shown in the previous chapters, a balanced SH mixer is very useful at millimeter wave frequencies in light of its advantages of subharmonic pumping, inherent local oscillator (LO) noise suppression, the rejection of certain spurious responses and the enhancement of inherent LO-to-RF isolation. For the application requirement of broadband millimeter-wave wireless systems, we have proposed a new type of uniplanar broadband balanced SH mixer. The designed two versions of balanced SH mixers have experimentally demonstrated an impressive performance with a low and flat conversion loss, a high isolation between ports and excellent suppression of some unwanted LO/RF harmonics and mixing frequency responses over a wide bandwidth of RF operating frequency. The mixers were made of CPW and slot lines. Such a mixer can be seen as a balanced SH mixer with infinite ground planes.

In the coplanar scheme, another kind of coplanar transmission line, Coplanar Strip (CPS), is also useful to build uniplanar circuits to save circuit space and make circuits compact. It may also be used to suppress the leakage due to parallel-plate

mode or dielectric slab mode caused by infinite grounded CPW discontinuities. In our previous work, we already used the CPS coplanar transmission line to realize a CPW_{fgp}-CPS double-Y balun. The designed double-Y balun has demonstrated low-loss and small-size properties through our experimental results, as outlined in Chapter 3.

In this chapter, we propose another type of uniplanar broadband subharmonically pumped mixer, which is implemented in CPW_{fgp} and CPS format. This type of mixer can similarly be regarded as a balanced SH mixer with finite ground planes. In this work, the design procedure of balanced SH mixer with infinite ground planes is applied to the design of its counterpart with finite ground planes.

6.2 Mixer with Finite Ground Planes

6.2.1 Structure and Design

The scheme layout of the proposed uniplanar balanced subharmonically pumped mixer is shown in Figure 6.1. Similar to the mixer with infinite ground planes, the mixer with finite ground planes consists of two anti-parallel diode pairs, a CPW_{fgp}-CPS balun, a tapered CPS T-junction, a tapered CPW_{fgp}-to-CPS ring divider, a CPW_{fgp} DC-blocking filter, a CPW_{fgp} RF-choke and a CPW_{fgp} low-pass filter. All the three ports related to RF, LO and IF signals are interfaced to CPW_{fgp} input/output lines.

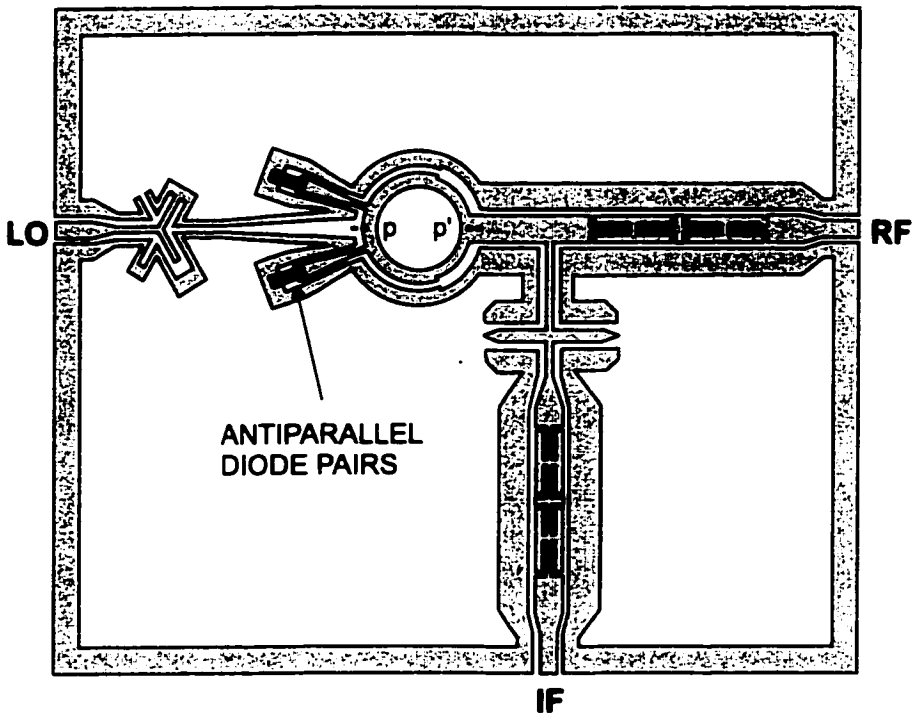

Figure 6.1 Proposed architecture of balanced SH mixer with finite width ground plane.

According to the developed technique of the double-Y baluns, we have designed a CPW$_{fgp}$-CPS double-Y balun which was synthesized at the upper edge of 16 GHz. Our measured results indicate that the designed CPW$_{fgp}$-CPS balun offers a good performance with a low insertion loss less than 1.5 dB and a good VSWR less than 1.3 over a broadband of DC-20 GHz frequency range. Since the balun is used for the subharmonic LO path, the low-loss frequency range is well suited to the proposed mixer design.

The hybrid is a combination of the tapered CPS T-junction and the tapered CPW$_{fgp}$ divider in connection with a $\lambda_{LO}/2$ CPS ring and two balanced CPW$_{fgp}$

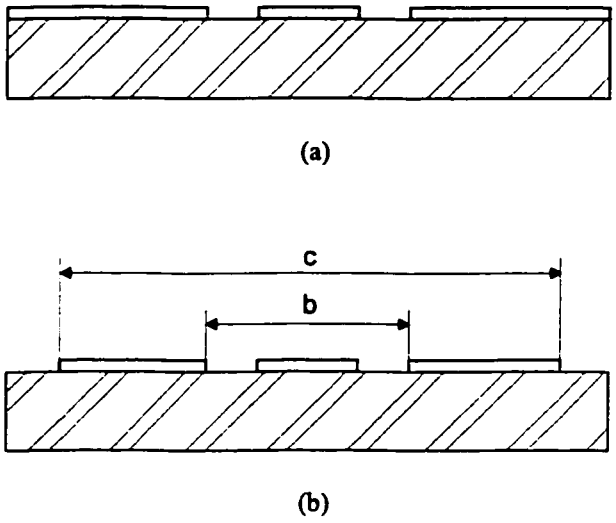

Figure 6.2 Two types of coplanar waveguide transmission lines: (a) CPW with infinite width ground planes; (b) CPW with finite width ground planes.

format outputs. Judging from the balanced characteristics of CPS and slotline, the hybrid should have the same properties as the one in the previous mixer with infinite ground planes. The reference point denoted by P' at which it yields a short circuit is a virtual ground (electrical wall) for the LO excitation (the right-hand side). The reference point P presents a virtual open circuit (magnetic wall) for the RF excitation (the left-hand side). This arrangement guarantees a high isolation between the LO and RF/IF ports. Meanwhile, the $\lambda_{LO}/2$ length of the CPS ring is also used to design two-section impedance transformers to obtain a good match over a broadband of frequencies. The intermediate sections of the impedance transformer are designed as $Z_1=1.53Z_o$ and $Z_2=1.16Z_o$. Its physical dimensions for the hybrid are synthesized using HP Momentum.

CPW with infinite width ground planes can be seen as CPW_{fgp} with the ground

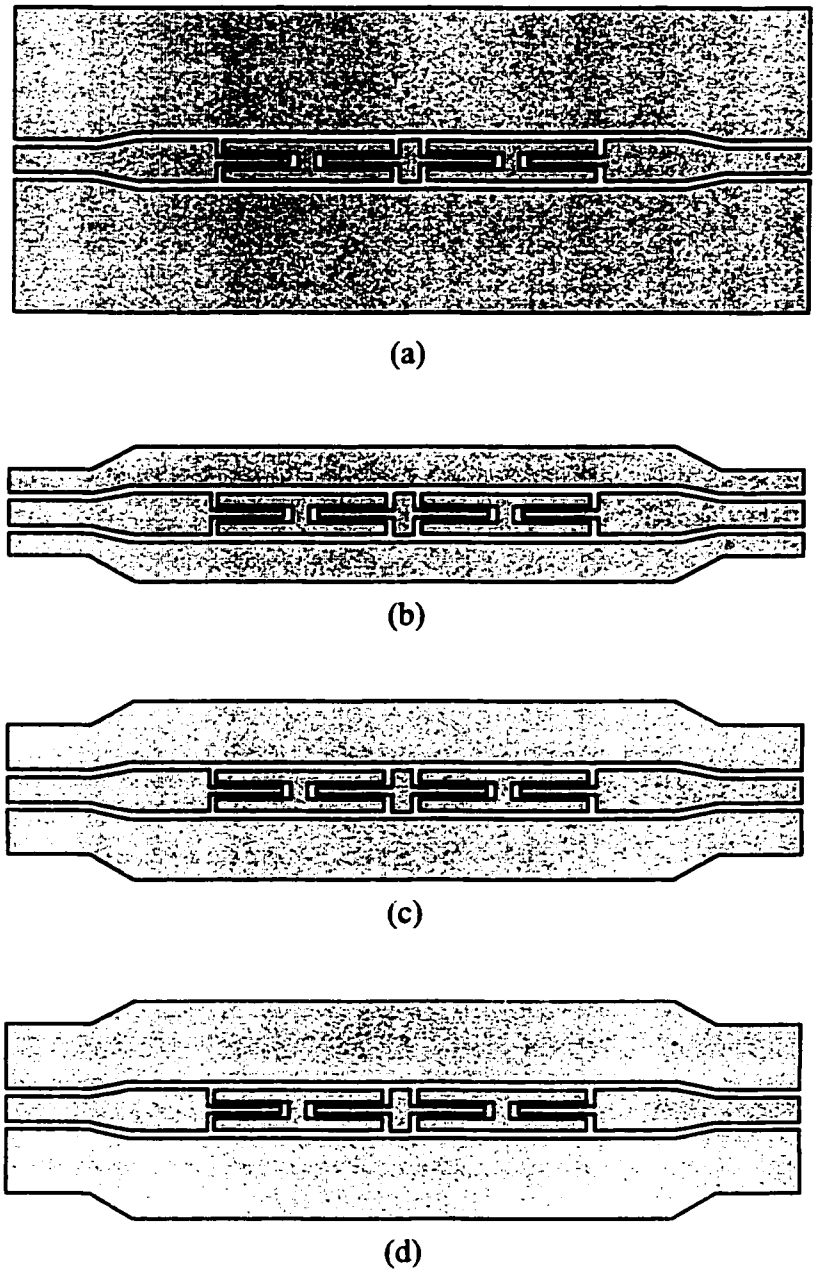

Figure 6.3 A class of CPW DC-block filters with infinite width as well as with three different widths: (a) with infinite ground width, (b) with c/b=3.8, (c) with c/b=4.5, (d) with c/b=5.

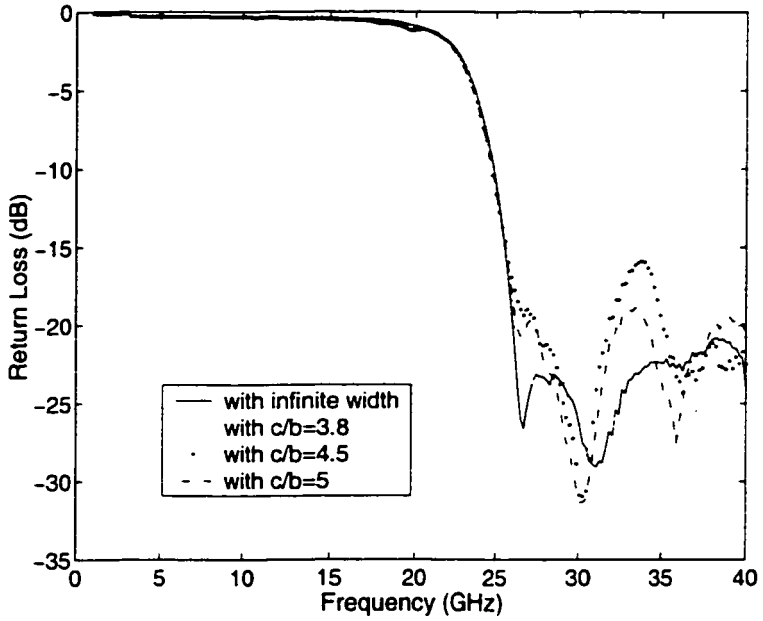

Figure 6.4 Measured results of a class of DC-block filters.

width approaching to be infinite, as illustrated in Figure 6.2. Theoretical studies [42] indicate that the CPW$_{fgp}$ characteristics are close to the CPW ones when c/b>3. As a result, our previous design approaches for the CPW DC-block filter, RF choke and low-pass filter are directly applied to the CPW$_{fgp}$ ones. For the purpose of comparison, a class of DC-block filters with three different ground plane widths (c/b=3.8, 4.5, 5) as well as with infinite width is fabricated on a 10-mil alumina substrate, as shown in Figure 6.3. Accurate measurements are performed over the frequency band of interest (1-40 GHz), and measured results are plotted in Figure 6.4. It is shown that it would be better to choose the finite ground plane width with c/b> 5. However, concerning our realizable mixer structure, we select the ratio c/b to be 4.5.

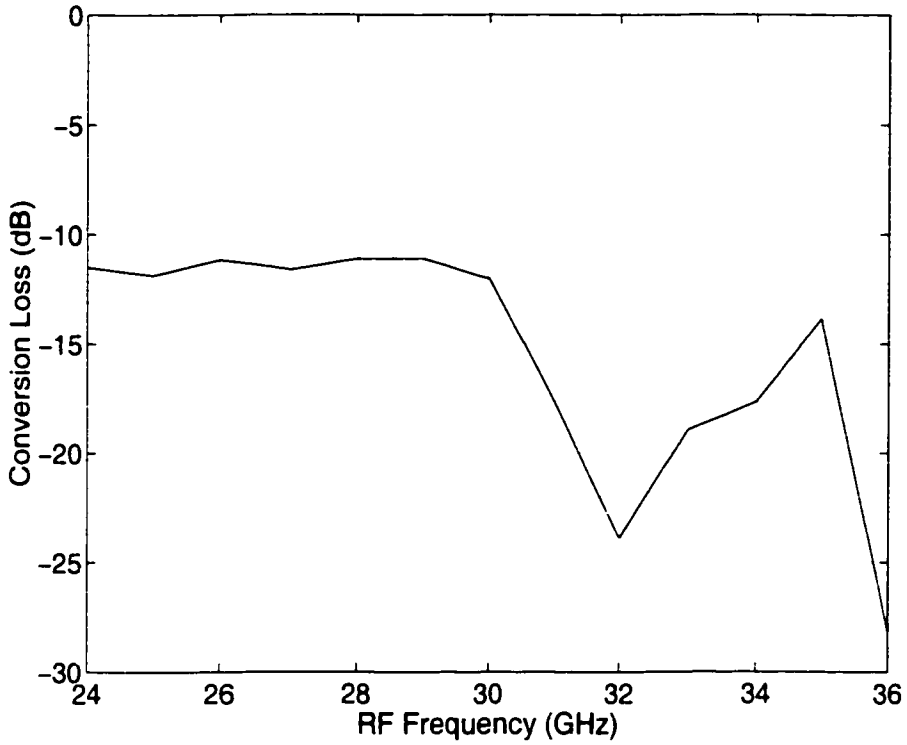

Figure 6.5 Measured conversion loss of the modified mixer. The LO and RF are swept from 11.5 to 18.5 GHz and 24 to 36 GHz.

Here, we should mention that there is a little difference in the RF choke circuit between CPW and CPW$_{fgp}$ formats. In the CPW$_{fgp}$ RF choke, a circular open stub is taken away (see Figure 6.1). The reason is that the circular open stub is too close to the CPS ring and it would affect the CPS transmission characteristics in the ring.

6.2.2 Performance

The proposed balanced SH mixer with finite width ground planes is fabricated on a 10 mil think ceramic substrate with a dielectric constant of 9.9. The overall

size chip is 600×460 mil^2. Two diode pair chips (ALPHA DMK2308-000) are flip-chip mounted on the line with silver epoxy. Air-bridges are included at various points in the circuit, particularly around the junctions, to suppress the excitation of some undesired slot (even) modes in the CPW$_{fgp}$ lines. The mixer is tested with 68 μm-pitch 40 GHz coplanar waveguide probes.

For the purpose of comparison, the designed mixer circuit is tested over 24-36 GHz RF frequency range. Figure 6.5 shows the measured conversion loss at a fixed IF frequency of 1 GHz: the RF signal is swept from 24 to 36 GHz and the LO is from 11.5 to 17.5 GHz with the 10-dBm power injected at the LO port. It is noted that the conversion loss smoothly varies from 11 to 12 dB over a 24-30 GHz RF range. However, beyond the 30 GHz RF frequency, the conversion loss has significantly been deteriorated.

Figure 6.6 depicts the measured LO-to-IF and RF-to-IF isolations. The LO-to-IF isolation is higher than 35 dB over a LO frequency range of 11.5-17.5 GHz. The RF-to-IF isolation is higher than 40 dB over most of RF frequency range.

Figure 6.7 plots the measured LO-to-RF and 2LO-to-RF isolations. The LO-to-RF isolation is higher than 40 dB over the LO frequency range of 11.5-17 GHz. The 2LO-to-RF isolation is higher than 55 dB over the entire LO frequency range.

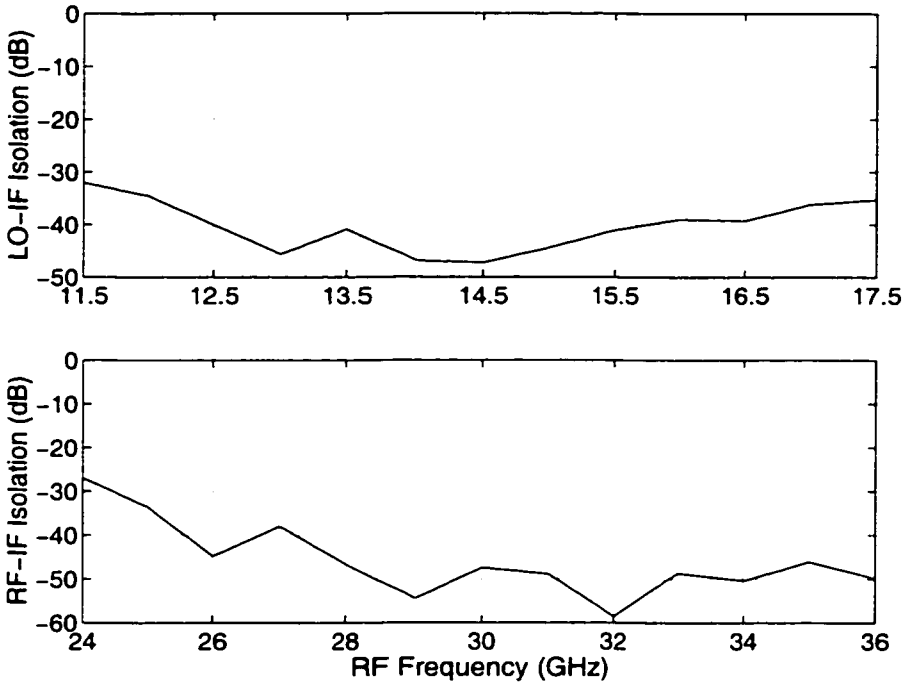

Figure 6.6 Measured LO-to-IF and RF-to-IF isolations.

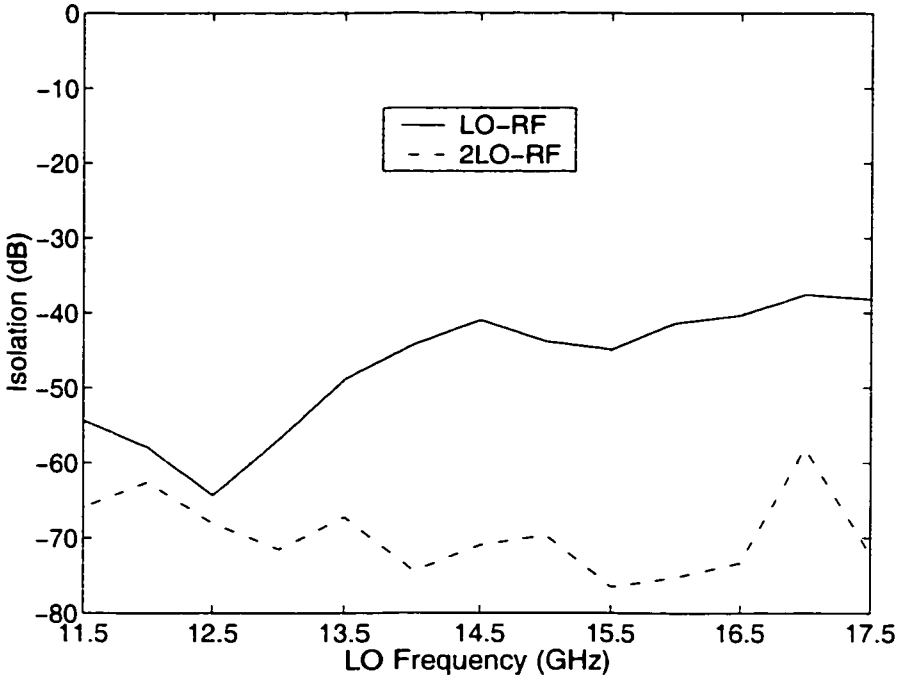

Figure 6.7 Measured LO-to-RF and 2LO-to-RF isolations.

6.3 Discussion

As presented above, the design method for the balanced SH mixer with infinite ground planes is directly applied to the design of the balanced SH mixer with finite ground planes. Especially, the physical dimensions of the CPW DC-block filter, RF choke and low-pass filter are the same as the ones of the CPW_{fgp} DC-block filter, RF choke and low-pass filter in the second version of balanced SH mixer with finite ground planes. However, the actual measured results of both structures are different. The mixer with finite ground planes has a good and flat conversion loss only over a narrow bandwidth of 24-30 GHz RF frequency. And also its isolations between ports are not so high as more than 45 dB over the entire RF or LO frequency range. The main problem causing narrow bandwidth performance may be coming from the significant discontinuities in the CPS-CPW_{fgp} parallel T-junctions and CPS ring.

Hence, we built two balanced SH mixer circuits with a little difference, as shown in Figure 6.8. In comparison to the previous mixer structure, the only difference is in the present the DC-block filter having two sections. As a result, the overall chip size is smaller and it is 540×460 mil^2.

For the two mixer, a small difference is in the T-junction of the tapered CPW_{fgp}-to-CPS ring divider. In the first structure, the connection between CPS and CPW_{fgp} is made common by extending the center conductor of CPW_{fgp} line to

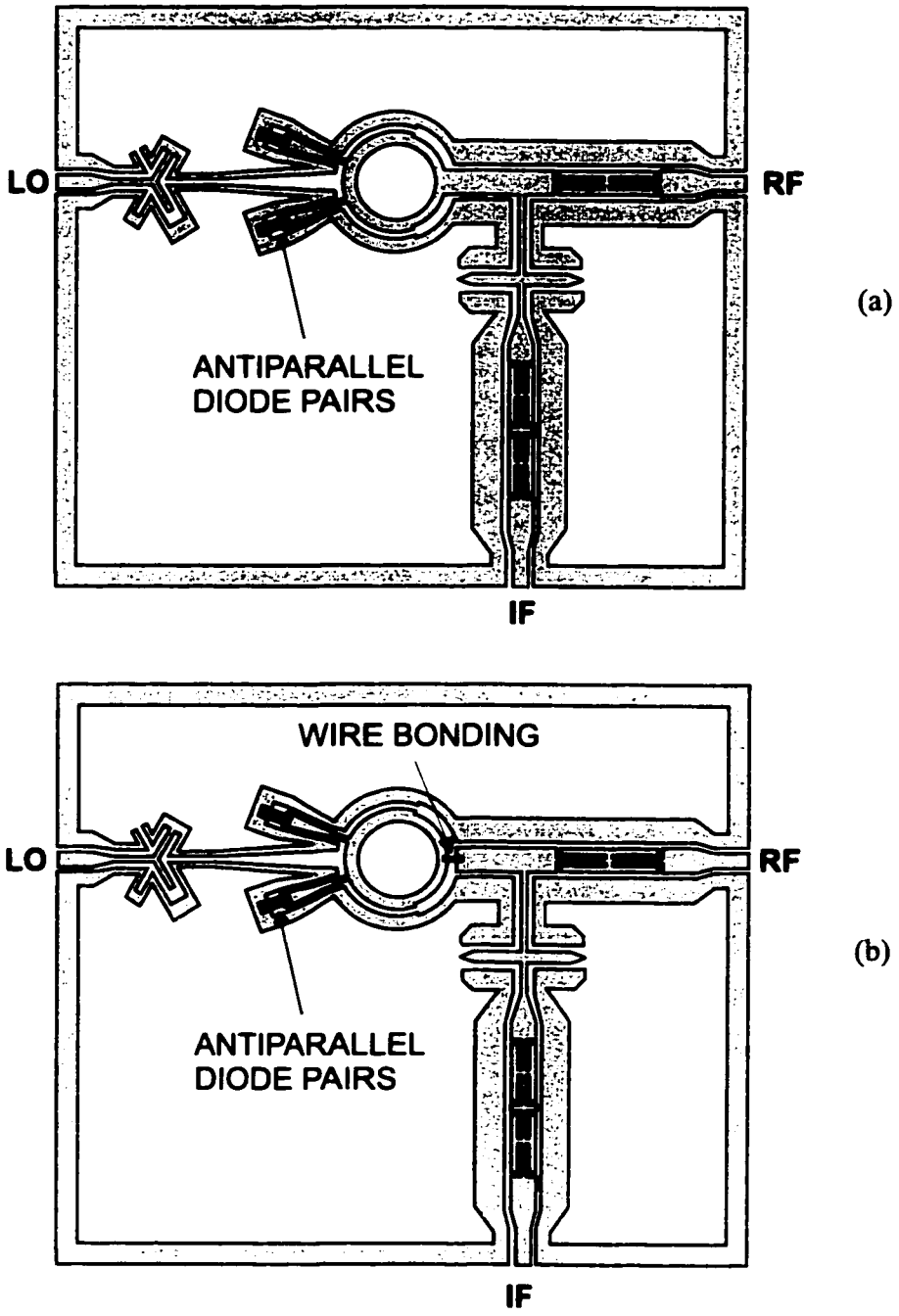

Figure 6.8 Two different balanced SH mixers with finite width ground plane: (a) without wire connection and (b) with a wire connection.

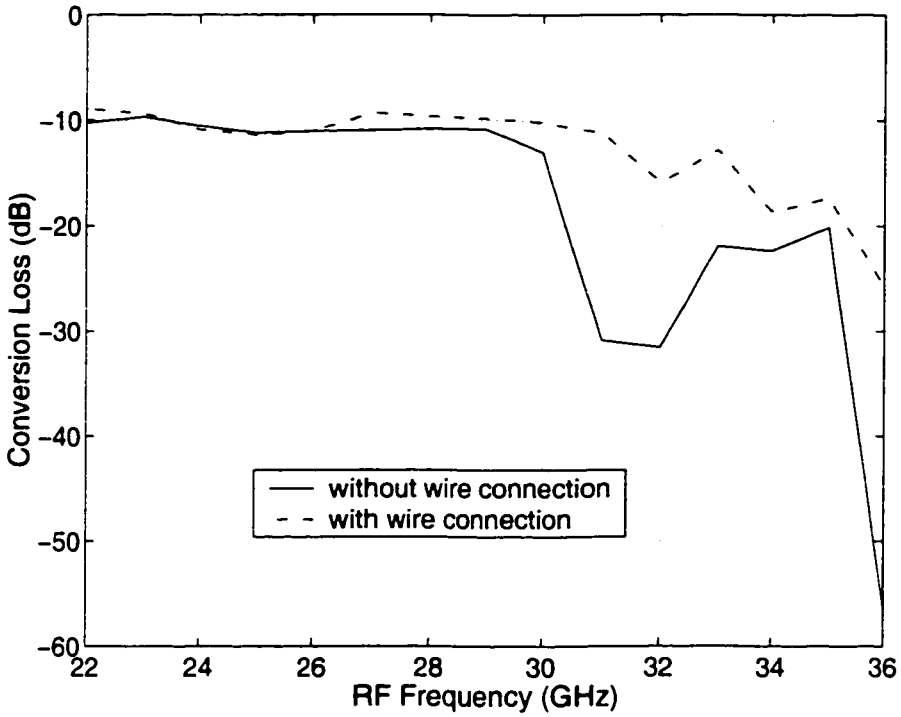

Figure 6.9 Measured conversion loss of two mixers with finite ground planes. The LO and RF are swept from 10.5 to 17.5 GHz and 22 to 36 GHz.

the CPS line. In the second one, strips of the two transmission lines are joined to each other through a metal wire.

They are fabricated on a 10 mil think ceramic substrate. Figure 6.9 shows their measured conversion loss at a fixed IF frequency of 1 GHz: the RF signal is swept from 22 to 36 GHz and the LO is from 11.5 to 17.5 GHz with the 10-dBm power injected at the LO port. From this figure, it can be seen that the conversion loss of the second mixer having a wire becomes much better specially over a RF range of 30-36 GHz. Actually the wire inductance changes the CPW$_{fgp}$-CPS T-junction characteristics. This validates our initial judgement: the main problem causing the

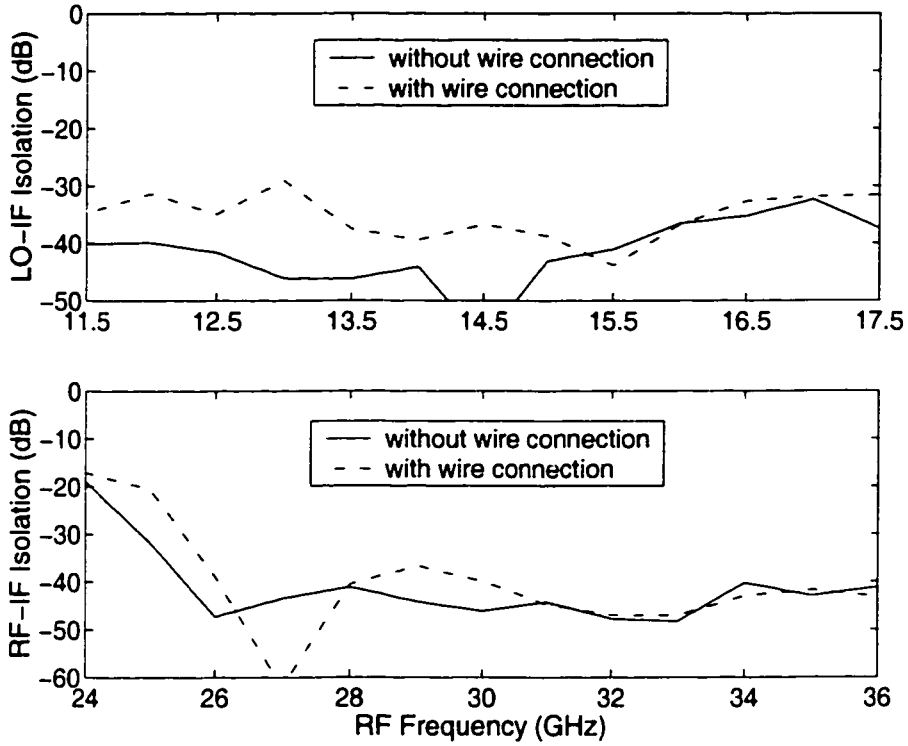

Figure 6.10 Measured LO-to-IF and RF-to-IF isolations.

deterioration of conversion loss beyond 30 GHz is due to the discontinuity of the CPW$_{fgp}$-CPS T-junction.

Figure 6.10 depicts the measured LO-to-IF and RF-to-IF isolation characteristics. The RF-to-IF isolation curves for both mixers look similar over the entire RF range of 22-36 GHz. The LO-to-IF isolation for the second mixer with a wire is at least 6 dB lower than that for the first mixer over the entire LO range of 10.5-17.5 GHz. The significant difference of the two measured LO-to-IF isolations indicates that the wire inductance enhances a coupling from slot mode to CPW mode in the T-junction. That way, the LO leakage to the RF or IF port increases.

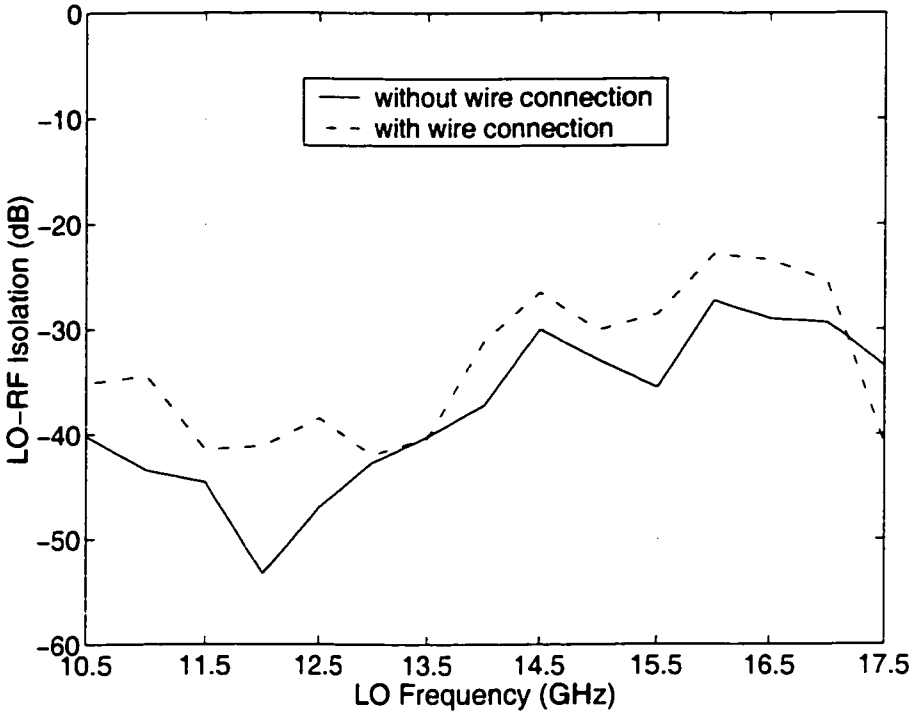

Figure 6.11 Measured LO-to-RF isolation.

Figure 6.11 depicts the measured LO-to-RF isolation characteristic. The LO-to-RF isolation for the second mixer with a wire is also lower than the one for the first mixer. This further proves that the wire makes the isolation between LO and RF/IF ports worse.

6.4 Conclusion

Another new uniplanar architecture of balanced subharmonically pumped mixer has been proposed. It is implemented in CPW$_{fgp}$ and CPS configuration. The proposed mixer has demonstrated a low and flat conversion loss over a 22-30 GHz RF frequency range. Although the isolations between ports are not so high as the

balanced SH mixers with infinite ground planes have. such a uniplanar balanced subharmonically pumped mixer with finite ground planes should be well suited for narrow bandwidth wireless system application with respect to its smaller size and more compact properties.

CONCLUSION AND RECOMMENDATIONS

Our objective is to realize a low cost, small size and high quality downconverter for the receiver front-end of LMCS subscriber terminal. The front-end module consists of low-noise amplifier (LNA), RF bandpass filter, downconverter and IF bandpass filter. In this case, the mixer is the key element and the core of the module. Therefore, the study of a broadband RF mixer becomes the research focus of the thesis work. In particular, our work is oriented to the development of multi-purpose broadband millimeter-wave mixer that can find many applications in broadband wireless access (LMDS/LMCS) and mobile satellite communication terminal.

To begin with, the advantages of balanced mixer and subharmonically pumped-(SH) mixer have been discussed and combined in our proposed mixer architecture, which results in a new type of balanced SH mixer. Approximating nonlinear diode characteristics by power series, we have derived out analytical features of such a mixer. In order to optimize the design of the mixer, a generic approach has been developed. We have also validated this modeling approach with the implementation of a balanced SH mixer at 14 GHz on the basis of microstrip line technique. The best port-to-port conversion loss is equal to 7.2 dB at the 14 GHz RF frequency. Considering roughly 2 dB losses of the practical circuit, the measured performance is almost identical to the simulated result.

Then, a number of useful discussions and considerations have been made for designing double-Y baluns on the basis of uniplanar techniques. The use of uniplanar schemes is to explore some unique properties of this class of planar lines for millimeter-wave design. According to those design considerations, two different double-Y baluns have been designed using a commercial full-wave simulator. They have been realized in MHMIC format and have experimentally demonstrated a low-loss and flat response over a wide bandwidth. The designed CPW-slotline balun has exhibited a rather good performance with a low insertion loss of less than 1 dB and a flat response over 2-3 octave frequency range. The designed CPW$_{fgp}$-CPS balun has demonstrated a less than 1.5-dB insertion loss over the DC-to-22 GHz frequency range. In order to reduce potential radiation as well as leakage losses for CPW open end, a concept of the anti-symmetrical CPW modal electrical fields that are "elastically" converged into a circular aperture has been applied to the design of RF chokes and tapered DC-blocking filters. Through a comparative study of different RF chokes and different DC-blocking filters, the compensated RF choke and DC-blocking filter have experimentally exhibited a better performance with lower loss and wider bandwidth.

Moreover, two types of uniplanar balanced SH mixers related to the infinite and finite ground planes have been proposed and implemented in MHMIC format. The first type of the mixer with infinite ground planes has achieved some unparalleled advantages: a very flat conversion loss of 9.5-11.6 dB over a wide bandwidth of 24-38

GHz RF bandwidth driven by a subharmonic LO source of 11.5-18.5 GHz and high isolations of more than 45 dB between ports. It shows an impressive broadband performance that features very good conversion loss, record high isolation between three sets of ports and excellent suppression capability of even-order harmonics and some spurious signals. The second type of mixer with finite ground planes has also achieved a good performance with a low conversion loss and a high suppression of some even-order harmonics and spurious signals over a narrow bandwidth. The conversion loss varies from 9 to 11 dB over a RF bandwidth of 24-30 GHz by a subharmonic LO source of 11.5-14.5 GHz. The isolations between ports are higher than 35 dB. The finite ground format allows the reduction of circuit space as well as the reduction in potential interference and leakage loss. Our proposed architectures allow reducing the demand on LO source so that it becomes very useful for low-cost millimeter-wave transceiver design.

Finally, a small and compact Ka-band downconverter has been suggested for LMCS application (see the Appendix I). It consists of our developed broadband balanced SH mixer and a commercial MMIC LNA. Due to our purchased MMIC LNA chips that have some technical problems, we could not obtain results for the real downconverter design. But we can expect that it should be no problem for us to realize such a small-size downconverter in the future.

We have designed the broadband uniplanar balanced SH mixer. It serves as a downconverter mixer. If the parts on the side of RF and IF ports are redesigned,

a similar balanced SH mixer used in the construction of an upconverter can be expected. But it is necessary for us to take into account how the ring in the hybrid circuit is designed to match the input CPW line over an IF frequency range and also to have quarter-wave shorted stubs for the slotline or CPS feed port at LO frequency. Since the IF frequency is much lower than the LO frequency in the upconverter SH mixer, the $\lambda_{LO}/2$ ring can be designed to behave as a quarter-wave shorted stubs at LO frequency, but multi-section impedance transformers over a broadband of IF frequency are not possible to be realized with the same ring. This requires a further intensive research.

Our developed uniplanar double-Y baluns have shown a good performance of low loss, small size and broadband. Such a balun transforms unbalanced line to balanced line. Hence, we can apply the baluns to design a broadband uniplanar double-balanced mixer which is implemented in CPW-slotline or CPW$_{fgp}$-CPS structures. The uniplanar double-balanced mixer consists of two baluns, a diode quad and IF interface lines. It will demonstrate a compact and small-size property with no metalization on or connections to the backside.

The innovative uniplanar baluns and novel uniplanar balanced subharmonically pumped mixers have been realized in an MHMIC format. Since no via holes are needed to connect devices with the ground conductor and all conductors are on one side of the substrate, the circuit fabrication process is the same as that of conventional MMICs. As such, the balun and mixer schemes are also suitable for

MMIC implementations with both lumped and distributed element approaches to make the circuits much smaller and to reduce their cost. Such a MMIC mixer can also be integrated with low noise amplifier, power amplifier and IF filter to realize a T/R module chip for broadband application.

REFERENCES

[1] "LMDS: The giant begins to stir" Information Provider Newsletters. 1996 VIPC. Video Information Provider Consulting.

[2] Dougla A. Gray, "A broadband wireless access system at 28 GHz", Technical paper FM-96-1.1. Wireless Cable Europe, 27-28 Feb. 1996. London.

[3] Bill Manley, "Announcement of LMCS licenses", Speaking Notes. October 29. 1996.

[4] , "Introduction and overview of millimeter waves", Inferred and Millimeter-wave, Academic Press, Inc. Vol. 4, Ch.1, pp. 1-21, 1981.

[5] Holger H. Meinel, "Commercial applications of millimeterwaves history, present status, and future trends", IEEE Trans. Microwave Theory Tech., vol. 43, pp. 1639-1653, July, 1995.

[6] Tai Ri Lee, "28 GHz solid state channelized transceiver for digital LMCS", page 16, Proc. of the 1997 IEEE MTT-S Int. Topical Symp. On Tech. For Wireless Appl. Feb. 23-26, 1997.

[7] P. H. Siegel, R. J. Dengler, I. Mehdi, J. E. Oswald, W. L. Bishop, T. W. Crowe, and R. J. Mattauch, "Measurements on a 215-GHz subharmonically pumped

waveguide mixer using planar back-to-back air-bridge Schottky diodes". IEEE Trans. Microwave Theory Tech., vol. 41, no. 11, Nov. 1993.

[8] J. W. Archer, R. A. Batchelor, and C. J. Smith, "Low-parasitic, planar Schottky diodes for millimeter-wave integrated circuits". IEEE Trans. Microwave Theory Tech., vol. 38, no. 1, Jan. 1990.

[9] D. G. Garfield, R. J. Mattauch, and S. Weinreb, "RF performance of a novel planar millimeter-wave diode incorporating an etched surface channel". IEEE Trans. Microwave Theory Tech., vol. 39, no. 1, Jan. 1991.

[10] W. L. Bishop, T. W. Crowe, R. J. Mattauch, and P. H. Ostdiek, "Planar Schottky barrier mixer diodes for space applications at submillimeter wavelength", Microwave Opt. Technol. Lett., vol. 4, no. 1, Jan. 1991.

[11] S. A. Mass, Microwave Mixers, Artech House, 1993.

[12] S. A. Mass, Nonlinear Microwave Circuits, Artech House, 1988.

[13] M. Cohn, J. E. Degenford, and B. A. Newman, "Harmonic mixing with antiparallel diode pair". IEEE Trans. Microwave Theory Tech., vol. MTT-23, no. 8, Aug. 1975.

[14] P. S. Henry, B. S. Glance, and M. V. Schneider, "Local-oscillator noise cancellation in the subharmonically pumped down-converter", IEEE Trans. Microwave Theory Tech., vol. MTT-24, no. 8, May 1976.

[15] R. Kawasaki and M. Akaike, "A broadband second-harmonic mixer covering 76-106 GHz", IEEE MTT-S Int. Microwave Symp. Digest, pp. 425-427, June 1978.

[16] S. D. Vogel, "Design and measurements of a novel subharmonically pumped millimeter-wave mixer using two signal planar Schottky-barrier diodes", IEEE Trans. Microwave Theory Tech., vol. 44, no. 6, pp. 825-831, June 1996.

[17] S. Raman, F. Rucky and G. M. Rebeiz, "A high-performance W-band uniplanar subharmonic mixer", IEEE Trans. Microwave Theory Tech., vol. 45, no. 6, June 1997.

[18] F. D. Flavis, T. Rozzi, F. Moglie, A. Sgrecia, and A. Panzeri, "Accurate analysis and design of millimeter wave mixers", IEEE Trans. Microwave Theory Tech., vol. 41, no. 5, pp. 870-873, May 1993.

[19] H. Gu and K. Wu, "A generic approach for the optimum design of microwave and millimeter-wave balanced subharmonically pumped mixers", Asia-Pacific Microwave Symp. Digest, pp. 480-484, Dec. 1999.

[20] S. B. Cohn, "Slot line on dielectric substrate", IEEE trans. Microwave Theory Tech., vol. MTT-17, pp. 768-778, Oct. 1969.

[21] G. H. Robinson and J.L. Allen, "Slot line application to miniature ferrite devices", IEEE Trans. Microwave Theory Tech., vol. MTT-17, pp. 1091-1096, 1969.

[22] J. B. Knorr, "Slot line transition", IEEE Trans. Microwave Theory Tech., vol. MTT-22, pp. 548-554, May 1974.

[23] A. Podcameni and M. L. Coimbra, "Slotline-microstrip transition on ISO/anisotropic substrate a more accurate design", Electronics Lett., vol. 16, no. 20, pp. 780-781, 1980.

[24] B. Schuppert, "Microwave/slotline transitions modeling and experimental investigation", IEEE Trans. Microwave Theory Tech., vol. MTT-36, pp. 1272-1282, Aug. 1988.

[25] V. Fouand Hanna and L. Rambroz, "Broadband planar coplanar waveguide-slotline transition", 12th Europ. Microwave Conf., pp. 628-631, 1982.

[26] D. Cahana, "A new coplanar waveguide/slotline double balanced mixer", IEEE MTT-S Int. Microwave Symp. Digest, pp. 967-968, June 1989.

[27] V. Trifunovic and B. Jokanovic, "New uniplanar balun", Electronics Letters, vol. 13, no. 17, pp. 510-511, 1977.

[28] J. H. Cloete, "Graphs of circuit elements for the Marchand balun", Microwave Journal, pp. 125-128, May 1998.

[29] D. M. L. Bartholomew, "Optimum design for a broadband balun", Electronics Letters, vol. 27, no. 10, pp. 813-815, 1991.

[30] V. Trifunovic and B. Jokanovic, "Four decade bandwidth uniplanar balun", Electronics Letters, vol. 28, no. 6, pp. 534-535, 1992.

[31] W. Grammer and K. S. Yngvesson, "Coplanar waveguide transitions to slotline: design and microprobe characterization", IEEE Trans. Microwave Theory Tech., vol. 41, no. 9, pp. 1653-1658, Sept. 1993.

[32] V. Trifunovic and B. Jokanovic, "Review of printed Marchand and double Y balun: characteristic and application", TELSIK'97, pp. 287-298, Oct. 1997.

[33] H. Gu and K. Wu, "Broadband design consideration of uniplanar double-Y baluns for hybrid and monolithic integrated circuits", IEEE MTT-S Int. Microwave Symp. Digest, pp. 863-866, June 1999.

[34] C. P. Wen, "Coplanar waveguide: a surface strip transmission line suitable for nonreciprocal gyromagnetic device applications", IEEE Trans. Microwave Theory Tech., vol. MTT-17, pp. 1087-1090, Dec. 1969.

[35] K. Wu, R. Sadat, D. Klemer, and R. G. Bosisio, "A class of radiationless wideband coplanar waveguide open stubs for monolithic and hybrid integrated circuits", IEEE MTT-S Int. Microwave Symp. Digest, pp. 277-280, 1994.

[36] R. W. Jackson, "Mode conversion at discontinuities in finite-width conductor-backed coplanar waveguide", IEEE Trans. Microwave Theory Tech., vol. MTT-37, no. 8, pp. 1582-1589, Oct. 1989.

[37] H. Shigesawa, M. Tsuji and A. A. Oliner, "Conductor-backed slot line and coplanar waveguide: dangers and full-wave analysis", IEEE MTT-S Int. Microwave Symp. Digest, pp. 199-202, 1988.

[38] I. Huynen and G. Dambrine, "A novel CPW DC-blocking topology with improved matching at W-band", IEEE Trans. Microwave Theory Tech., vol. 8, no. 4, pp. 149-151, April 1998.

[39] H. Gu and K. Wu, "Broadband uniplanar building blocks for monolithic and hybrid millimeter-wave integrated circuits", 30th Europ. Microwave Conf., pp. 628-631, 2000.

[40] F. D. Flaviis, T. Rozzi, F. Moglie, A. Panzeri, "Accurate analysis and design of millimeter wave mixers", IEEE Trans. Microwave Theory Tech., vol. 41, pp. 870-873, May 1993.

[41] H. Gu and K. Wu, "A novel broadband uniplanar balanced subharmonically pumped mixer", IEEE MTT-S Int. Microwave Symp. Digest, pp. 635-637, June 2000.

[42] K. C. Gupta, Ramesh Garg, Inder Bahl and Prakash Bhartia, Microstrip lines and slotlines, Artech House, 1996.

Appendix I

BROADBAND UNIPLANAR BALANCED SUBHARMONICALLY PUMPED MIXER WITH BUFFER LNA FOR KA-BAND LMCS SUBSCRIBER TERMINAL

I.1 Introduction

To study and develop a low-cost integrated millimeter-wave transceiver (T/R module) intended for application in the design of high-performance LMCS, we should build a transceiver system T/R RF module which is shown in Figure I.1. The receiver has an input buffer amplifier proceeding to the mixer. This pre-amplifier or sometimes AGC is used to increase the strength of the received signal so that it exceeds the noise level of the following mixer.

For the purpose of compact and high performance, we intend to combine our developed balanced subharmonicllly pumped mixer with a commercial MMIC low noise amplifier (LNA) to build a Ka-band downconverter, that is, the mixer and the MMIC LNA are integrated into single chip using miniaturized hybrid MIC process.

I.2 A MMIC Low Noise Amplifier

In order to accommodate our developed broadband uniplanar balanced SH mixer, the commercial LNA chosen for a Ka-band downconverter is a Ka-band

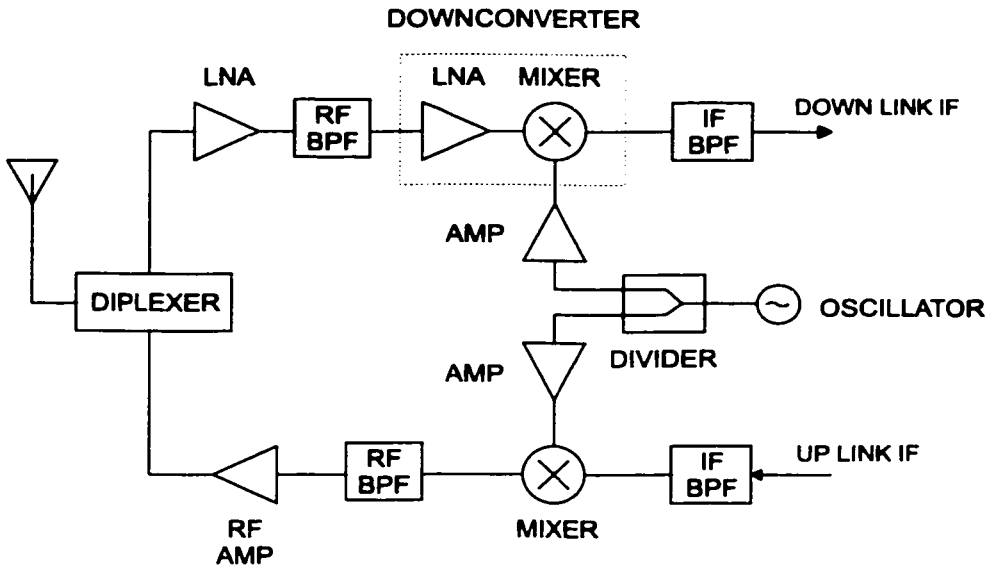

Figure I.1 Transceiver T/R RF module block diagram.

HEMT low-noise amplifier (ALH140C, TRW), which is a broadband, two-stage, low-noise amplifier. The performance characteristics of the amplifier chips are shown in Table I.1 as given by the manufacturer.

The amplifier ALH140C is compatible with eutectic die attach, thermocompression and thermosonic wire bonding assembly techniques. Since the MMIC LNA wafer is going to be combined with our uniplanar mixer, it must be connected to the coplanar line. Here it is noted that the MMIC amplifier is in microstrip format. The microstrip-to-CPW transition is nonplanar in nature. The CPW is terminated at one end by joining the ground plane at a short distance away from the strip. The ground planes of the CPW and the MMIC chip are made common by placing the chip on top of the CPW ground plane. Strips of the two transmission lines are joined to each other through a metal ribbon. However, the open-end capacitance of

Table I.1 Ka-band HEMT low-noise amplifier performance characteristics (T_a=25°)

Specification	Minimum	Typical	Maximum	Unit
Frequency	24		40	GHz
Gain	10	11.5		dB
Noise figure		4.0		dB
Input VSWR			1.95	
Output VSWR			1.76	
Frequency	24		27	GHz
Gain	10	12		dB
Noise figure		4.0		dB
Input VSWR		1.6	1.95	
Output VSWR		1.4	1.7	
Frequency	27		30	GHz
Gain	10	12		dB
Noise figure		4.0		dB
Input VSWR		1.3	1.70	
Output VSWR		1.3	1.51	
Frequency	37		40	GHz
Gain	10	11.5		dB
Noise figure		4.0	5.5	dB
Input VSWR		1.20	1.50	
Output VSWR		1.40	1.50	
V_d		+4		V
V_g	-1	-0.2	+0.3	V
I_{dl}		75		mA
Thermal resistance		195		oC/W

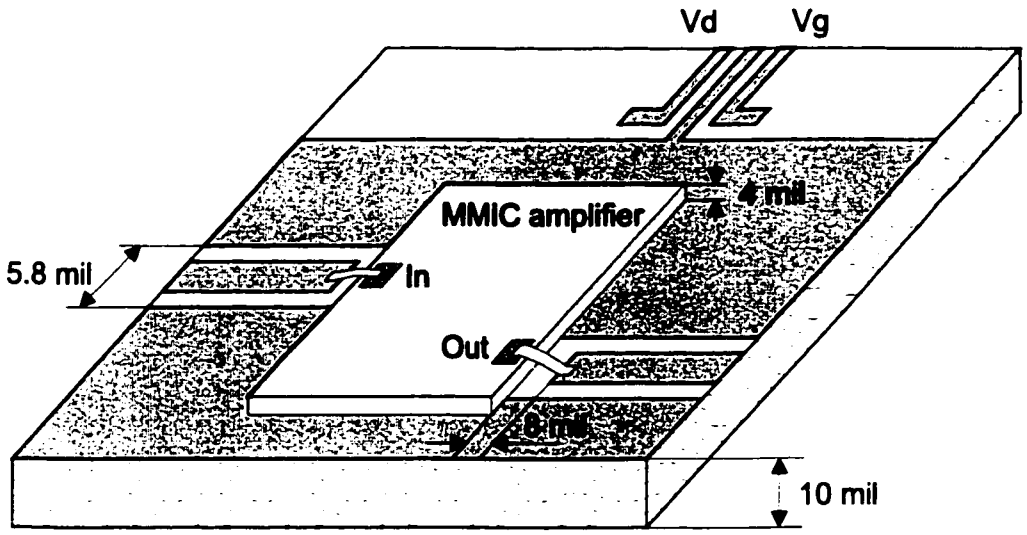

Figure I.2 MMIC LNA test board.

the microstrip line, ribbon inductance, and the open-end capacitance of the CPW constitute a low-pass filter whose cutoff frequency can be varied by varying the length of the metal ribbon. Therefore, it is necessary to measure the MMIC amplifier with a special test board, which matches our designed mixer interface, before the MMIC LNA is integrated with the mixer into one chip.

According to the recommended assembly notes from the manufacturer, the test board is designed and shown in Figure I.2. It is fabricated on Epsilon 9.9 alumina substrate with a thickness h=10 mil. In practice, the connection between two strips, however, is a 0.7-mil diameter wire available in our lab. This size wire is not the same as the ribbon recommended by the manufacturer.

The amplifier is tested with 68 um-pitch 40 GHz coplanar waveguide probes. The LNA DC bias network requires a bipolar power source. To prevent transient

burnout of the HEMT LNA during turn-on, the proper turn-on sequence is: first apply a negative bias to V_g and then apply a positive bias to V_d by gradually increasing from zero voltage. Following this turn-on rule, we test three pieces of MMIC LNA chips but two of them have no power gain output. The situation is that the I_d goes up to its maximum limitation 100 mA when the V_d is increased to around 2 V.

However, only one of the three pieces works with an unstable quiescent point. Figure I.3 shows the measured input and output VSWR. The maximum input and output VSWRs are 2.7 and 2.5, respectively, over the entire frequency range of 24-40 GHz. The minimum gain is 9.3 dB over the entire range. From the two figures, it can be seen that the achieved performance is not as good as suggested by the manufacturer. Specially, it becomes worse with frequency. This may be caused from the connection between the MMIC LNA wafer and the CPW line because the wire inductance and open-end capacitance constitute a low-pass filter. To reduce the wire inductance effect, it would be better to use two wire lines for approaching the 3×0.5 mil^2 ribbon required by the manufacturer.

I.3 Broadband Downconverter

As presented in Chapter 5, a Ka-band uniplanar balanced subharmonically pumped mixer has been developed and it has experimentally demonstrated a very good performance with a low conversion loss and high isolations between ports

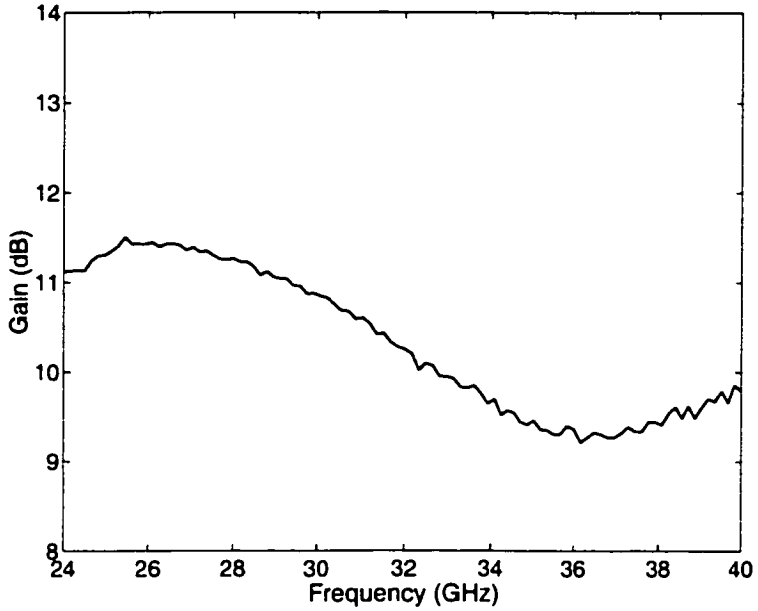

Figure I.3 Measurement MMIC LNA gain under V_g=-1 V, V_d=4 V and I_d=70 mA.

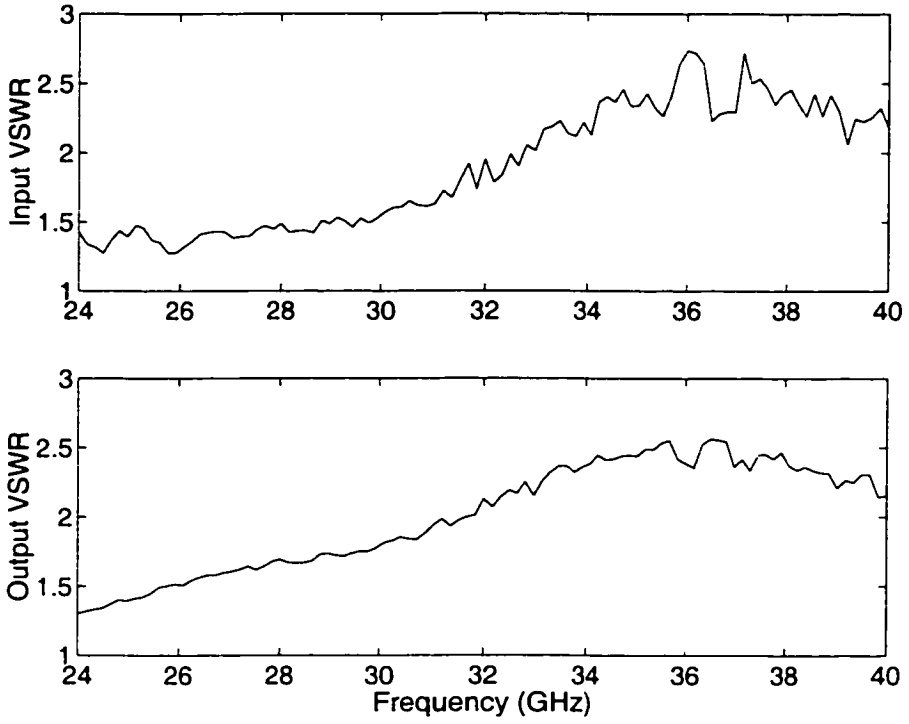

Figure I.4 Measurement of input and output VSWR under V_g=-1 V, V_d=4 V and I_d=70 mA.

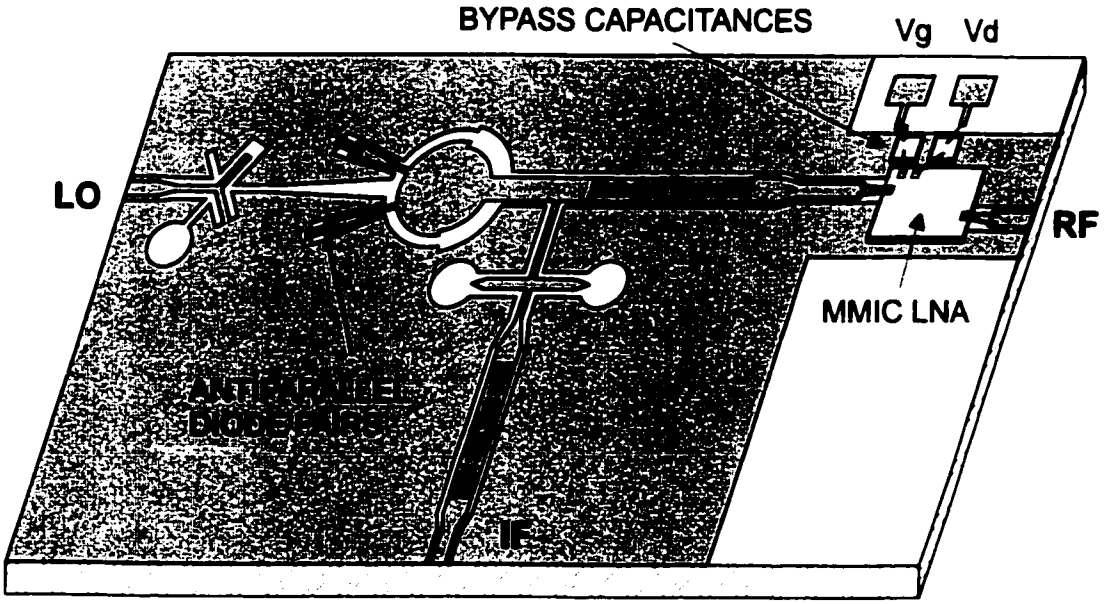

Figure I.5 Construction of broadband downconverter.

as well as good suppression of some undesired mixing frequency elements. Therefore, we intend to build a Ka-band downconverter by combining the mixer and commercial MMIC LNA into one chip.

Figure I.5 shows the uniplanar construction of Ka-band downconverter. It consists of a uniplanar balanced SH mixer and a MMIC LNA. Two diode pair chips (ALPHA DMK2308-000) and one MMIC LNA chip (TRW ALH140C) were flip-chip mounted on their locations with silver epoxy. It is tested with 68 μ-pitch 40 GHz coplanar waveguide probes.

To be careful, we test each of both mixer and LNA separately before making the connection between the mixer and LNA. The mixer itself works well but the LNA had no power gain output. The situation is the same as the previous scenario

before. Then, we try to replace it by new one, but the same problem happens again. Through the five tests, it is obvious that there should be some problem in the MMIC LNA chips. Hence, we could not proceed with the final testing of the whole circuit.

I.4 Conclusion

A uniplanar downconverter architecture with compact size has been suggested. The downconverter consists of our developed broadband balanced subharmonically pumped mixer and a commercial MMIC LNA chip. It is implemented in a uniplanar configuration. As such, the downconverter should have the advantages of easy fabrication, good performance and small size.

Due to the problem related to our purchased MMIC LNA chips, we could not get the final results of the Ka-band downconverter. However, we can expect that it should be no problem to realize a Ka-band downconverter if we have a good quality of MMIC LNA chip.